NTNU – Trondheim
Norwegian University of
Science and Technology

Water Alternating Gas in Stratified Reservoirs

A Sensitivity Study of WAG Parameters

Jonas Sørbel

Petroleum Geoscience and Engineering
Submission date: June 2015
Supervisor: Jan-Åge Stensen, IPT

Norwegian University of Science and Technology
Department of Petroleum Engineering and Applied Geophysics

Abstract

Water alternating gas (WAG) injection is an EOR method where water and gas is injected in cycles. The process exploits the microscopic displacement advantages of gas while using subsequent water slugs for mobility control. The gas is also effective in displacing attic oil not reached by water, and as such WAG can improve both microscopic and macroscopic sweep.

Heterogeneities and high permeability streaks and channels can be an issue for effective WAG application. However, the distribution and location of these heterogeneities are not irrelevant and can in some situations be advantageous for gas injection. This study investigates the importance of the position of the high quality units in immiscible WAG by using a modified simulation model of a Gullfaks satellite. The simulations use a black oil fluid description and are run in Eclipse 100. In addition to selected sensitivities, six different stratification sequences are investigated. The layers are moved within the model to explore stratifications where the highest quality layers are on top of the formation, termed "downwards fining", the other way around, termed "upwards fining", and other varieties.

The study showed WAG provided additional recovery between 1.0 % and 3.0 % in all simulations. WAG was 25-50 % more effective in upwards fining sequences than downwards fining sequences and gas breakthrough is reduced and delayed. Vertical permeability was found to have a large impact on results in both waterflooding and WAG in the base case. Increased vertical permeability reduced the incremental oil of WAG over waterflood in the base case, but it is not given that this is the case in other setups. Further investigation is recommended on the matter.

Sammendrag

Alternerende vann- og gass (WAG) injeksjon er en EOR-metode hvor vann og gass blir injisert i sykluser. Prosessen utnytter de mikroskopiske fortrengningsfordelene til gass mens påfølgende vann sykluser sørger for mobilitetskontroll. Gassen er også effektiv i å fortrenge olje høyt i formasjonen som ikke nås med vann, og som sådan kan WAG forbedre både mikroskopisk og makroskopisk sveip.

Heterogeniteter og høypermeable lag og kanaler kan være en hindring for WAG. Distribusjonen og plasseringen av disse heterogenitetene er imidlertid ikke irrelevant, og kan i enkelte tilfeller være fordelaktig for gassinjeksjon. Denne studien undersøker betydningen av posisjonen til høykvalitetslagene i ikke-blandbar WAG ved hjelp av en modifisert simuleringsmodell fra en Gullfaks satellitt. Modellen bruker en «black oil» væskebeskrivelse og kjøres i Eclipse 100. I tillegg til utvalgte sensitiviteter, er seks forskjellige lagdelingssekvenser undersøkt. Lagene blir flyttet rundt i modellen for å utforske sekvenser hvor høykvalitetslagene er øverst i formasjonen, kalt nedover forfinende, og motsatt, kalt oppover forfinende, i tillegg til andre varianter.

Studien viste at WAG ga mellom 1.0 % og 3.0 % ekstra oljeutvinning i alle simuleringer. WAG var 25-50 % mer effektiv i oppover forfinende enn nedover forfinende sekvenser, og gassgjennombruddet var redusert og forsinket. Vertikal permeabilitet ble funnet å ha stor innvirkning på resultatene i både vannfløming og WAG i basistilfellet. Økt vertikal permeabilitet reduserte mengden inkrementell olje fra WAG i basistilfellet, men det er ikke gitt at dette er tilfelle i andre oppsett. Videre undersøkelser anbefales på området.

Acknowledgements

I would like to thank my supervisor, Jan Åge Stensen, for providing advice and guidance whenever called upon. His experience and suggestions has been greatly appreciated during the specialization project and master thesis.

I would also like to thank Øyvind Breivik for keeping military grade discipline during our night sessions at times when progress was most needed and Jørgen Olsen for constructive criticism on my writing during proofreading.

Last, but not least, I would like to thank Hanna Vølstad for her encouraging words and positive attitude whenever problems arise.

Table of Contents

List of Figures

List of Tables

1 Introduction

Water alternating gas (WAG) injection has been utilized in many fields since the first field application in 1957 (Christensen, Stenby, & Skauge, 1998). The method seeks to combine the advantages of water flooding and gas flooding to increase the ultimate recovery. Most WAG applications have been considered a technical success (Christensen, Stenby, & Skauge, 1998), but the sales potential of the gas and required up front capital expenditure necessitates accurate evaluation before a decision is made. Both waterflooding and gas flooding is well understood individually, but uncertainties still surround WAG. The presence of three phases in the reservoir introduces infinite sets of saturation paths, where conventional two-phase hysteresis models are not accurate. Many studies have been conducted on relative permeability hysteresis and relative permeability of oil in a three phase system, but none of the proposed models are universally better than others (Element, Masters, Sargent, Jayasekera, & Goodyear, 2003; Pejic & Maini, 2003). Consequently meticulous research and experimental data is required for each individual reservoir where WAG is considered.

Due to the density difference between gas and oil/water, accurate representation of the geological environment is a key factor to successful prediction of WAG performance. The vertical permeability is particularly important to the WAG process. The position of the best quality reservoir units will also play a role in the feasibility of WAG.

1.1 Objective

This thesis investigates WAG in a heterogeneous reservoir based on a reservoir model from a Gullfaks satellite. The model is severely altered and bears minimal resemblance to the real field. The main objective is to identify the role of reservoir quality distribution in a WAG process. In other words, how the WAG efficiency will be in a system with the high reservoir quality units on top and lower quality units on the bottom compared to the other way around. Several others variations will also be investigated, including the original field layering.

A set of sensitivities is also selected to examine the parameters' influence on WAG simulation.

Simulations are run in Eclipse 100 with a black oil fluid description.

1.2 Why WAG?

WAG is the most applied EOR technology in the North Sea to date. In addition to being a widely used EOR technology, knowledge of three-phase flow behavior is also applicable in reservoirs where WAG is not implemented. Examples are; fields with a gas cap and aquifer/water injection and fields produced by solution gas drive that are later water flooded. WAG is an interesting subject both because of the complexity and its regular application.

2 Water Alternating Gas – Theory and Application

Water alternating gas (WAG) injection seeks to combine the advantages of both waterflooding and gasflooding. WAG injection is an EOR method where water and gas is injected in cycles. The technique exploits the microscopic displacement advantages of gas while using subsequent water slugs for mobility control. WAG was initially proposed as a method to control the mobility in gas flooding projects (Christensen, Stenby, & Skauge, 1998), but in later years WAG is more often used to improve the recovery of a waterflood by introducing the gas component. Gas is also effective in displacing attic oil not reached by water and as such WAG can improve both microscopic and macroscopic sweep. Typically WAG is applied as a tertiary recovery method, but some fields in the North Sea have applied WAG early in the field life (Instefjord & Todnem, 2002; Lien, Lie, Fjellbirkeland, & Larsen, 1998). In a summary of reported field applications by Christensen, Stenby & Skauge (1998) the reported increased oil recovery is mostly around 5% of STOOIP, but up to 20 % has also been reported in some fields.

WAG is usually divided into miscible WAG (MWAG) or immiscible WAG (IWAG), but other less used variations also exist, like simultaneous WAG (SWAG), foam assisted WAG (FAWAG) and hybrid WAG (HWAG). Further detail on miscible and immiscible WAG is provided in section 2.1.

2.1 Miscibility

The section on miscibility is previously used in (Sørbel, 2014) *and has not been written specifically for this study.*

Depending on pressure, temperature and fluid composition of the injected fluid and reservoir fluid, three types of displacements can occur; first contact miscibility (FCM), multicontact miscibility (MCM) and immiscible displacement. FCM is where interfacial tension (IFT) between the injectant and reservoir fluid is zero, and they behave as a single phase. MCM is where mass exchange between the oil and gas phase lead to miscibility in multiple contacts (see Figure 2-1). Immiscible displacement is slightly misleading because a gas will always extract some oil components and the gas is soluble in undersaturated oil (Sheng, 2013, pp. 12-13). MCM processes can be divided into vaporizing-gas drive and

condensing-gas drive. For vaporizing-gas drive the injected lean gas will vaporize some methane from the reservoir oil and eventually become miscible with the virgin reservoir fluid. Successively injected lean gas will be miscible with the previously injected gas, typically through several contacts. For condensing-gas drive, enriched gas is injected and gives up heavier components to the oil. Eventually the reservoir oil becomes sufficiently enriched to be miscible with the freshly injected gas (Holm, 1986). Usually it is a combination of both as shown in Figure 2-1 C.

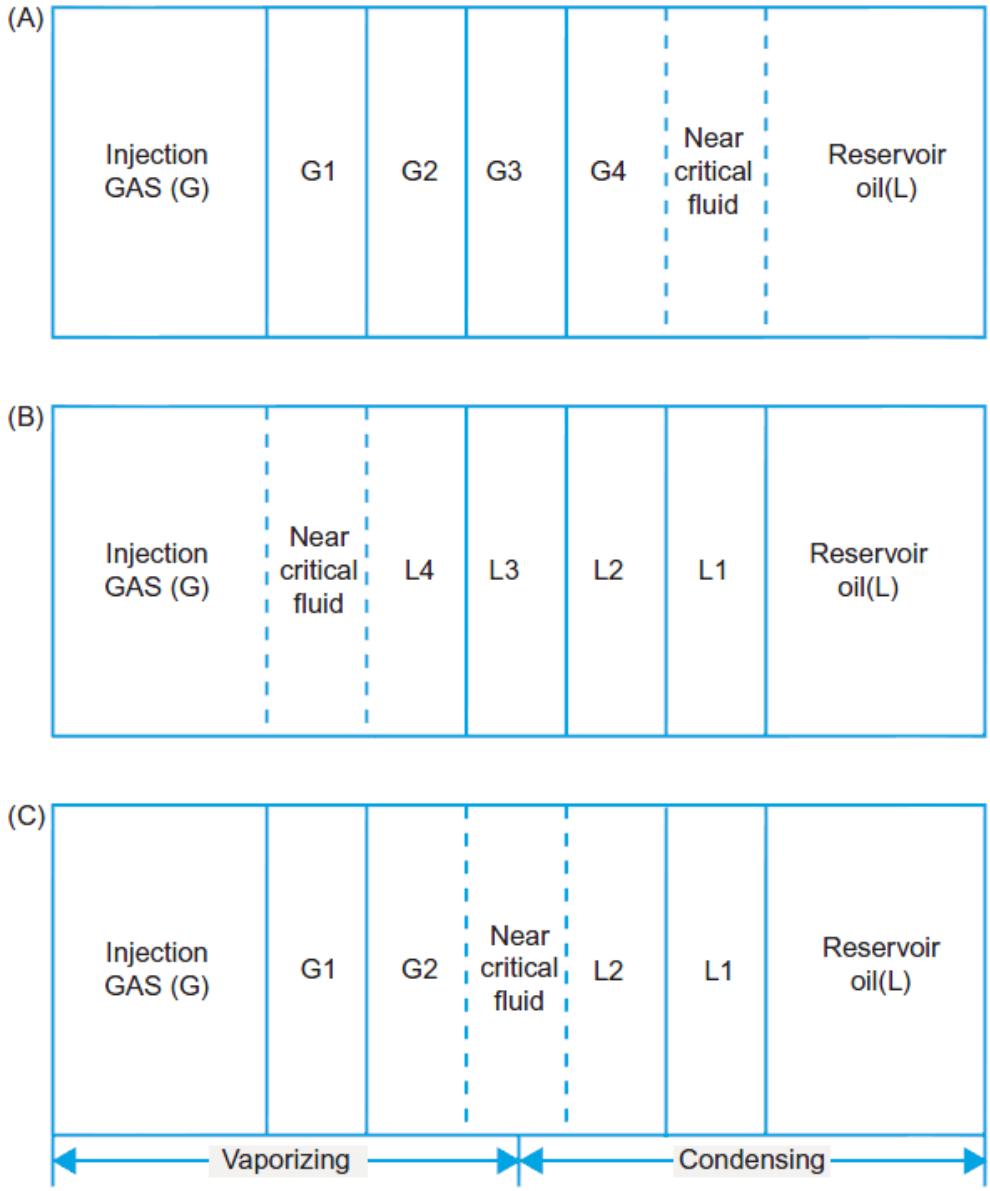

Figure 2-1 – Location of the low IFT fluidrelative to location of injection and production wells for vaporizing-gas drive (A), condensing-gas drive (B) and combination of both (C). (Sheng, 2013, p. 14)

The minimum pressure to achieve multicontact miscibility (MCM) can be determined in a number of ways. Besides empirical correlations and analytical methods, the most used experimental method is the slim-tube test. The tube is long and thin, typically packed with glass-beads and filled with oil sampled from the field. Gas is injected at a constant pressure and recovery at a specific time (e.g. 1.2 PV) is measured, before the experiment is repeated at a higher pressure. The definition of minimum miscible pressure (MMP) is somewhat arbitrary. The most common are; the MMP of a MCM process is 90 % recovery at 1.2 PV injected and the MMP for FCM process is near total recovery at 1.2 PV injected. A typical result from this test is seen in Figure 2-2. Another definition of MMP is the pressure where the slope changes. (Wu & Batycky, 1990)

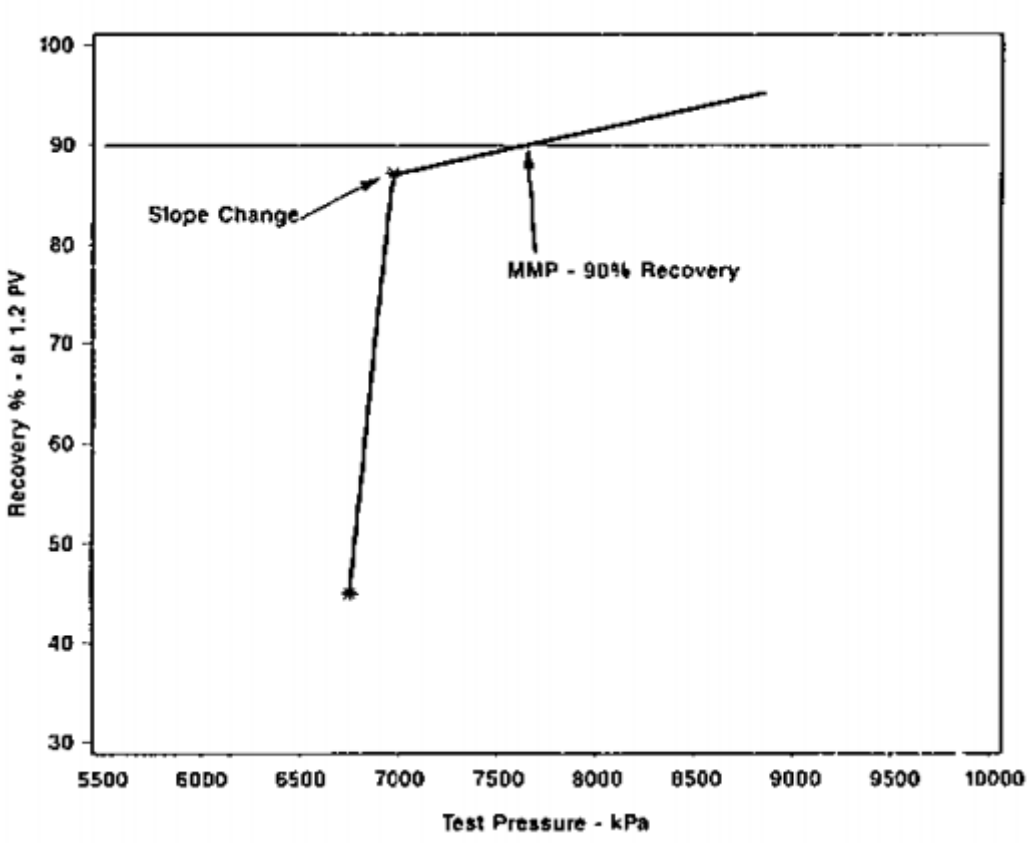

Figure 2-2 – Recovery at 1.2 PV CO_2 injection vs test pressures (Wu & Batycky, 1990)

Miscibility is an important factor for gas flooding because it directly influences the residual oil saturation in the swept areas. In an immiscible displacement process some oil is trapped as isolated drops, stringers or pendular rings, directing the fluid flow around the trapped oil. This residual oil is kept in place by capillary forces that restrict oil droplet deformation and passage through the pores. Injection of a miscible gas will not have interfacial tension with

the oil and can mix with the trapped oil to extract it. The microscopic displacement of oil can approach 100 % for a miscible displacement. (Green & Willhite, 1998, p. 186)

Pure carbon dioxide can be miscible from about 100 bara at 40 C, enriched gas can be miscible between 120 and 200 bara (Donaldson, Chilingarian, & Yen, 1989) while nitrogen usually requires over 350 bara to be miscible (Sebastian & Lawrence, 1992). The pressure in this study is too high to rule out some compositional exchange and development of multicontact miscibility, but it is assumed in this simulation that the process is immiscible.

2.2 WAG Recovery Mechanisms

2.2.1 Microscopic Sweep

Gasflooding provides several advantages over waterflooding. Hydrocarbon gas is soluble in oil up to a certain point, depending on temperature, pressure and hydrocarbon composition. When gas contacts undersaturated oil, some gas will solute in the oil and cause swelling and viscosity reduction. The swelling will increase the local oil saturation and mobilize some of the oil, effectively reducing the stock tank oil left as residual even if the residual oil saturation does not change. The reduced viscosity causes a more favorable mobility ratio and increases the efficiency of a subsequent waterflood.

The interfacial tension (IFT) between oil and gas is typically lower than the IFT between oil and water. Reduced IFT affects the capillary pressure which in turn affects the relative permeability and end point saturations. The IFT between gas and oil will be zero for a first-contact-miscible process and the residual oil saturation can theoretically reach zero. First-contact miscible injection is usually not achieved, but the residual oil to gas is often lower than the residual oil to water.

2.2.2 Macroscopic Sweep

Gas has a much lower viscosity than oil and water. This leads to viscous fingering and bypassing of oil. In other words, the advantages of gas floods in microscopic sweep are negated by the disadvantages in macroscopic sweep. WAG aims to gain the advantages in microscopic sweep of gas floods without the disadvantages in macroscopic sweep by chasing the gas with water. This is often just partially achieved because the gas segregates and does not flow over the entire net pay as it moves further from the injector. While gas segregation

reduces the area affected by enhanced microscopic sweep, it can have positive effects as well. It will be particularly helpful in recovering attic oil because the gas will take a different flow path from oil.

2.2.3 Relative Permeability Hysteresis

Relative permeability is known to be dependent not only on phase saturation, but also phase saturation history. Typically this is represented by differing imbibition and drainage curves in simulation models. Most studies investigating relative permeability hysteresis have found that the hysteresis effect is large for the non-wetting phase and small for the wetting phase (Braun & Holland, 1995). For two-phase flow, relative permeability and hysteresis effects are quite easily measured in laboratory experiments. Since the saturation path is predefined, the assumption that a phase's relative permeability is only dependent on its own saturation and saturation history is valid. In a three-phase system, relative permeability is a much more advanced mechanism. Not only does the number of process paths increase, but the entire saturation path is initially unknown (Larsen & Skauge, 1998). Gas will always be the non-wetting phase in a three-phase system, while oil and water can be both wetting and intermediate wetting. This review will consider water as the wetting phase and oil as the intermediate wetting phase. Several studies investigating three-phase flow (Corey, Rathjens, Henderson, & Wyllie, 1956; Leverett & Lewis, 1941; Saraf, Batycky, Jackson, & Fisher, 1982) have found that the relative permeability of the wetting and non-wetting phase is primarily a function of its own saturation. The intermediate wetting phase is strongly affected by the saturation history and the saturations of the other two phases. They also found that hysteresis effects are small for the wetting phase and significant and pronounced for the non-wetting phase, i.e. gas.

Despite the complexity of the intermediate wetting phase relative permeability, three-phase relative permeability is often represented by functions of one- or two-phase saturations. While reasonably accurate for the wetting and non-wetting phase, the intermediate wetting phase, most commonly considered oil, is much more complex. This has resulted in many correlations and models for calculating oil relative permeability in a three-phase system from two-phase relative permeability sets. The most used methods include Stone I (Stone, 1970), Stone II (Stone, 1973) and Baker (Baker, 1988). Only a limited number of experimental three-phase data sets exist, but none of the correlations are able to be reasonably accurate

to all of them. Pejic & Maini (2003) compared 8 different correlations to three complete three-phase relative permeability sets and found that no single correlation was able to match all sets. They also found that the accuracy of each correlation was strongly related to wettability. The models that performed well in water-wet medium did not perform well in intermediate wet medium. Of the most used models, Stone I works well in water-wet medium, while Baker's models work better in intermediate wet medium.

More recent research has shown that the two-phase hysteresis model for gas is not accurate in a three-phase system. The two-phase gas hysteresis model is often accurate during the first gas cycle, but gas relative permeability has been observed to be reduced when water saturation is increased above the connate saturation (Skauge & Larsen, 1994). The conventional hysteresis models of Carlson (1981) and Killough (1976) assume that the hysteresis process is reversible and only dependent on gas saturation. This difference can have a large impact on gas breakthrough and displacement, subsequently affecting the oil recovery. The reduced gas mobility in secondary drainage has been implemented in Eclipse under the WAGHYSTR keyword. This model ignores the input gas imbibition curve and uses a combination of an analytic version of Carlson's model and Land's parameter (Land, 1968). As long as the water saturation is close to the connate water saturation, the standard reversible two-phase hysteresis model is used. When the water saturation increases over a threshold value, a three-phase model with reduced gas mobility is applied.

Although the wetting phase does not exhibit strong relative permeability hysteresis, reduced water mobility has been observed in intermediate wet three-phase systems (Skauge & Larsen, 1994). Reduced injectivity of water during WAG processes has also been reported (Schneider & Owens, 1976). This effect is also included in the WAGHYSTR keyword of Eclipse and is linked to gas saturation. During two-phase flow the regular water relative permeability curve is used for both imbibition and drainage, but once gas is introduced in the reservoir the water relative permeability is created by scanning curves between a two-phase curve and a three-phase curve.

2.2.4 Residual Oil Saturation

Several studies have linked residual oil saturation to the trapped gas saturation (Holmgren & Morse, 1951; Element, Masters, Sargent, Jayasekera, & Goodyear, 2003), but the effect is

most dominating in water-wet reservoirs. Element, Masters, Sargent, Jayasekera & Goodyear (2003) noted that trapped gas did not significantly affect residual oil saturation in intermediate wet cores, while Kralik, Manak, Jerauld & Spence (2000) found no effect in an oil-wet system. The reduction in residual oil saturation is often an important contributor to incremental recovery in immiscible WAG, but as discussed later in 3.1.4 the reservoir in question is considered more intermediate wet. As a consequence the residual oil will not be directly linked to trapped gas in this thesis. An additional benefit is that this enables sensitivity to observe the effect of reducing water and gas relative permeabilities in the presence of trapped gas.

2.3 Field Application of WAG

Hydrocarbon gas injection gained popularity during the 50's with propane or liquid petroleum gas to achieve miscibility, but increasing price of these solvents soon made continuous gas injection economically unfavorable for fields with an export route (Stalkup, 1983). As a result, alternating the gas injection with water or injection of a miscible slug followed by chase gas and/or water has become a popular alternative. The first WAG application reported in literature is in 1957 and since then WAG has been used in combination with HC gas, CO_2 and nitrogen in many projects (Christensen, Stenby, & Skauge, 1998). Hydrocarbon gas injection remains as a popular alternative when gas export is not a possibility, exemplified by Alaska North Slope (Ma & Youngren, 1994) and some fields in the North Sea (Zhang, Brodie, Daae, Erbas, & Duncan, 2013).

Hydrocarbon gas injection, both continuous gas injection and WAG injection, has only made a marginal contribution to the oil production in North America in the last decades, but is a popular EOR option in some areas. Most notable is the North Sea, where a majority of the applied EOR projects have been hydrocarbon gas injection processes. In addition to some continuous miscible gas floods, at least 14 WAG floods have been initiated in the North Sea between 1975 and 2006. Of these 7 were immiscible WAG, 4 were miscible WAG and 3 were Simultaneous WAG (SWAG) or Foam Assisted WAG (FAWAG). Awan, Teigland & Kleppe (2008) reported data and available results for 12 of the WAG projects in the North Sea. Nearly all of the North Sea WAG applications have been considered a success, with only the immiscible WAG initiated in Ekofisk considered a failure due to instant hydrate formation around the pilot well. Miscible WAG typically results in higher recovery than immiscible

WAG, witnessed by data collected by Christensen, Stenby, & Skauge (1998) which showed higher incremental recovery for miscible WAG (9.7 %) than for immiscible WAG (6.4 %). Both miscible WAG and immiscible WAG has been successful in the North Sea. BP have successfully applied miscible WAG in Magnus and Ula (Brodie, Zhang, Hetland, Moulds, & Jhaveri, 2012; Haadjizadeh, Narayanan, & Waldren, 2001; Zhang, Brodie, Daae, Erbas, & Duncan, 2013), and both are estimated to have achieved more than 10 MMSTB of incremental oil from WAG injection. Ula is expected to have incremental recovery from WAG of 8 % of STOOIP or nearly 100 MMSTB at the end of field life, but could increase to up to 15 % of STOOIP if more gas becomes available. The most successful immiscible WAG injection in the North Sea may be in the Brent formation of the Statfjord field. Following a successful WAG pilot to target attic oil initiated in 1997, WAG was implemented in the entire Brent formation and already by 2002 the incremental oil was estimated to 22 MMSTB (Crogh, Eide, & Morterud, 2002). Now, more than 10 years later, it is safe to assume that the incremental oil is substantially increased, even if no public estimation of incremental oil can be found.

The typical motivation for WAG methods in the North Sea has been disposal of excess and stranded gas. WAG injection enables higher flexibility and reduces the need for expensive gas export solutions in smaller fields and satellites. This is an additional benefit to increased oil recovery. A well-known problem for gas injection is the existence of high permeability streaks and thief zones, which can severely reduce the efficiency of a WAG process. Due to the difficulty of predicting the presence of these zones the efficiency of WAG can vary not only from field to field, but from well-pair to well-pair. This has been seen in several North Sea applications, where WAG injection as a whole has been considered a success, but certain well-pairs were forced to be excluded from the gas injection cycle. Examples are Snorre (Slotte & Stenmark, 1996), Gullfaks (Instefjord & Todnem, 2002) and Brage (Lien, Lie, Fjellbirkeland, & Larsen, 1998). Snorre experienced gas breakthrough in one well within a month, while the other producers did not see an increase in GOR for almost two years. Gullfaks had WAG injection success in the pilot and fault block I5, while the WAG injection in fault block H2 was not particularly effective. Brage applied WAG injection in 6 wells, but the pilot well had to be left out of the cycle due to a thief zone.

3 Model Background

3.1 Original Model

The model applied in this thesis is largely created fit for purpose. However, some of the petrophysical properties are from a model of the Gullfaks satellite Rimfaks, created by Statoil and provided to NTNU through a joint project. The Rimfaks reservoir is in the Statfjord formation located about 18 km south-west of the Gullfaks A platform (Knudsen, 1999). A typical stratigraphic log of the reservoir is shown in Figure 3-1. The top reservoir consists of Nansen, Eiriksson 2-A and Eiriksson 2-B and is a marginal marine fluvial deposit with good reservoir qualities and permeabilities in the Darcy range, approximately 120 m thick. The deeper Eiriksson-1 unit is not of the same quality as the upper section, but still has good continuity and moderate reservoir qualities. The bottom Raude section has reduced N/G ratio and continuity and poor reservoir qualities.

The reservoir contains a 100 m gross oil column with a 200 m gross thickness gas cap on top. The top of reservoir is at 2775 m depth, with the GOC at 2975 m and OWC at 3080 m. The initial reservoir pressure is 426 bara at GOC. STOOIP is 12.4 MSm^3 and 2.0 MSm^3 of condensate, of which 93 % is in the Nansen and Eiriksson units. The field also contains 6.8 GSm^3 of gas, including both free and solution gas.

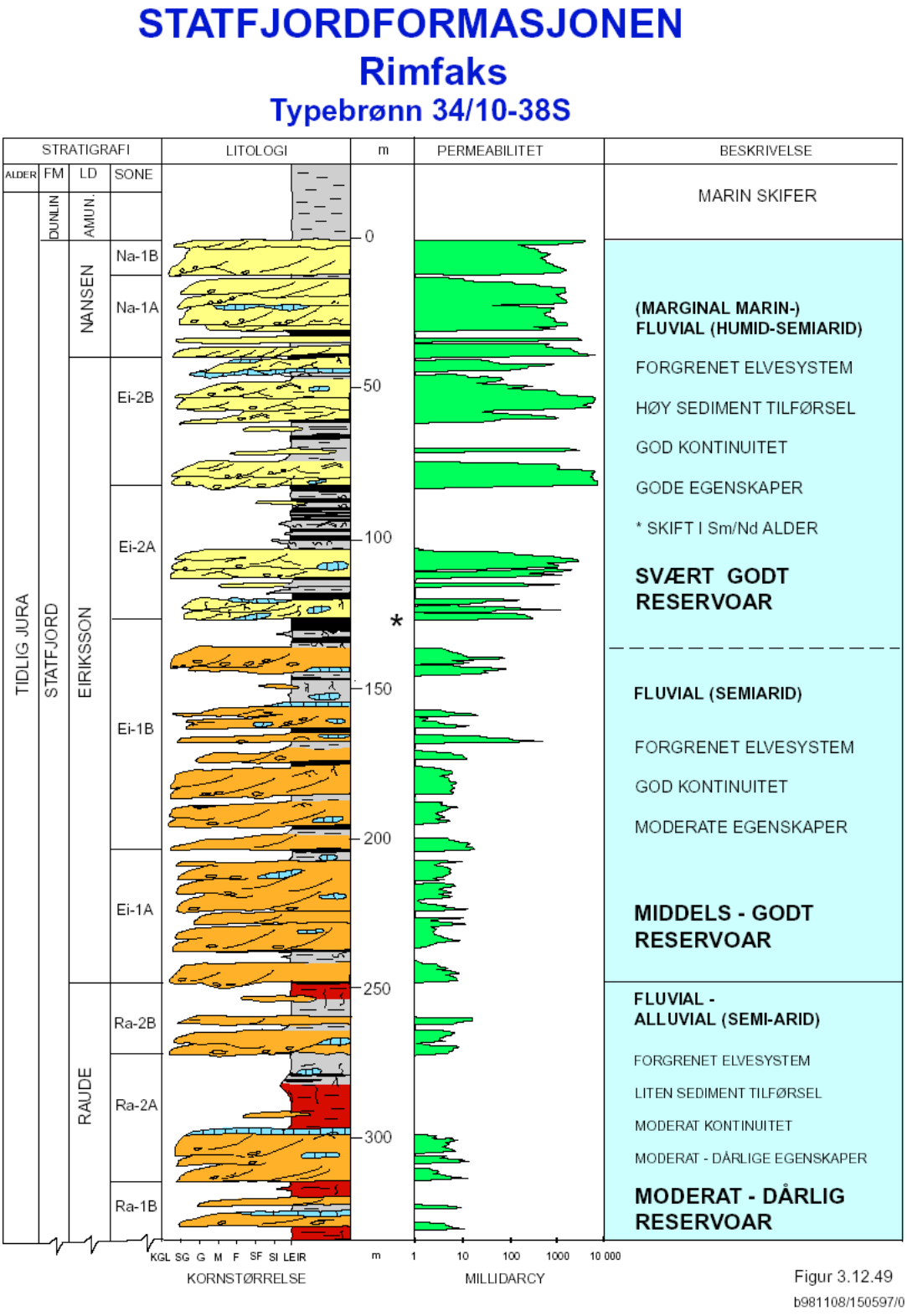

Figure 3-1 – Stratigraphic log from Rimfaks reservoir (Statoil, 2005)

3.1.1 Grid Modification

The model grid is 45x75x26 with a total of 44 905 active cells. The Nansen unit is represented by 5 layers, Eiriksson by 15 layers and Raude by the bottom 6 layers. As opposed to other reservoirs in the area, Rimfaks is not heavily faulted, with only a few major faults and no isolated compartments. The original model is shown in Figure 3-2, displaying PERMX and cells with k_x > 1000 mD are blue. The cell dimensions are typical for a reservoir model, with DX and DY mostly between 40 m and 50 m and DZ generally between 10 and 20 m. The spread in DZ is more notable with some layers as thin as 2 m, while others are more than 30 m thick. This is too thick for the purpose of this study and hence the grid requires some refinement. In addition, the reservoir volume and area is too large for the simple two well setup used in this study.

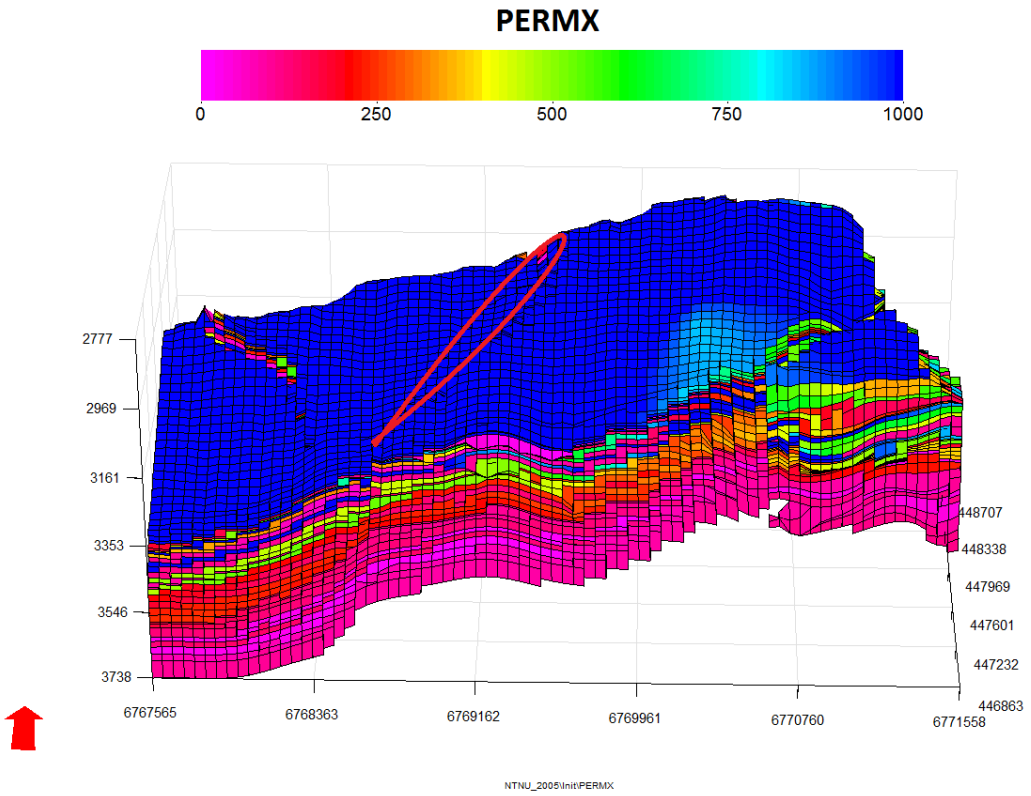

Figure 3-2 – Original Rimfaks model displaying permeability in X-direction capped at 1000 mD. A major center fault is illustrated by the red circle.

The first step of modification is to cut the reservoir in half and remove the left hand side of the fault illustrated in Figure 3-2, by deactivating grid cells with Y<39. This makes the new total size of the model 45x37x26. While the grid cells' X and Y dimensions are acceptable, the large DZ in some of the layers are not appropriate for accurate modelling of the WAG

injection process. Application of local grid refinement in Eclipse is not a practical solution in a field wide refinement, and the corner point grid geometry and large variation in DZ make layer splitting a tedious and cumbersome process if the layers are to have consistent thickness.

The solution to the problem is to construct a new grid entirely and populate it with the petrophysical properties from the Rimfaks model. The new model will not bear much resemblance to the original model in terms of shape and size, but the permeability, porosity and N/G characteristics of the Rimfaks model remains. This provides a more realistic heterogeneity, rather than creating layers of constant permeability, porosity and N/G ratio.

The new grid has DX and DY of 40 m and a dip of 7.2 degrees. It is built with three different layer thicknesses, DZ of 4 m, 2 m and 1 m, to enable a sensitivity study of the importance of layer thickness. The models with a layer thickness of 2 m and 1 m have repeated layers in order to keep reservoir volume consistent with the 4 m layer thickness model. The model with 4 m layer thickness has 26 layers, while the 2 m and 1 m layer thickness models have 52 and 104 layers respectively. The new grid with DZ of 4 m is shown in Figure 3-3. To reduce the runtime and volume the cells to the right of the red line is deactivated. These cells are barely reached by the gas and water injected and marginally impacts the simulation. In addition the cells between X= 41 and X=45 are deactivated. Most of these cells are already inactive and the affected cells are in the low quality Raude unit, behind the producer. The dimension of the model is reduced to 40x28 cells in the XY-plane.

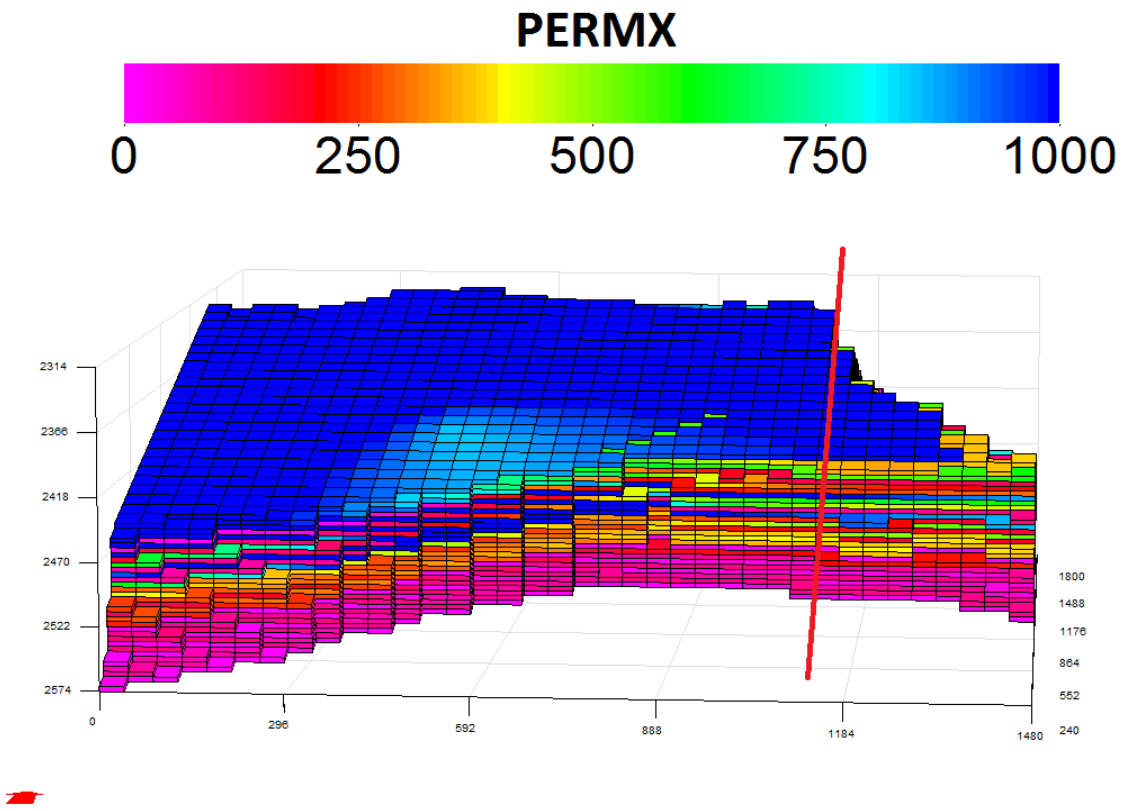

Figure 3-3 – Modified Rimfaks model displaying permeability in X-direction capped at 1000 mD. The right hand side of the grid is later deactivated.

3.1.2 PVT Data Modification

The Pressure-Volume-Temperature (PVT) data from Rimfaks defines a light oil with API gravity of 38.5. The model contains both live oil and wet gas. No metadata about the creation or origin of the PVT data is available, making validation of the data difficult. Sørbel (2014) created a PVT data set of a typical light Brent crude oil from correlations at 90 °C. The oil and gas of the Rimfaks model have remarkable similarities with the input data used by Sørbel (2014). They have API oil gravity of 38 and 38.5, the same gas specific gravity of 0.72 and reservoir temperatures of 96 °C in the Rimfaks data and 90 °C in Sørbel's data. Sørbel created his data set in the following manner: He applied correlations from Glasø (1980) to calculate solution gas-oil ratio and formation volume factors at bubblepoints ranging from 50 to 300 bara (725 to 4352 psia). Glasø used fluids from North Sea reservoirs with API gravity mostly between 33 and 38, thus the correlations should give reasonable results. To calculate oil FVF and viscosity for undersaturated oil the correlations of Vazquez & Beggs (1980) was used. The procedure for calculating viscosity is; dead oil viscosity from Beggs & Robinson (1975), bubblepoint viscosity from Chew & Connally (1959) and undersaturated oil

viscosity from Vazquez & Beggs (1980). For gas properties Sørbel applied the correlation for pseudocritical properties developed by Sutton (1985), then the Hall & Yarborough (1977) representation of the Z-factor chart presented by Standing & Katz (1942) to calculate Z-factors and corresponding gas densities. Gas viscosity was calculated with the correlation presented by Lee, Gonzalez & Eakin (1966). Note that an error was found in the oil FVF calculation of Sørbel (2014), giving reduced values. This comparison is with the corrected data.

Although Sørbel's data set only includes dry gas and live oil while the Rimfaks PVT data includes live oil and vaporized oil in the gas phase, a comparison of gas properties can be made by only looking at Rimfaks data with no vaporized oil in the gas. Figure 3-4 shows the oil FVF vs pressure for both data sets. The range of Sørbel's data is considerably smaller, but it is clear that the differences are not large in the relevant pressure region of 200-400 bar. Sørbel's data set is able to hold about 10 % more solution gas at bubblepoint, causing the faster growth of FVF at bubblepoint as pressure increases.

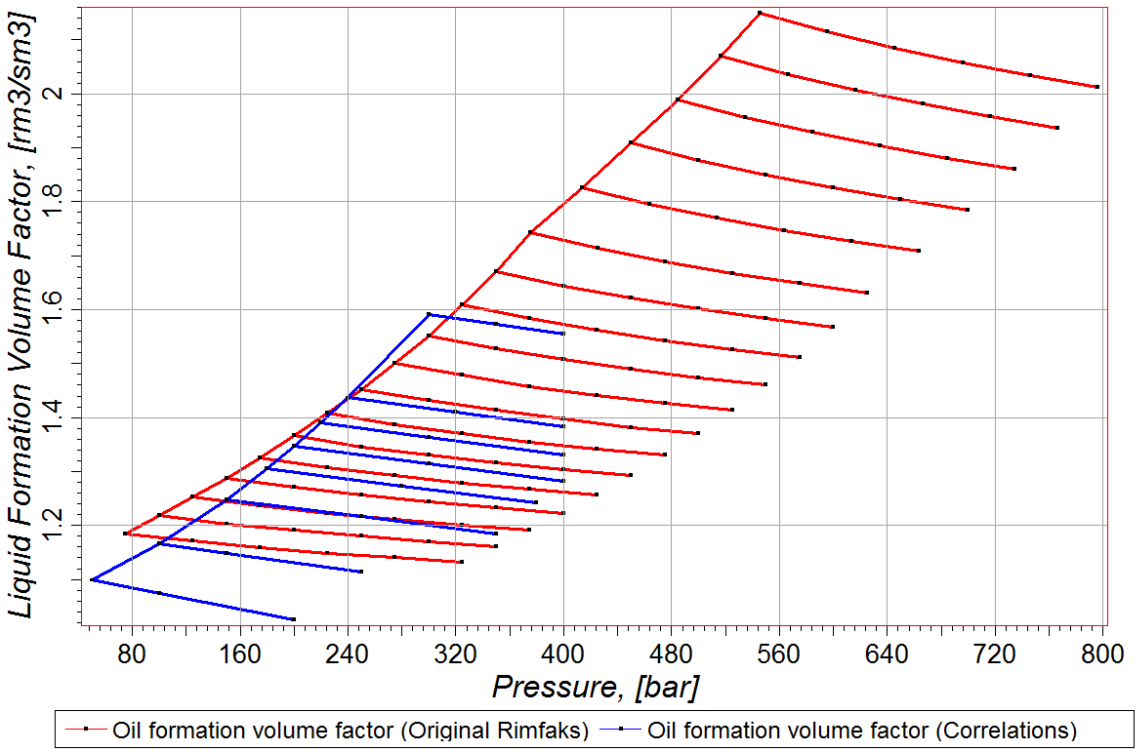

Figure 3-4 – Comparison of oil FVF vs pressure for the original Rimfaks data and (Sørbel, 2014).

Viscosity data shown in Figure 3-5 is also quite coherent. The Rimfaks oil viscosity is consistently slightly lower than Sørbel's data, but always within 20 %. All in all the oil PVT data of the Rimfaks model is close to and similar of PVT data created by correlations using similar oil.

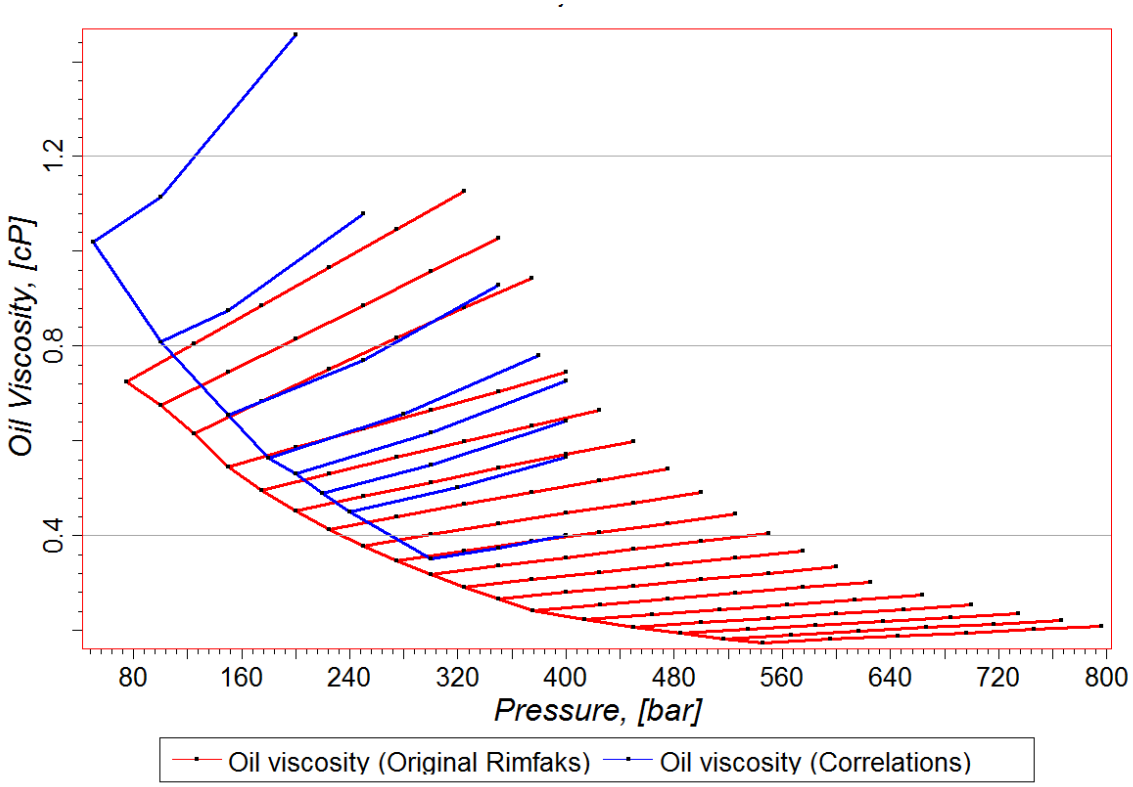

Figure 3-5 – Comparison of oil viscosity vs pressure for the original Rimfaks data and (Sørbel, 2014).

The gas formation volume factor and gas viscosity of dry gas from the original Rimfaks data and Sørbel is shown in Figure 3-6. While the gas viscosity correlates very well over the entire range, the difference in gas formation volume factor is larger than it appears in Figure 3-6. Calculating the Z-factors for the Rimfaks data and comparing with the Standing-Katz diagram, they follow a curve of pseudo reduced temperature of about 2.2. The pseudo reduced temperature in Sørbel's data set is 1.71. Since the temperature of the reservoirs is very close, the critical temperature of the gas mix must be the difference maker. Even if the difference is significant it does in no way fall outside realistic range. It should also be noted that laboratory work is the likely background for the Rimfaks data while Sørbel (2014) used correlations. Thus it can be safely assumed that the Rimfaks data are realistic and will be used without modification in the WAG simulations.

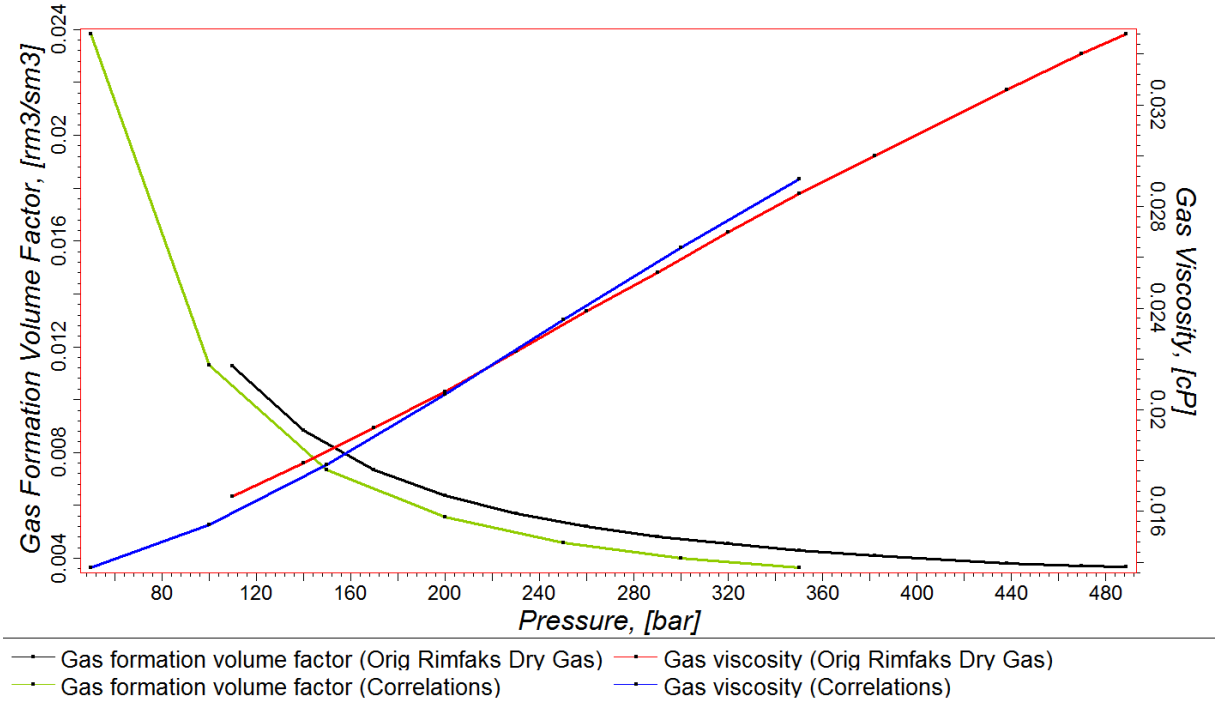

Figure 3-6 – Comparison of gas formation volume factor and gas viscosity vs pressure for the original Rimfaks data and (Sørbel, 2014).

3.1.3 Equilibrium Modification

The original model contains a gas cap above a layer of oil, but a WAG injection scheme is usually not applicable in such an environment. With the grid modifications described in 3.1.1, the depth and vertical and lateral extension of the grid has changed. The GOC is set above top of the reservoir, which indicates no initial free gas. The OWC is set at 2450 m, which is at the top of the structure down-dip, seen in Figure 3-7. The datum depth is at the OWC, where the pressure is 250 bara. The solution gas in saturated oil at 250 bara is 137.5 Sm^3/Sm^3. The initial oil will have Rs of 100 Sm^3/Sm^3 at the top of the structure (2317 m) and decline linearly to 90 Sm^3/Sm^3 at the OWC. Figure 3-7 shows the initial oil saturation. The total pore volume is 10.92 million m^3 and the base case STOOIP is 5.42 MSm^3. The total injected volume at the end of simulation is 10.95 MRm^3 or about 1 PV.

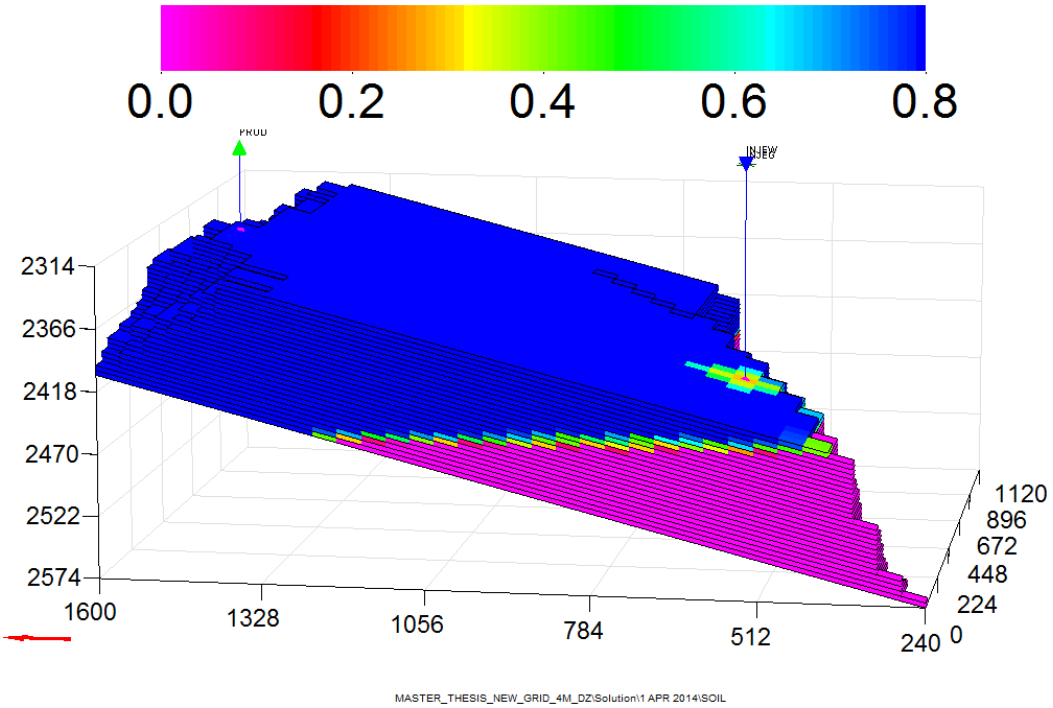

Figure 3-7 – Initial oil saturation in the model

3.1.4 Relative Permeability Modification

The original Rimfaks model had 8 sets of imbibition and drainage relative permeability curves. These were split into two different lateral sets, one south (left side in Figure 3-2) of the fault indicated in Figure 3-2 and one north (right side in the figure) of the fault. Since the south side of the fault has been removed from the model used in this study, the relative permeability curves from this area are ignored. The remaining four sets are; the top Nansen unit, the Eiriksson 2 unit, Eiriksson 1b unit and Eiriksson 1a and Raude combined. All sets are created using the power equations, commonly called Corey equations, given by Lake (1989, p. 61)

$$k_{rw} = k_{rw,max} * \left[\frac{S_w - S_{wc}}{1 - S_{wc} - S_{orw}}\right]^{n_w} \quad 3.1$$

$$k_{ro} = k_{row,max} * \left[\frac{1 - S_w - S_{orw}}{1 - S_{wc} - S_{orw}}\right]^{n_o} \quad 3.2$$

where $k_{rw,max}$ and $k_{ro,max}$ are end point water and oil relative permeabilities, S_w is water saturation, S_{wc} is connate water saturation and S_{orw} is residual oil saturation when only oil

and water is present. Water and oil has no separation on imbibition and drainage as they are the wetting phases, while gas relative permeability is calculated in a similar manner using

$$k_{rg}^{drainage} = k_{rg,max}\left[\frac{S_g - S_{gc}}{1 - S_{gc} - S_{wc} - S_{org}}\right]^{n_g} \quad 3.3$$

$$k_{rg}^{imbibition} = k_{rg,max}\left[\frac{S_g - S_{go}}{1 - S_{go} - S_{wc} - S_{org}}\right]^{n_g} \quad 3.4$$

where S_{gc} is the critical gas saturation, S_{go} is the maximum trapped gas saturation, S_{org} is the residual oil saturation to gas, n_g is an empirical constant for the gas curvature and the remaining are the same as before. The endpoints used for each relative permeability set is given in Table 3-1 and the empirical power terms n_w, n_o and n_g is 2, 3 and 1.6 respectively.

Table 3-1 – Original endpoints used in the relative permeability sets in Rimfaks. S_{gc} is critical gas saturation and S_{go} is maximum trapped gas saturation.

Unit	S_{wc}	S_{orw}	S_{org}	S_{gc}	S_{go}
Nansen	0.10	0.20	0.14	0.02	0.3
Eiriksson 2	0.12	0.20	0.14	0.02	0.3
Eiriksson 1b	0.20	0.25	0.28	0.05	0.3
Eiriksson 1a + Raude	0.20	0.25	0.28	0.05	0.3

Without access to the data behind these numbers, it is difficult to assess their validity. A quick comparison with available research can be used to consider the consistency of the data. Goda & Behrenbruch (2004) proposed a wettability matrix based on data from the Bonaparte basin offshore northwestern Australia, shown in Table 3-2. Based on this data the Rimfaks reservoir would be in the slightly oil wet category.

Table 3-2 – Wettability matrix from Bonaparte basin data (Goda & Behrenbruch, 2004)

Wetting Conditions	n_o	n_w
Oil Wet	6 - 8	2 – 3
Slightly Oil Wet	2 - 6	2 - 4

Slightly Water Wet	2 - 6	4 - 6
Water Wet	2 - 4	6 - 8

The connate water saturation is increasing with decreasing reservoir quality, which is typical as the pores get smaller and capillary pressure effects increase. Skauge & Sorbie (2014) presented core scale residual oil data from 11 different reservoirs. These showed residual oil to gas is typically lower than residual oil to water, but in some instances the opposite also applies. In the Rimfaks model, the Nansen and Eiriksson 2 units have lower S_{org} than S_{orw}, while the Eiriksson 1 and Raude units have higher S_{org} than S_{orw}. The data of Skauge & Sorbie (2014) also showed the three-phase residual oil saturation, S_{om}, was lower than both S_{orw} and S_{org} for all 11 reservoirs. Since the model will have no initial free gas and gas is not introduced until WAG injection starts, S_{org} is the equivalent of S_{om} in this simulation. To honor that three-phase residual oil saturation is lower than S_{orw}, an adjustment in S_{org} will be made in Eiriksson 1 and Raude, decreasing S_{org} to 0.2 from the original 0.28.

In the Rimfaks model the water relative permeability at residual oil saturation, $k_{rw,max}$, is 0.4, while $k_{ro,max}$ and $k_{rg,max}$ are both 1. When a water-wet reservoir is waterflooded the oil typically occupies the large pores. First water saturation increases in the smaller pores, then the larger pores previously occupied by oil. Pores containing oil can be cut off from the rest of the oil and become trapped in the large pores. As a result of trapped oil in the large pores, the maximum water relative permeability at residual oil saturation can be quite low, often around 0.25. In a mixed-wet reservoir, like the Rimfaks reservoir, the larger pores are usually oil-wet, while the smaller pores are water-wet. When water saturation increases water invades the larger pores first and stays in the middle of the pore (Abdallah, et al., 2007). The result is a continuous oil phase and less trapped oil, so $k_{rw,max}$ is larger than in the water-wet case, often 0.4 to 0.5. Treiber & Owens (1972) found in most of the reservoirs they tested the available relative permeability data matched the contact angle measured, thus being strongly correlated to the wettability. A $k_{rw,max}$ of 0.4 is in other words consistent with the assumed wettability in the Rimfaks reservoir.

Since gas is not introduced in the reservoir until most of it has been contacted by water, the water saturation will mainly be higher than the connate water saturation wherever gas

flows. As discussed in 2.2.3, gas relative permeability has been reported to be reduced in three-phase zones. To account for this $k_{rg,max}$ has been reduced to 0.5.

The critical gas saturation, S_{gc}, is the minimum required saturation for a gas to be mobile. Donnez (2007, p. 244) reported that a critical gas saturation of 5 % is a good starting point and Cosentino (2001, p. 183) reported the range to be from 2 to 10 %. A critical gas saturation of 2 % in Nansen and Eiriksson 2 and 5 % in Eiriksson 1 and Raude is reasonable and within the normal range.

The trapped gas saturation is an important parameter in gas reservoirs with aquifers or in WAG flooding. It is dependent on rock type and saturation history. The simplest correlation for the relationship between gas saturation history and trapped gas saturation, S_{go}, was presented by Naar & Henderson (1961) where S_{go} is half of the initial saturation, S_{gi}. Although reasonably accurate for many reservoirs, Keelan & Pugh (1975) showed that for two carbonate reservoirs with Sgi=0.8 the trapped gas saturation varied from 0.23 to 0.69. Land (1968) introduced a relationship between the initial nonwetting saturation and the trapped nonwetting saturation given in Eq. 3.5. This relationship is still in use today in many reservoir simulations.

$$C = \frac{1}{S_{nwr}} - \frac{1}{S_{nwi}} \qquad 3.5$$

The maximum trapped gas saturation in the Rimfaks field is set to 0.3 for all units. The maximum initial gas saturation ranges from 0.7 in the Nansen unit to 0.55 in Eiriksson and Raude. Hamon, Suzanne, Billiotte & Trocme (2001) found in sandstones with porosity above 14 % the trend is S_{go} between 25-35% from more than 300 samples. >90 % of the grid cells have porosity above 14 % and of the remaining cells, none are below 12 % porosity. S_{go} of 0.3 is as such a reasonable value. Land's constant is not used in the two-phase hysteresis model, but the S_{go} of 0.3 is equivalent to a Land's constant around 2.2 for all units.

In order to assure consistency, the relative permeability sets are recreated, even the oil-water sets where no changes have been made. The Eiriksson 1b and Eiriksson 1a+Raude sets are combined into 1 set, since they are identical. This result in three relative permeability

sets and the endpoints are shown in Table 3-3. Relative permeability tables and graphs are attached in Appendix A.

Table 3-3 – Endpoints used in the new relative permeability sets.

Unit	S_{wc}	S_{orw}	S_{org}	S_{gc}	S_{go}
Nansen	0.10	0.20	0.14	0.02	0.3
Eiriksson 2	0.12	0.20	0.14	0.02	0.3
Eiriksson 1 + Raude	0.20	0.25	0.20	0.05	0.3

3.1.5 Implementation of WAGHYSTR Keyword

The presence of trapped gas affects the gas and water relative permeability. This effect is extensively discussed in 2.2.3. To explore the importance of reduced gas and water permeability and more clearly defined trapped gas saturation, the WAGHYSTR keyword is implemented in the Eclipse simulation. Land's constant is defined so the maximum trapped gas saturation is 0.3 in every unit. The maximum reduction in gas and water relative permeability is set to a factor of 0.5, similar to what is used by Larsen & Skauge (1999). Reduction of residual oil related to trapped gas is not implemented, for reasons explained in 2.2.4, but the residual oil to gas is somewhat lower than residual oil to water and similar to the two-phase hysteresis case.

3.1.6 Well Placement

The base case features a vertical oil producer up-dip placed in cell stack (X,Y)=(37,12). Gas injection in a vertical injector will mainly inject in the top half of the reservoir, due to the pressure gradient difference between the gas column in the well and the oil/water column in the reservoir. To accommodate gas injection in every reservoir layer the injector is placed horizontally along the OWC, penetrating every layer in the model by cutting diagonally across the model. At the heel the distance between the injector and the producer is just over 1 km, while at the toe the distance is 540 m. The toe is in the poorer reservoir quality units Eiriksson 1 and Raude, so gas and water breaks through in Nansen and Eiriksson 2 first. Figure 3-8 shows the placement of the wells. The injector's heel is in the bottom left corner of the grid.

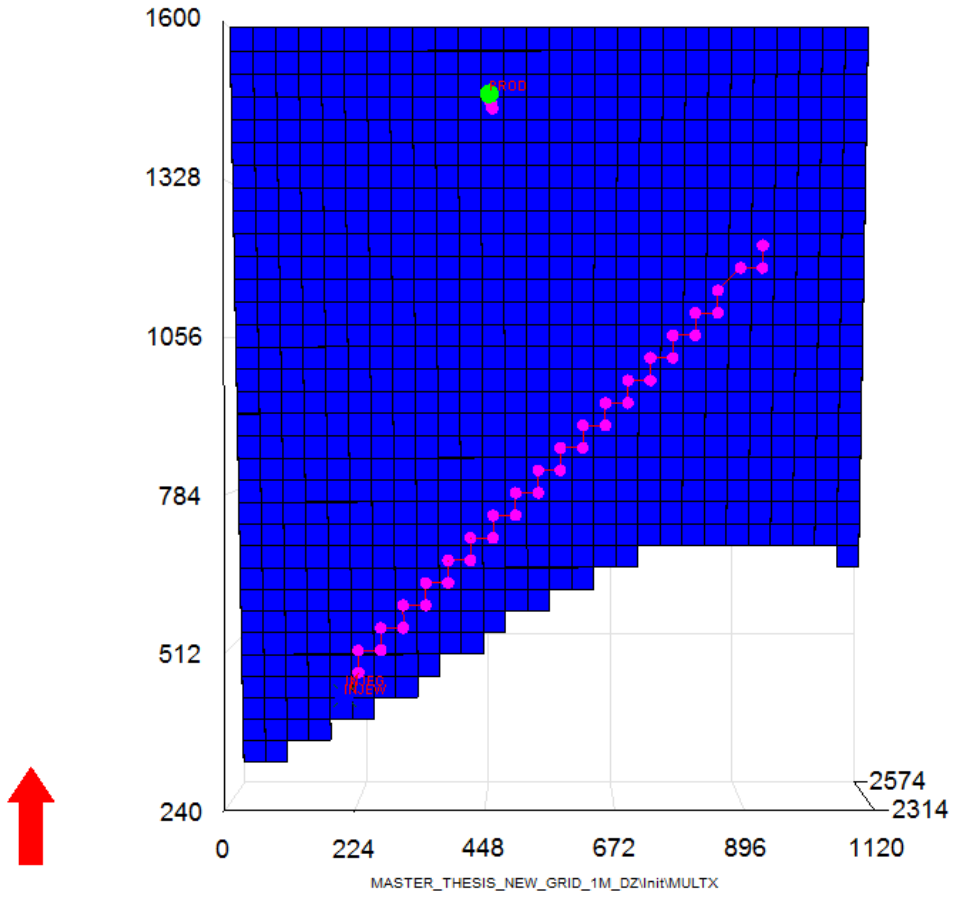

Figure 3-8 – Overview of the well placement. The producer is the vertical well, while the injector is the horizontal diagonally crossing well.

4 Simulation Setup

4.1 Base Case Description

Two cases are considered the base cases; one base case injecting only water (termed Water base case) and the WAG base case. Both base cases feature gas relative permeability hysteresis, 1 m DZ cells and the well placement given in 3.1.6. The base line production rate is 1500 Sm^3/day oil rate, controlled by BHP to keep reservoir pressure stable. Injection is controlled by reservoir volume. The total simulation time is 15 years and the total injection volume is very close to 1 PV. The WAG simulation is not as stable as the water base case and requires shorter time steps and some tuning tweaks. In order to keep these effects on the simulation to a minimum, the water base case will utilize the same tuning parameters.

4.2 WAG Schedule Creation

The reservoir is waterflooded for the first four years. At this point the water cut is 40 % in the base case, but this is different for each case. At this point a three month gas injection period is initiated. The injected reservoir volume is increased from 2000 Rm^3/d in the water injection phase to 2500 Rm^3/d. This is to keep the reservoir pressure and production stable as some of the gas will go into solution in the oil. The cycle time is 6 months, i.e. 3 months of gas injection followed by 3 months of water injection. The WAG cycle will be partially tapered as the gas breaks through faster and in larger volumes for each cycle. The first two cycles are similar and are followed by two cycles of 6 months with injection rate at 2000 Rm^3/d for both gas and water phase. Finally there are two cycles with two months of gas injection and 4 months of water injection. The overall water/gas ratio is 1.15, but the last half cycle can be counted as a part of the final waterflood. If so the WAG ratio is 0.91. The WAG period is followed by 8 years of waterflooding.

Optimization of the WAG flood is important to reach the maximum potential. However, this is a long and cumbersome process and not within the scope of this study. The WAG flood would also need individual optimization for each setup described in 4.4. Consequently the same WAG schedule is used for every case.

4.3 Parameter Sensitivities

A number of sensitivities will be run to determine their effect on the simulation. These are mainly focused on simulation parameters that only affect simulation results, but cannot be changed in the field, such as cell thickness and relative permeability hysteresis. Production rate has also been tested.

4.3.1 Relative Permeability Hysteresis Sensitivity

The WAG base case was originally intended to include the WAG hysteresis option, but the gas element created significant convergence issues and increased run time tenfold. The results did not differ enough from the two-phase hysteresis case to justify the increased run time. Results are reported in 5.3.1.

WAG injection is also run without relative permeability hysteresis on the gas phase, applying only the drainage curve. Since less gas will be trapped in the reservoir, the gas production and significance of the gas breakthrough is expected to increase.

4.3.2 Layer Thickness Sensitivity

The grid has been created with cell thickness of 4 m and 2 m in addition to the base case 1 m, as described in 3.1.1. This enables sensitivity runs, determining the effect of cell thickness. Results are reported in 5.3.2.

4.3.3 Oil Vaporization Sensitivity

The PVT data specifies a wet gas, i.e. when dry gas is injected it has the ability to vaporize part of the oil. If the gas contacts all of the oil, the residual oil saturation would theoretically drop to zero given enough throughput of gas. However the gas will not contact all the oil as it will only flow in a fraction of the pores. Eclipse includes a function to inhibit oil vaporization given in Eq. 4.1 (Schlumberger, 2011)

$$R_v = R_{v\,sat}\left(\frac{S_o}{S_{o\,max}}\right)^{vap1} \qquad 4.1$$

where R_v is the vaporized oil, $R_{v\ sat}$ is the vaporized oil of a saturated gas, S_o is the oil saturation of a cell, $S_{o\ max}$ is the largest oil saturation in the grid block so far and vap1 is the vaporization control parameter. The lower the oil saturation, the more oil vaporization is inhibited. The WAG base case has a vap1 constant of 2. The high case is a vap1 constant of 3

and the low case a constant of 0.5. Large values of this constant may cause convergence issues in the simulation and is not recommended. Results are reported in 5.3.3.

4.3.4 Production Rate Sensitivity

The base case applies a reservoir volume rate of 2000 Rm^3/day, which equates to 1500 Sm^3/day of oil with no water or free gas is in the production stream. A change in production rate will affect the ability of gas and water to migrate vertically and can affect the flow paths and sweep efficiency of in the reservoir. A low case will produce at 1500 Rm^3/day, while the high case will produce at 2500 Rm^3/day. It should be noted that this model operates without calculation of THP and the actual ability of the wells to deliver at such rates in reality has not been considered. Results are reported in 5.3.4.

4.3.5 Vertical Permeability Sensitivity

The base cases have a vertical permeability of 0.01 of the horizontal permeability. The WAG and water base cases are also run with vertical permeability of 0.1 and 0.05 of the horizontal permeability. Results are reported in 5.3.5.

4.4 Description of Simulation Setup

Because of the density difference between gas and liquid, the gas will migrate to the top of the reservoir. The amount of the injected gas that actually reaches the top of the reservoir depends on the vertical permeability and the relative location of the most permeable beds, among other factors. A very permeable bed directly beneath a vertical flow barrier can cause premature gas breakthrough, significant enough to effectively strangle the effect of WAG injection. Since the most permeable Nansen unit is on top of the reservoir in Rimfaks, the stratification of the reservoir is not ideal for a WAG process. This study will investigate the importance of the heterogeneity sequence by relocating the layers. The cases will not be directly comparable with each other as they will shuffle in-place volumes between different quality reservoirs, but they will be comparable to the pure waterflooding case under the same conditions.

Table 4-1 shows the average permeability in the X-direction for the 26 layers originally in the model. For the case with 1 m cell thickness, each layer has been split into four layers with exactly the same permeability, porosity and N/G ratio.

Table 4-1 – Overview of the average permeability in X-direction in the reservoir model

Unit	Layer	Average kx [mD]
Nansen	1	1271
	2	1039
	3	903
	4	187
	5	507
Eiriksson 2	6	144
	7	869
	8	456
	9	809
	10	106
	11	744
	12	154
	13	413
Eiriksson 1	14	345
	15	277
	16	298
	17	263
	18	20
	19	204
	20	113
Raude	21	28
	22	118
	23	30
	24	85
	25	102
	26	14

Five different setups are run in addition to the base case and each setup is run with both pure water injection and WAG injection. No adjustments are made to the injection schedule for each case and the WAG process will naturally not reach its potential. The well placement will not be adjusted. The setups are described below in 4.4.1 to 4.4.5.

4.4.1 Nansen and Eiriksson 2 switch

The top three layers in Nansen have Darcy-range permeability and gas able to migrate to these layers will break through rapidly. By placing the Nansen unit beneath the Eiriksson 2 unit, this gas can continue the migration into Eiriksson 2. The expected effect is slightly

slower GOR evolution, but Eiriksson 2 contains some very permeable layers and the overall effect may not be significant.

Table 4-2 – Layer ordering for the Nansen and Eiriksson 2 switch

Original Unit	Original Layer	Average kx [mD]
Eiriksson 2	6	144
	7	869
	8	456
	9	809
	10	106
	11	744
	12	154
	13	413
Nansen	1	1271
	2	1039
	3	903
	4	187
	5	507
Eiriksson 1	14	345
	15	277
	16	298
	17	263
	18	20
	19	204
	20	113
Raude	21	28
	22	118
	23	30
	24	85
	25	102
	26	14

4.4.2 Downwards fining sequence

A downwards fining sequence, i.e. where reservoir quality is decreasing deeper in the reservoir, would be considered the least favoring for WAG injection. When all layers are perforated, as in this study, most of the gas will be injected in the top layers and additionally it can easily migrate to the top of the reservoir. Gas breakthrough is expected to be fast and GOR evolution rapid. Since the reservoir is waterflooded both before and after the WAG

period, the overall recovery is not expected to be lower than waterflooding. The layers are sorted by permeability with the most permeable layer on top. The entire Raude unit is kept intact at the bottom.

Table 4-3 – Layer ordering for the downwards fining sequence

Original Unit	Original Layer	Average kx [mD]
Nansen	1	1271
Nansen	2	1039
Nansen	3	903
Eiriksson 2	7	869
Eiriksson 2	9	809
Eiriksson 2	11	744
Nansen	5	507
Eiriksson 2	8	456
Eiriksson 2	13	413
Eiriksson 1	14	345
Eiriksson 1	16	298
Eiriksson 1	15	277
Eiriksson 1	17	263
Eiriksson 1	19	204
Nansen	4	187
Eiriksson 2	12	154
Eiriksson 2	6	144
Eiriksson 1	20	113
Eiriksson 2	10	106
Eiriksson 1	18	20
Raude	21	28
Raude	22	118
Raude	23	30
Raude	24	85
Raude	25	102
Raude	26	14

4.4.3 Upwards Fining Sequence

In an upwards fining sequence the water can be expected to breakthrough faster than in the base case. There are two main reasons for this expectation. The water will segregate down to the most permeable units and with the current well trajectory of the injector, the distance between injector and producer in the highly permeable layer is reduced. Gas is expected to reach and sweep large parts of the reservoir not properly contacted by the water. Due to the

bad reservoir quality of the Raude unit, the Raude unit and layer 18 is placed on the bottom. From the bottom the remaining layers are sorted by permeability and the most permeable layer is placed as layer 19.

Table 4-4 – Layer ordering for the upwards fining sequence

Original Unit	Original Layer	Average kx [mD]
Eiriksson 2	10	106
Eiriksson 1	20	113
Eiriksson 2	6	144
Eiriksson 2	12	154
Nansen	4	187
Eiriksson 1	19	204
Eiriksson 1	17	263
Eiriksson 1	15	277
Eiriksson 1	16	298
Eiriksson 1	14	345
Eiriksson 2	13	413
Eiriksson 2	8	456
Nansen	5	507
Eiriksson 2	11	744
Eiriksson 2	9	809
Eiriksson 2	7	869
Nansen	3	903
Nansen	2	1039
Nansen	1	1271
Eiriksson 1	18	20
Raude	21	28
Raude	22	118
Raude	23	30
Raude	24	85
Raude	25	102
Raude	26	14

4.4.4 Upwards Fining Sequence with Interbedded Vertical Flow Barriers

This case is similar to the case described above, but contains four “units” that are upwards fining. The layers are sorted by permeability and the four layers with highest average permeability form the base of each unit. Layer 26 remains as the base and layer 23 is not included in a unit because it is not defined over the entire area. The units are not completely

sealed off from each other, but the low permeability layer on the top of each unit act as the vertical flow barrier.

Table 4-5 – Layer ordering for the upwards fining sequence with interbedded vertical flow barriers

Original Unit	Original Layer	Average kx [mD]
Eiriksson 1	18	20
Eiriksson 2	10	106
Eiriksson 2	12	154
Eiriksson 1	15	277
Eiriksson 2	8	456
Eiriksson 2	7	869
Raude	21	28
Eiriksson 1	20	113
Nansen	4	187
Eiriksson 1	16	298
Nansen	5	507
Nansen	3	903
Raude	24	85
Raude	22	118
Eiriksson 1	19	204
Eiriksson 1	14	345
Eiriksson 2	11	744
Nansen	2	1039
Raude	25	102
Eiriksson 2	6	144
Eiriksson 1	17	263
Eiriksson 2	13	413
Eiriksson 2	9	809
Nansen	1	1271
Raude	23	30
Raude	26	14

4.4.5 Downwards Fining Sequence with Interbedded Vertical Flow Barriers

The units in the case described above are reversed putting the most permeable layers on top of each unit. WAG is expected to perform worse than the reversed case, but it is difficult to predict WAG performance compared with the case described in 4.4.2. Analysis of this run found that the gas had better vertical sweep than intended in a limited area due to unintended non-neighbor connections (NNCs) created over cells made inactive by the MINPV keyword. The deactivated cells are mostly in the original layer 18 and because of the

placement of this layer in other setups, the effect is thought to have most impact in this setup. Additional simulations with NNCs disabled are run for this setup only. See 5.4.5 for results and for 6.2.5 further discussion and analysis.

Table 4-6 – Layer ordering for the downwards fining sequence with interbedded vertical flow barriers

Original Unit	Original Layer	Average kx [mD]
Eiriksson 2	7	869
Eiriksson 2	8	456
Eiriksson 1	15	277
Eiriksson 2	12	154
Eiriksson 2	10	106
Eiriksson 1	18	20
Nansen	3	903
Nansen	5	507
Eiriksson 1	16	298
Nansen	4	187
Eiriksson 1	20	113
Raude	21	28
Nansen	2	1039
Eiriksson 2	11	744
Eiriksson 1	14	345
Eiriksson 1	19	204
Raude	22	118
Raude	24	85
Nansen	1	1271
Eiriksson 2	9	809
Eiriksson 2	13	413
Eiriksson 1	17	263
Eiriksson 2	6	144
Raude	25	102
Raude	23	30
Raude	26	14

5 Results

5.1 Results Summary

Table 5-1 and Table 5-2 shows the recovery in all cases and the incremental recovery over the corresponding water case for all WAG cases.

Table 5-1 – Result summary for sensitivy runs

Case	Recovery [%]	Inc Recovery over Water [%]
Base Case Water	60.42	-
Base Case WAG	62.67	2.25
No Hyst WAG	62.27	1.85
WAGHYSTR WAG	63.37	2.95
2M Thickness Water	60.12	-
2M Thickness WAG	62.35	2.23
4M Thickness Water	59.46	-
4M Thickness WAG	61.83	2.37
High Rate Water	61.34	-
High Rate WAG	63.90	2.56
Low Rate Water	58.92	-
Low Rate WAG	60.71	1.79
Low Oil Vap WAG	63.12	2.70
High Oil Vap WAG	62.60	2.18

Table 5-2 – Result summary for stratification cases

Case	Recovery [%]	Inc Recovery over Water [%]
Base Case Water	60.42	-
Base Case WAG	62.67	2.25
Nansen Switch Water	58.84	-

Nansen Switch WAG	60.83	1.99
Down Fining Water	59.25	-
Down Fining WAG	61.19	1.94
Up Fining Water	53.80	-
Up Fining WAG	56.23	2.43
Down Fining Vertbarr Water	57.85	-
Down Fining Vertbarr WAG	59.55	1.70
Down Fining Vertbarr Water NoNNC	57.80	-
Down Fining Vertbarr WAG NoNNC	59.49	1.69
Up Fining Vertbarr Water	54.42	-
Up Fining Vertbarr WAG	57.03	2.61

5.2 Base Cases

Waterflooding achieves quite good sweep and recovery in the reservoir. 10 years after the start of waterflooding, in 2024, the water cut has reached 90 % and the overall field recovery is 56.7 %. The final recovery in 2029 is 60.4 % and the ending water cut is 96 %. Residual oil saturations in the best swept areas are typically around 25-30 %, but oil saturations of up to 50 % is not uncommon. Figure 5-1 shows the oil saturation in the water base case in 2024. The sweep is mostly good in the permeable Nansen and Eiriksson 2 layers, but not as good in the lower quality Eiriksson 1 and Raude units. Further south, where injection is in the lower units, the sweep is not as good. Shown in Figure 5-2, the oil saturation is mostly around 40 % and in some layers up to 50 %. Since these units have less favorable petrophysical properties, most of the injected fluids will enter the formation in the higher quality Nansen and Eiriksson 2 units.

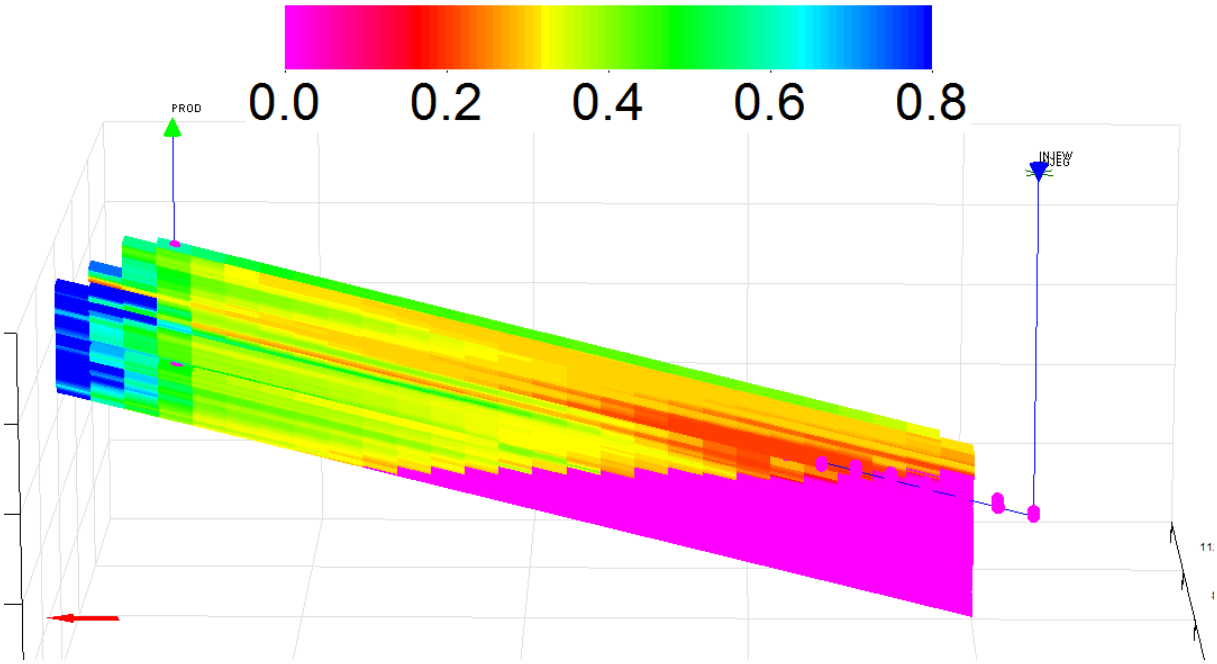

Figure 5-1 – Oil saturation of the water base case in 2024 in XZ slice with Y=12.

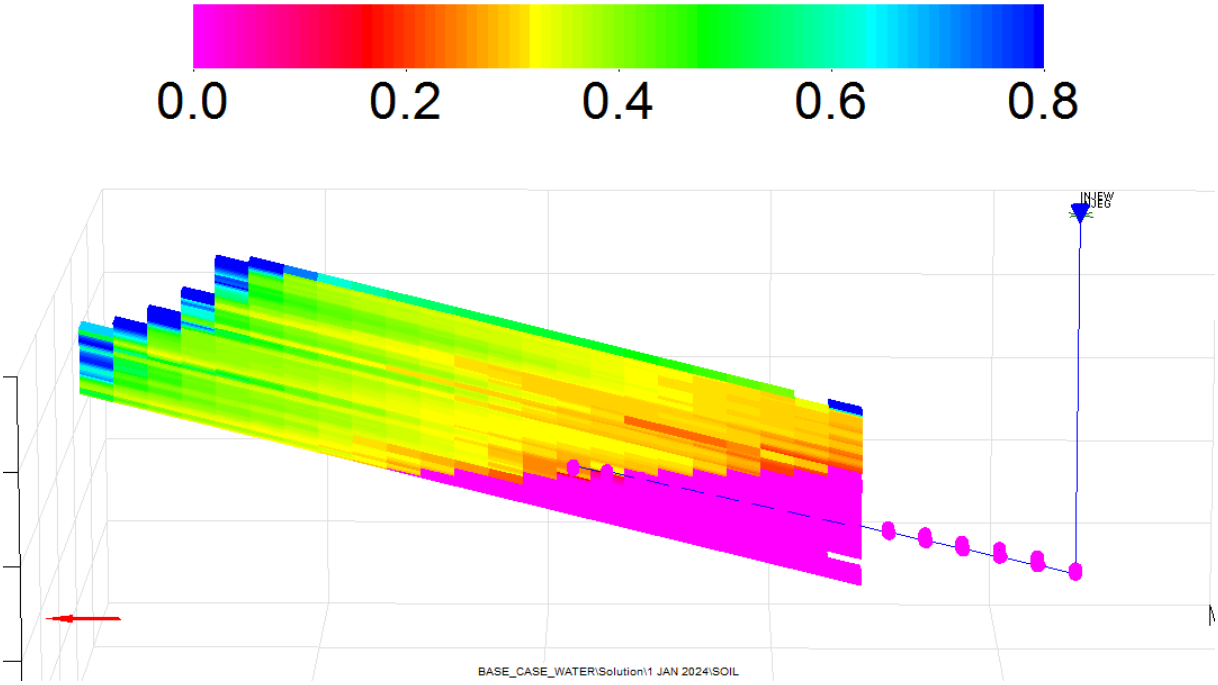

Figure 5-2 – Oil saturation of the water base case in 2024 in XZ slice with Y=20.

As seen in Figure 5-3, the final WAG oil recovery is slightly higher than the waterflood case. Most of the incremental oil is achieved after the WAG period. The producer is controlled by BHP and the presence of free gas can affect the inflow performance. That results in dropping production in this case, but in a real application the added gas would reduce the production fluid density and increase THP, allowing higher production rates. It should be noted that WAG is not expected to make a large impact on production in the base case, because the

high permeable units are on the top of the structure and most of the gas will quickly move to these layers. After 10 years of production, 1st January 2024, the oil recovery is 58.2 %, 1.5 % more than the water base case. At the end of simulation the recovery is 62.7 %, 2.3 % more than the water base case and an increase in produced oil of 3.75 %. On 1st April 2019, at the end of the 3rd WAG cycle, gas has broken through and GOR is rapidly increasing. At this time 46 % of the gas and 8 % of the oil is produced through the top layer. Clearly much of the injected gas is segregated to the top layer.

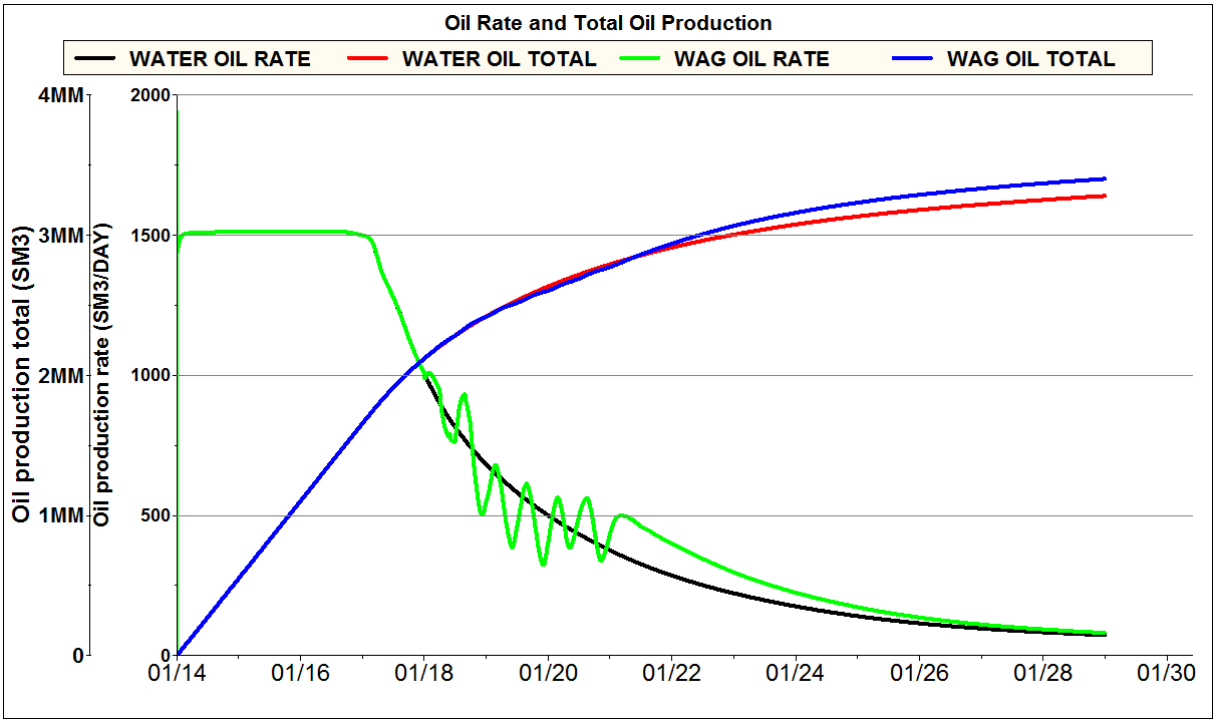

Figure 5-3 – Oil rate and total oil production in the water and WAG base cases.

5.3 Sensitivities

5.3.1 Relative Permeability Hysteresis Sensitivity

In addition to the base case, WAG has been applied without hysteresis and with the WAGHYSTR keyword as described in 3.1.5. Oil rate and total oil production is shown in Figure 5-4 and GOR is shown in Figure 5-5. When comparing the base case to the run without hysteresis, the gas production from the first and second WAG cycle is larger, while in the later cycles about the same amount of gas breaks through, but at a slower pace and over more time.

When the WAGHYSTR keyword is implemented, the simulation shows many of the same tendencies, but less gas breaks through in the early cycles and similar amounts in the later cycles. GOR also drops off faster after a gas cycle. Additional insight and discussion is offered in 6.1.1.

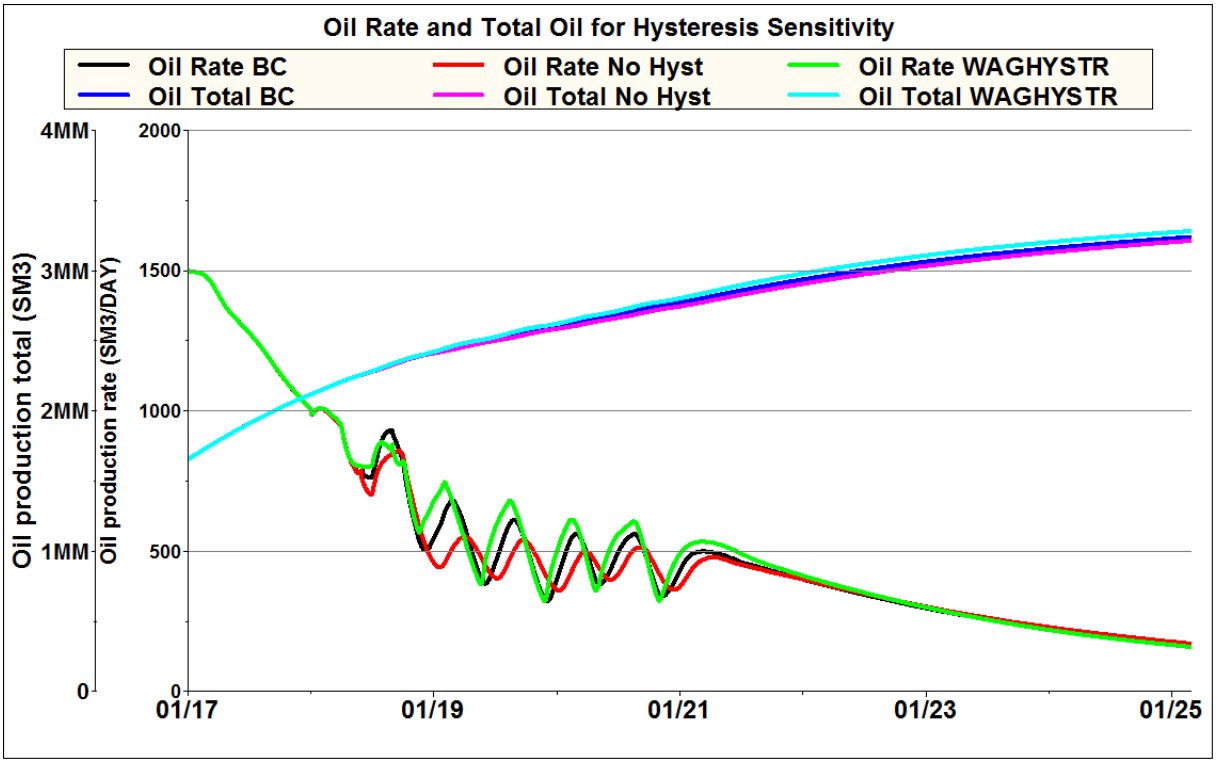

Figure 5-4 – Oil rate and total oil production for the hysteresis sensitivity. The graph only shows between 2017 and 2025, while the simulation ran from 2014 to 2029. Only waterflooding was used outside the graph's area.

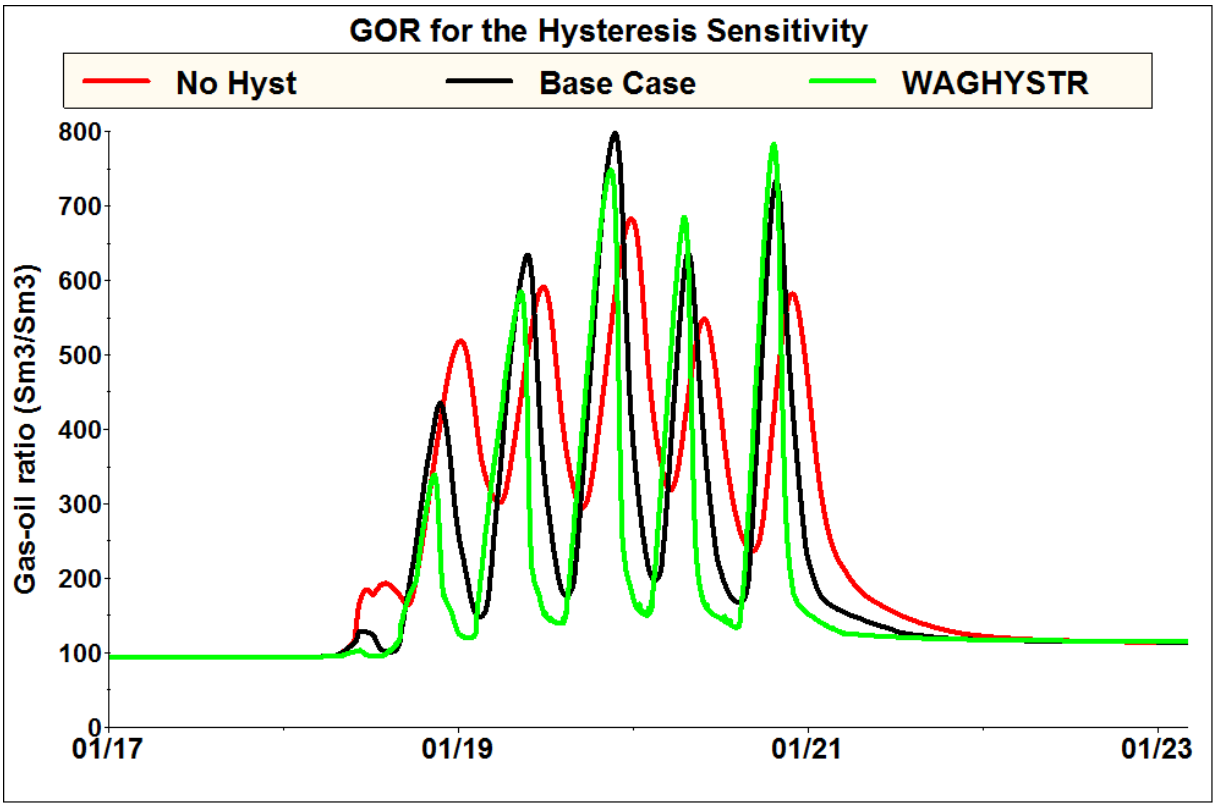

Figure 5-5 – Gas-oil ratio for the hysteresis sensitivity. The graph only shows between 2017 and 2023 of the 15 years of simulation.

5.3.2 Layer Thickness Sensitivity

The main format of the simulations is a layer thickness of 1 m. However the WAG and water base cases have also been run with 2 m and 4 m layer thickness. As shown in Figure 5-6, the difference in oil rate and oil production is very minor. Figure 5-7 shows that the GOR also shows minor deviation. The peak GOR is a little lower in the 4m DZ case, but all in all the results are very consistent. The spread in ultimate recovery is only 0.8 %.

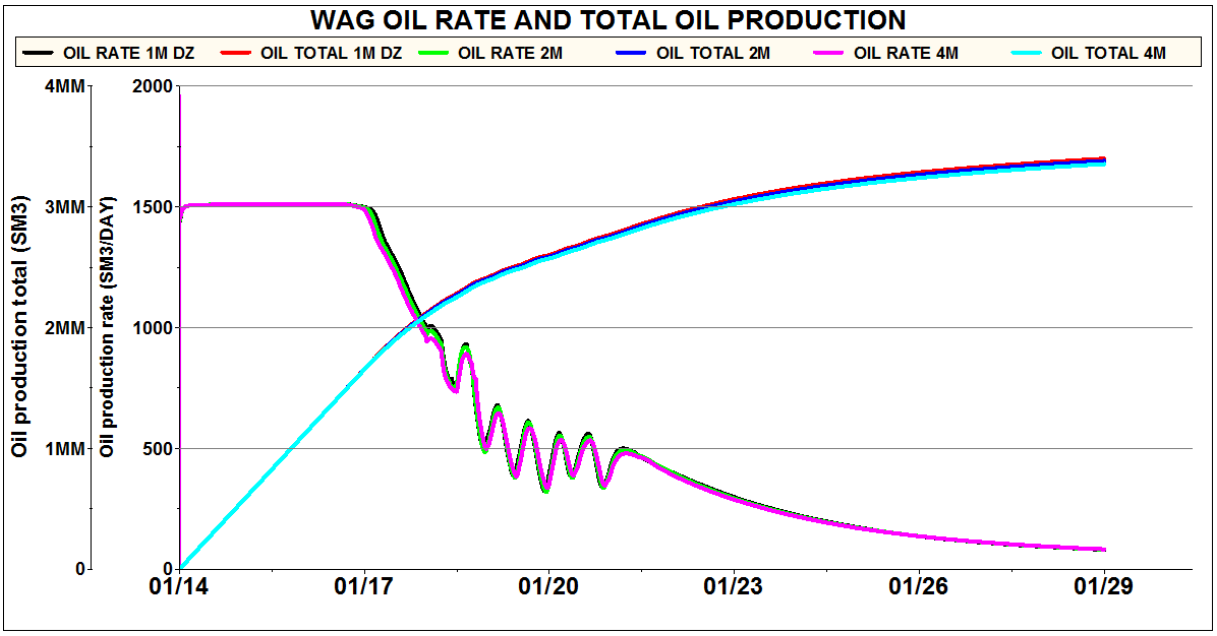

Figure 5-6 – Oil rate and total oil production of the WAG cases with layer thickness of 1, 2 and 4 meters respectively.

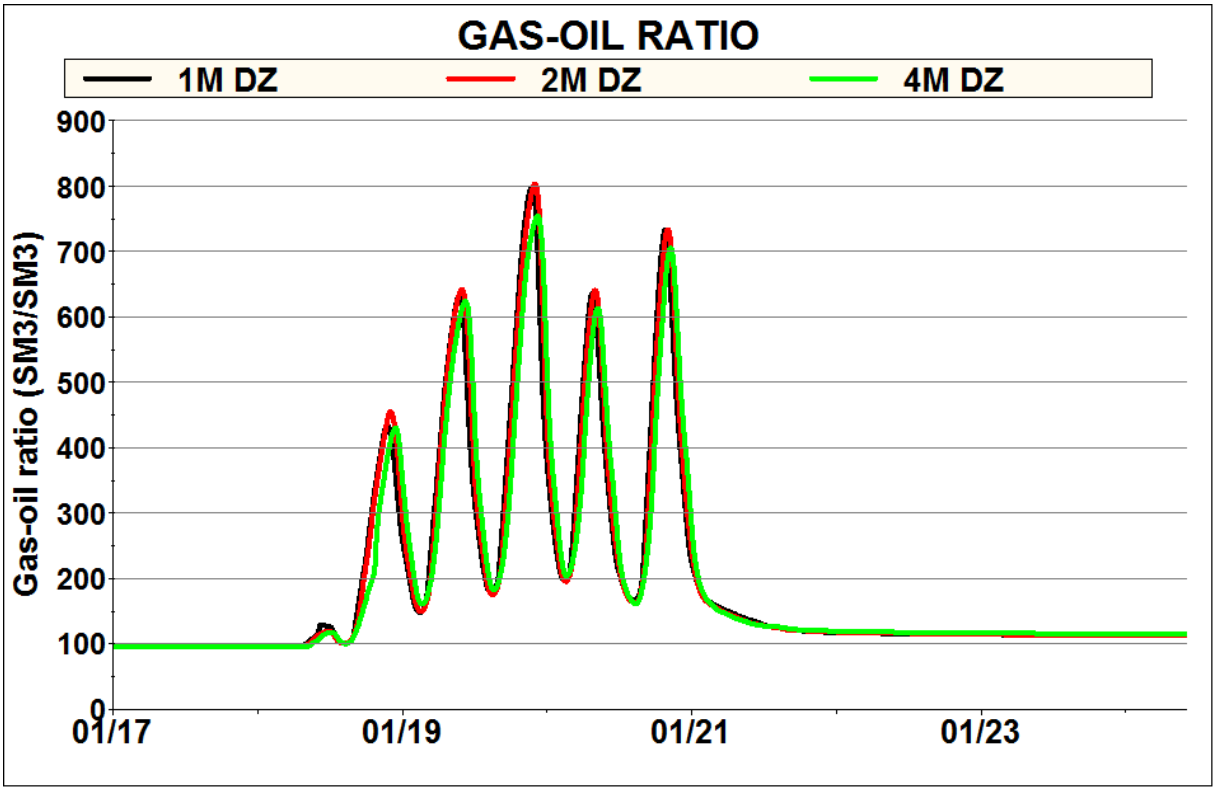

Figure 5-7 – Gas-oil ratio of the WAG cases with layer thickness of 1, 2 and 4 meters respectively.

The results are similar for the waterflood cases, shown in Figure 5-8. Reduced layer thickness delay the water breakthrough, but only within a matter of days. The spread in ultimate oil recovery is nearly as low as for the WAG cases, at 1.0 %. Additional discussion on the matter is offered in 6.1.2.

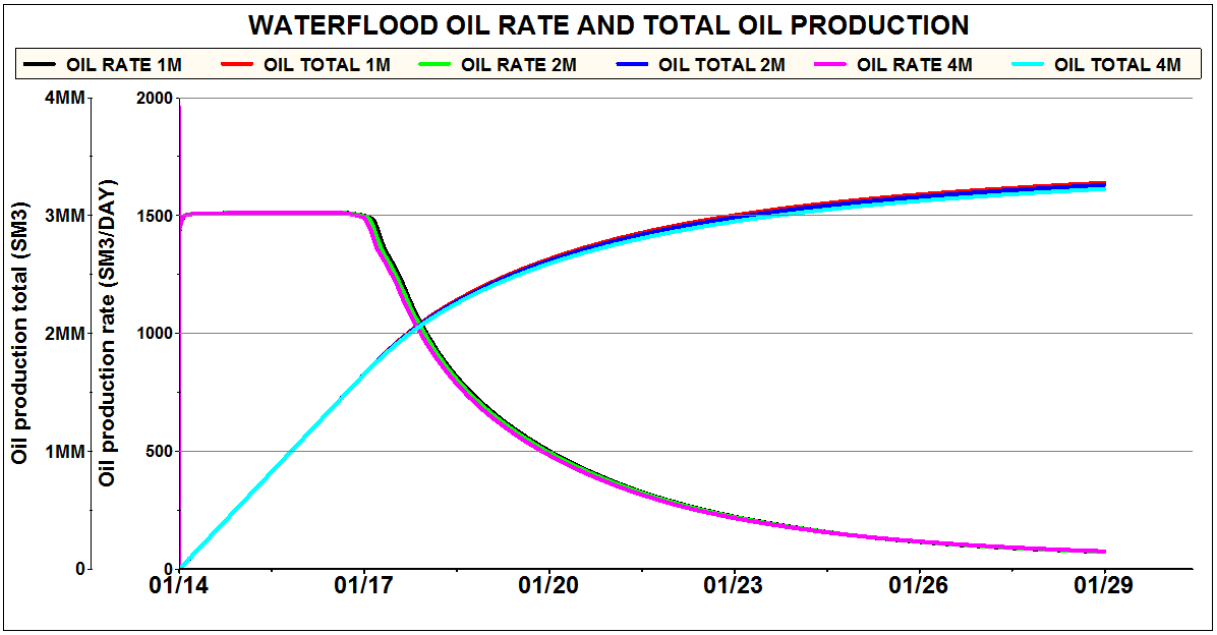

Figure 5-8 – Oil rate and total oil production of the water cases with layer thickness of 1, 2 and 4 meters respectively.

A secondary sensitivity has also been run with a very different setup. This simulation used a vertical WAG injector down dip and a vertical producer up dip with entirely different production rates and schedule. The reservoir is waterflooded for 4.5 years before 6 WAG cycles are initiated. 7 years of waterflooding follows the WAG cycle.

As seen in Figure 5-9, the layer thickness does not affect the simulation result much with vertical wells either. There is some difference in the GOR, shown in Figure 5-10, but the magnitude of change as well as the trend is the same as for a horizontal injector.

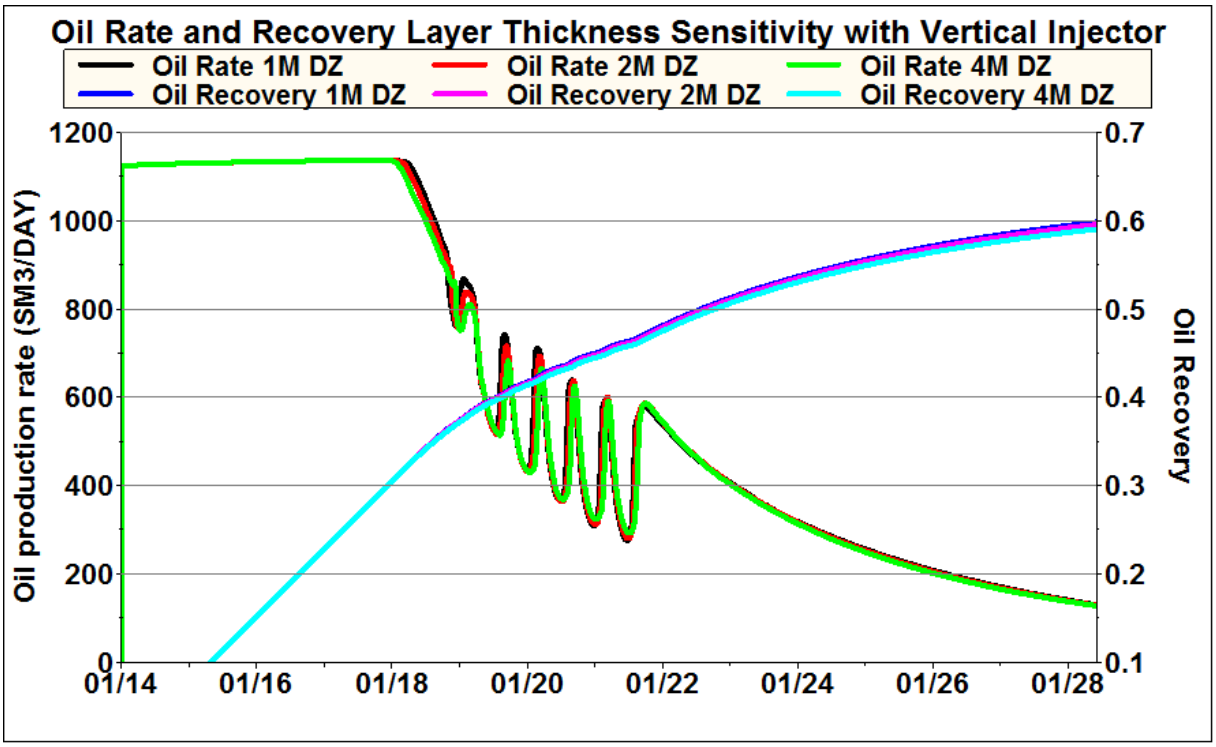

Figure 5-9 – Oil rate and oil recovery for different layer thicknesses with vertical injector.

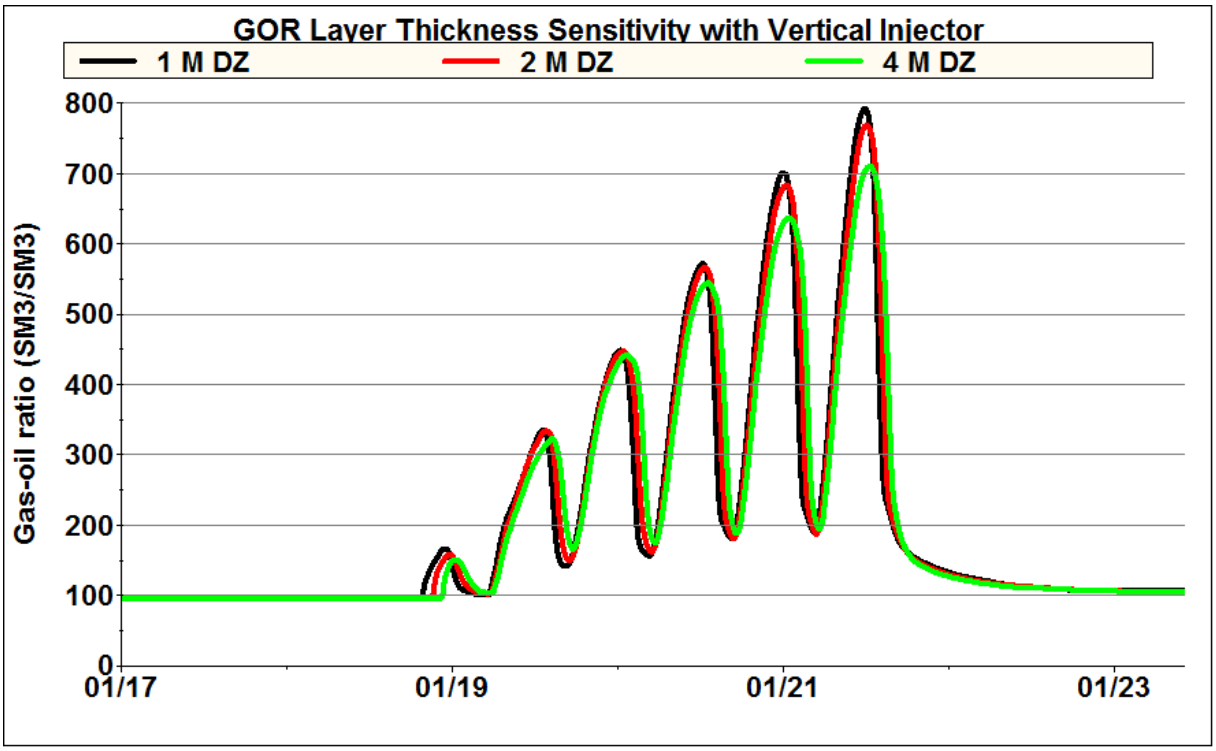

Figure 5-10 – Field GOR vs time for different layer thicknesses with vertical injector.

5.3.3 Oil Vaporization Sensitivity

The effect of changing the oil vaporization control parameter was not very large. The oil rate and total oil production is shown in Figure 5-11 and the GOR is shown in Figure 5-12. Increasing the oil vaporization control parameter described in 4.3.3 from 2 to 3 did not make any noteworthy impact. The GOR is reduced slightly at the peaks, while the oil recovery is reduced by 0.06 % with the increased parameter.

Increasing the impact of oil vaporization by reducing the parameter to 0.5 has more effect. The GOR is clearly reduced at the peaks since the gas breaking through contains more oil. The oil recovery is increased by 0.34 %. A side effect of reducing this parameter is that the oil saturation close to the injection well can be reduced to 0, where the gas throughput is large.

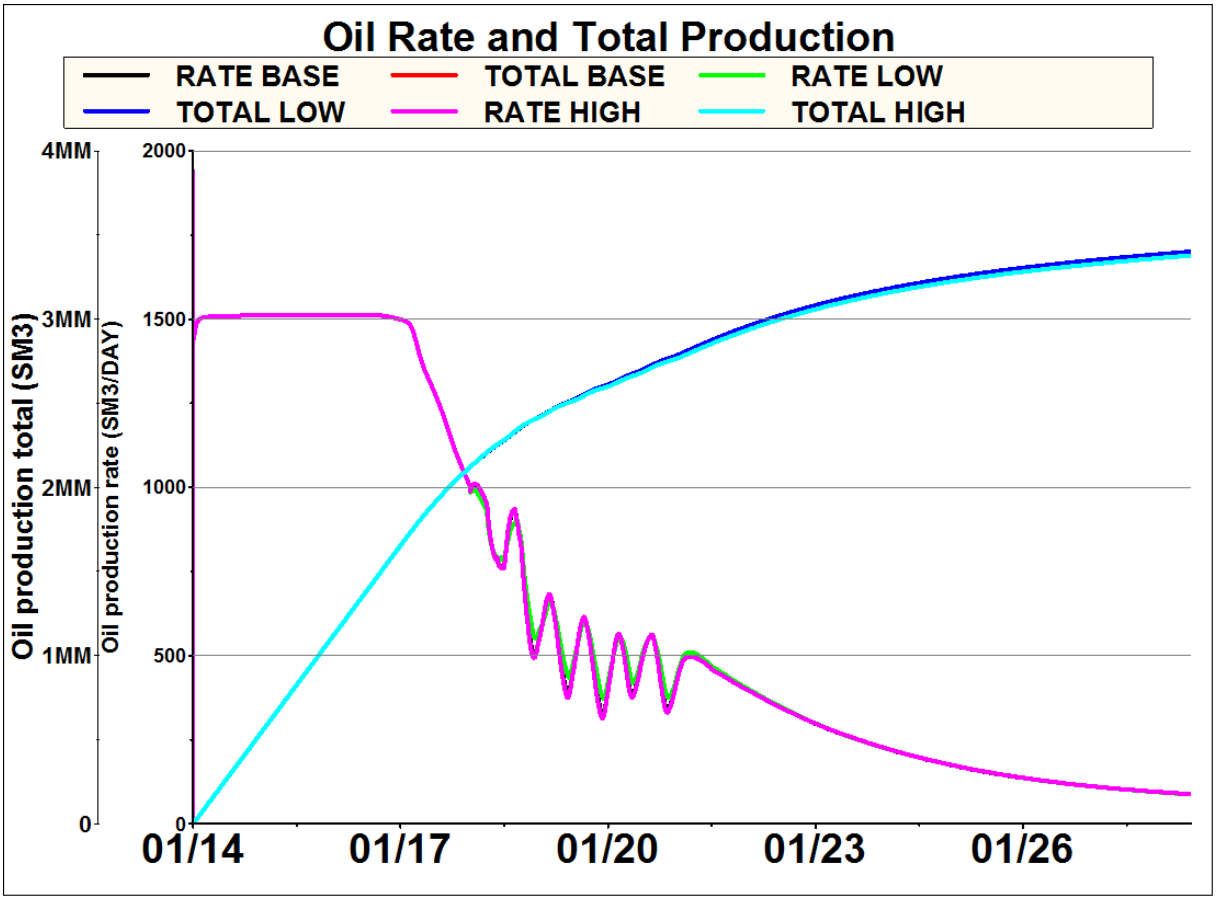

Figure 5-11 – Oil rate and total oil production in the oil vaporization sensitivity study.

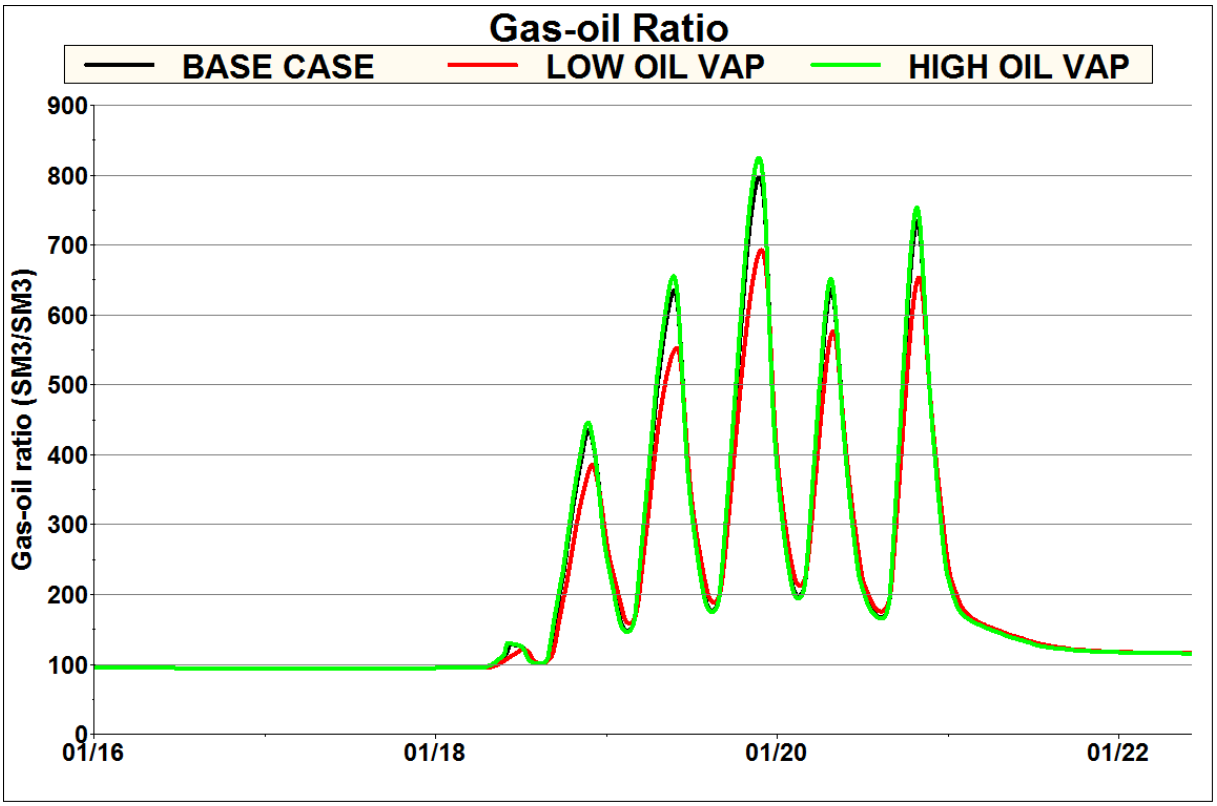

Figure 5-12 – Gas-oil ratio in the oil vaporization sensitivity study.

5.3.4 Production Rate Sensitivity

The base case production rate is 2000 Rm^3/day. WAG and waterflood cases have been run with high rate of 2500 Rm^3/day and low rate of 1500 Rm^3/day. Figure 5-13 and Figure 5-14 shows the oil rate and total oil production for high flow rate and low flow rate respectively. The equivalent plot for the base cases is shown in Figure 5-3. WAG performs better than waterflooding for all flow rates in the tested range. Between the base cases and the high flow rate cases the tendency and development is very similar. In the base case, WAG provided 2.3 % incremental recovery and in the high flow rate case WAG provided 2.6 % incremental recovery. The low flow rate WAG case appears to have a discrepancy with the other two WAG cases, with a large drop in production rate after the second WAG cycle. This is however related to the simultaneous breakthrough of both water and gas. Water breakthrough is naturally delayed due to the reduced flow rate. The incremental oil in the low flow rate WAG case is 1.8 % of STOOIP over waterflood.

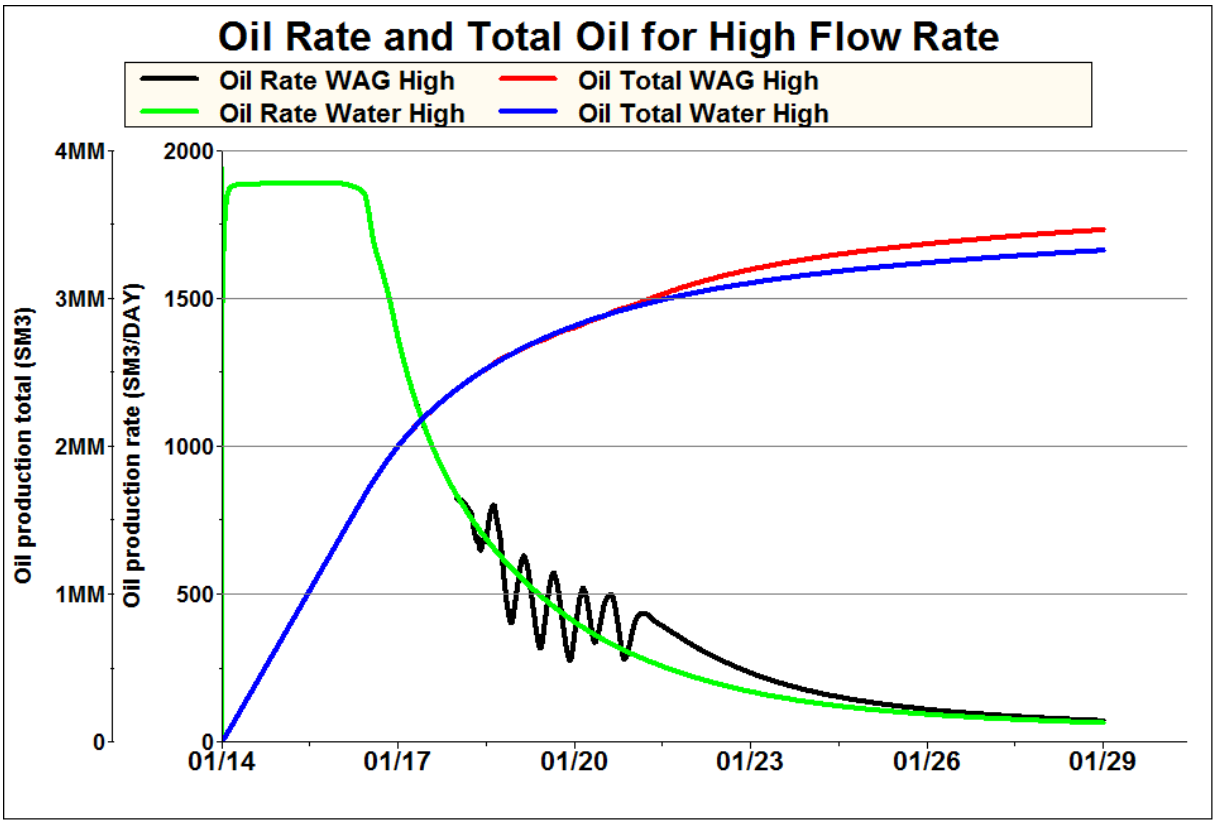

Figure 5-13 – Oil rate and total oil production with production rate of 2500 Rm^3/day for waterflooding and WAG.

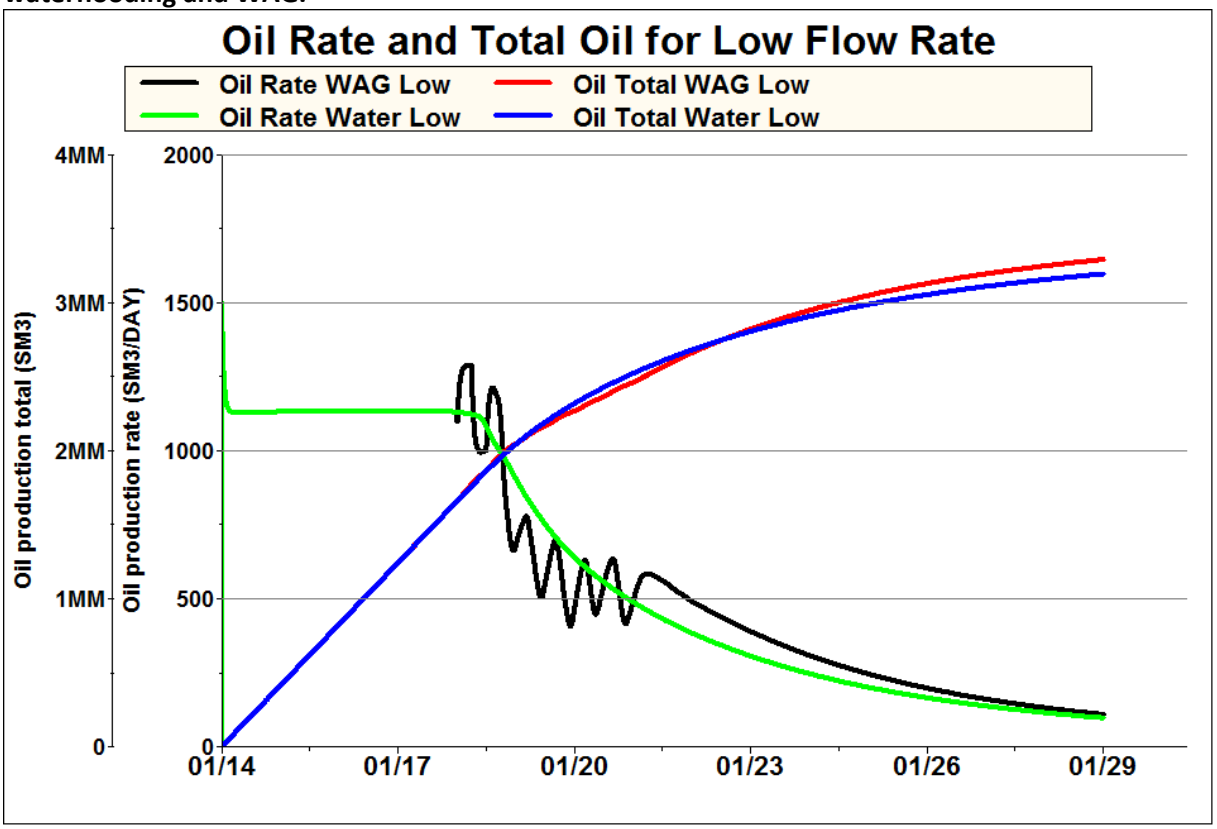

Figure 5-14 – Oil rate and total oil production with production rate of 1500 Rm^3/day for waterflooding and WAG.

5.3.5 Vertical Permeability Sensitivity

The base case has a vertical permeability of 0.01 of the horizontal permeability. The WAG and water base cases are also run with vertical permeability of 0.1 and 0.05 of the horizontal permeability. Figure 5-15 and Figure 5-16 shows the oil rate and total oil production of the WAG and water cases respectively. In both scenarios a higher vertical permeability results in higher recovery and later water breakthrough. The higher the vertical permeability, the higher are the fluctuations in oil production rate. The GOR is shown in Figure 5-17 and the gas breakthrough is faster and larger in the high vertical permeability case, naturally causing the fluctuations in oil production rate.

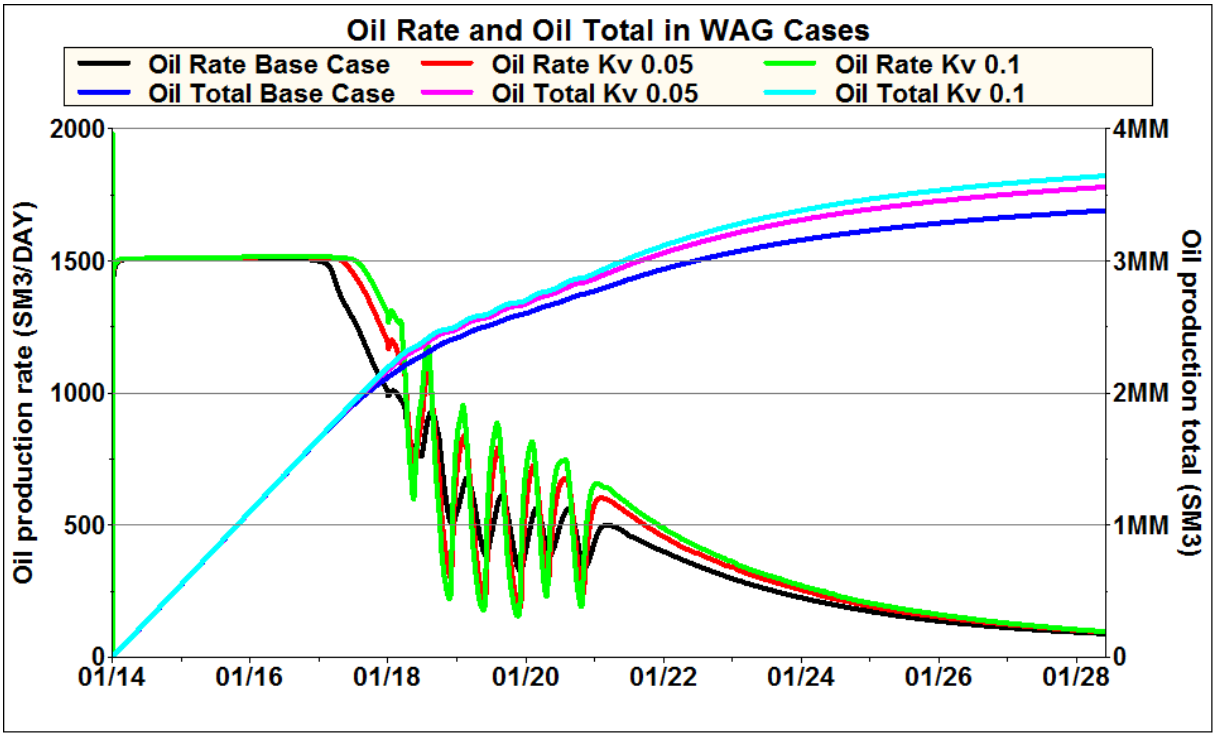

Figure 5-15 – Oil rate and total oil in WAG cases of different vertical permeability.

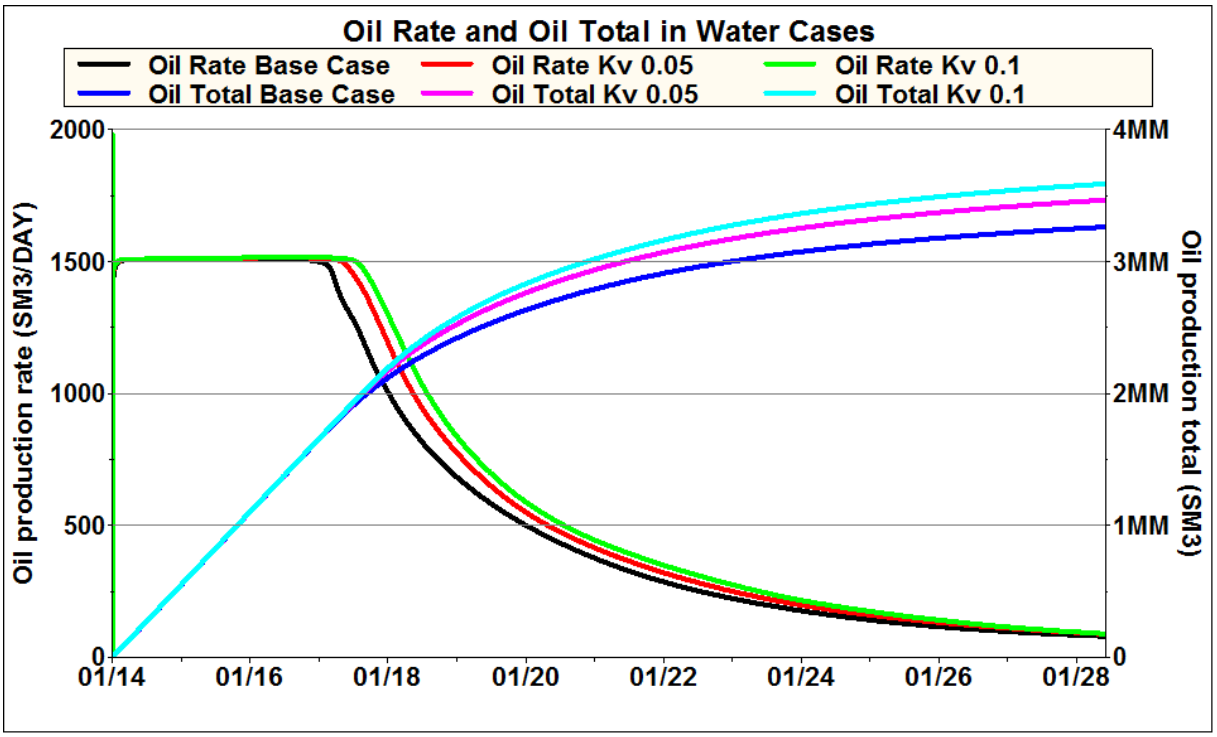

Figure 5-16 – Oil rate and total oil in water cases of different vertical permeability.

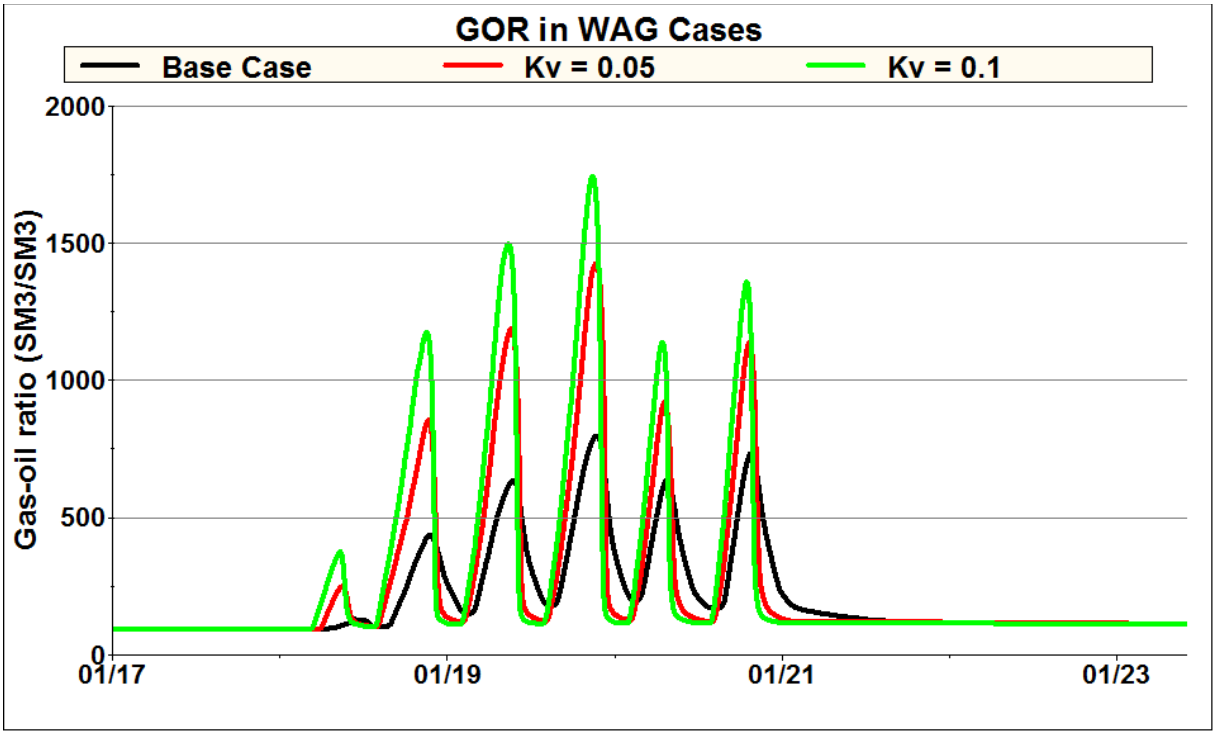

Figure 5-17 – Gas-oil ratio in WAG cases of different vertical permeability.

Figure 5-18 and Figure 5-19 shows the oil rate and total oil production for both water and WAG cases in Kv/Kh of 0.05 and 0.1 respectively. WAG is less efficient for higher the vertical permeability. The additional recovery is 1.7 % for the 0.05 case and 1.0 % for the 0.1 case, compared to 2.3 % for the base case.

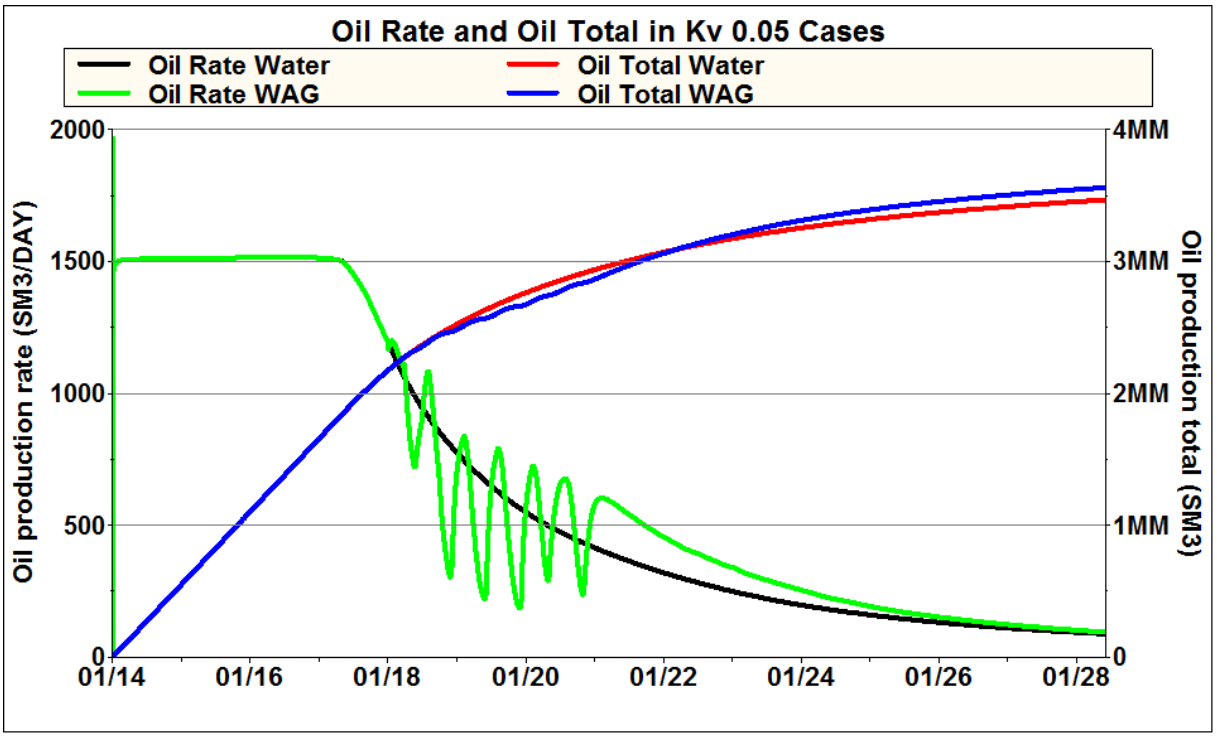

Figure 5-18 – Oil rate and total oil production in water and WAG cases with Kv/Kh = 0.05.

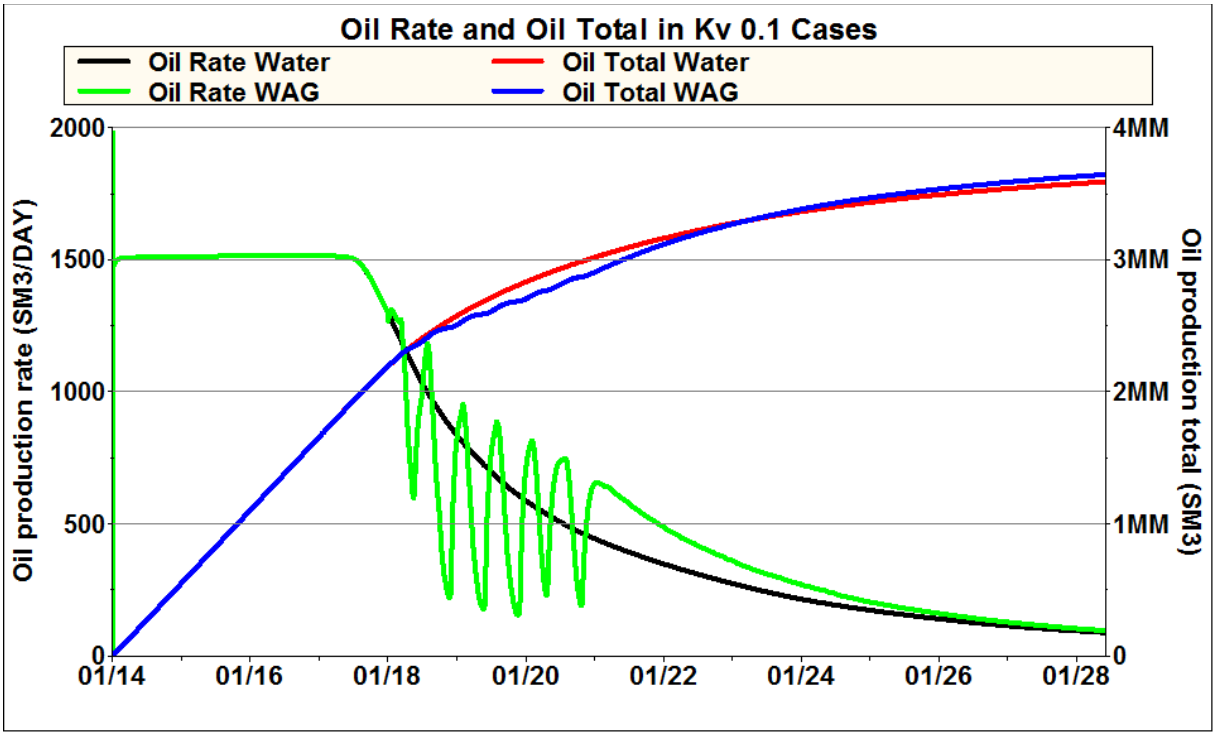

Figure 5-19 – Oil rate and total oil production in water and WAG cases with Kv/Kh = 0.1.

5.4 Stratification Sequences

5.4.1 Nansen and Eiriksson 2 Switch

In this case the top unit Nansen and the second unit Eiriksson 2 has been switched. Oil rate and total oil production for the WAG and water cases in this setup is shown in Figure 5-20. WAG performance is not much different from the base case, shown in Figure 5-3. Again the incremental oil is produced by the final waterflood after WAG has ended. The incremental oil recovery at the end of simulation is 2 % of STOOIP, compared to 2.3 % for the base case. Comparison of the waterflood base case and Nansen switch in Figure 5-21, shows that waterflooding has reduced efficiency in the Nansen switch case. Ultimate recovery is 1.6 % lower and in 2021 the recovery is 2.8 % lower. Water breaks through sooner in the Nansen switch case (when oil drops off plateau) and recovery is not able to "catch up" in the later stages.

The WAG base case and WAG Nansen switch case has very similar performance. As can be seen in Figure 5-22, most of the difference in recovery is from before WAG starts and during the first two cycles. After this, production rate and WAG response is nearly identical. Figure 5-23 shows the GOR for the WAG base and Nansen switch cases. Gas breakthrough in the first two WAG cycles is faster and more severe. Later cycles also shows faster breakthrough and similar decline, except for a temporary stabilization in the GOR late in the cycle.

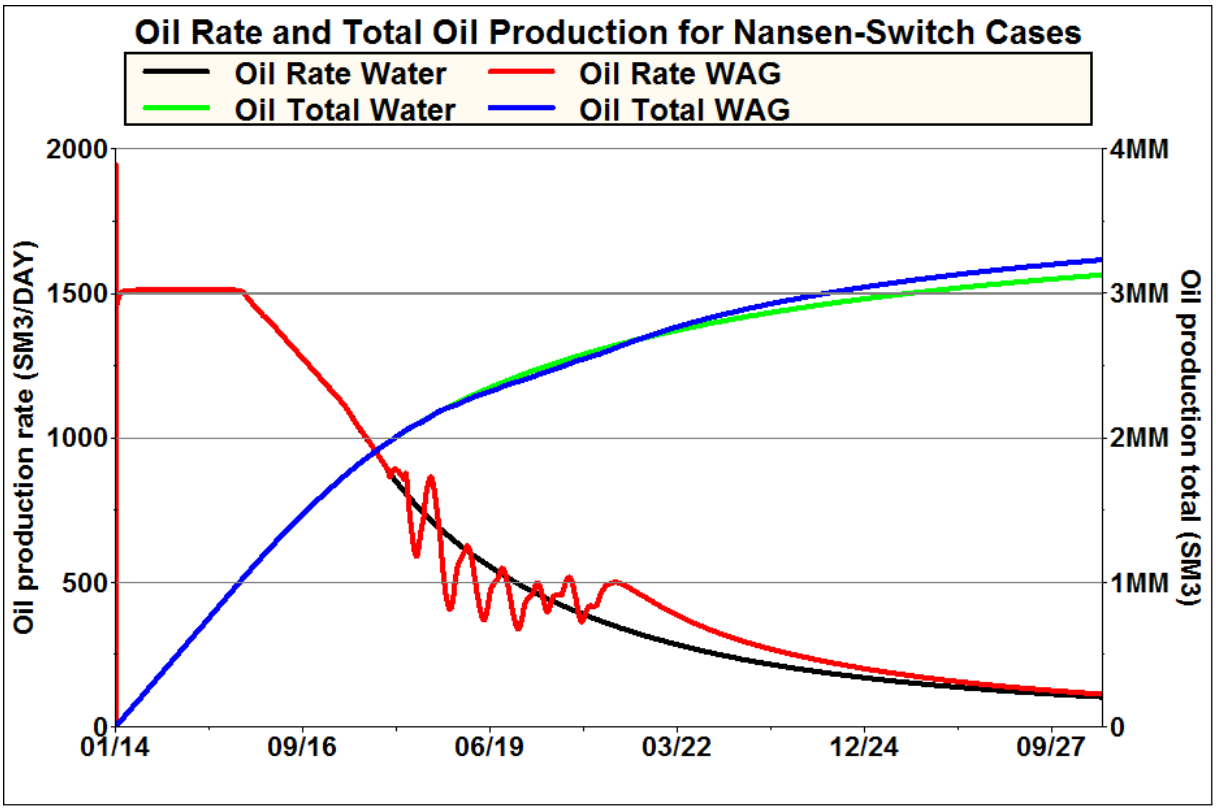

Figure 5-20 – Oil rate and total oil for the water and WAG Nansen switch cases.

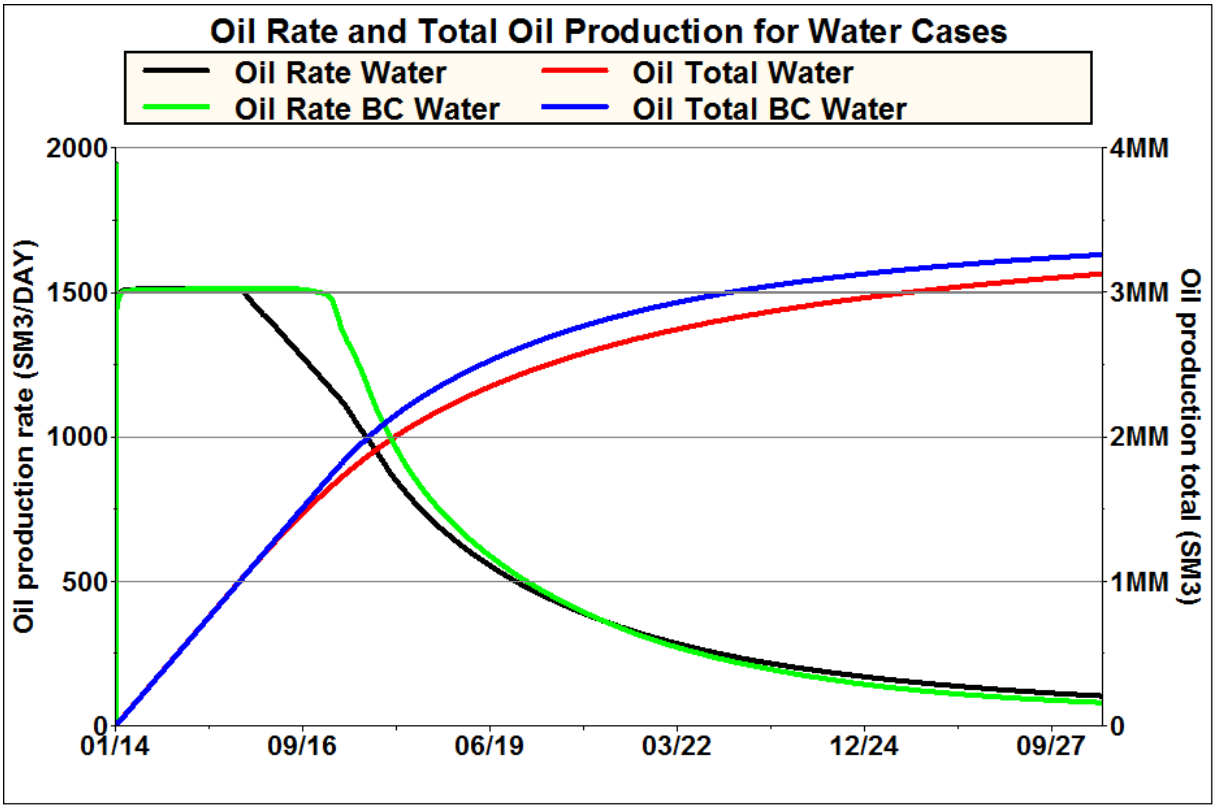

Figure 5-21 – Oil rate and total oil for the base case and Nansen switch water case.

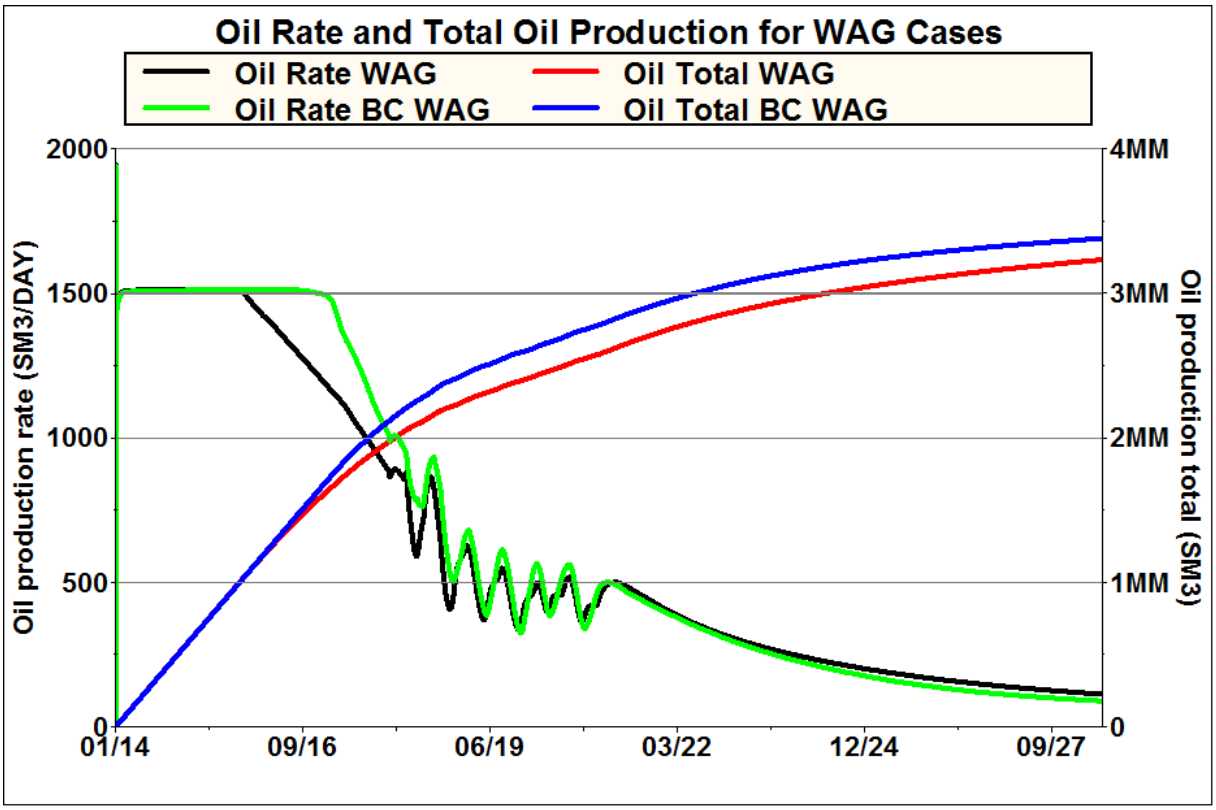

Figure 5-22 – Oil rate and total oil for the base case and Nansen switch WAG case.

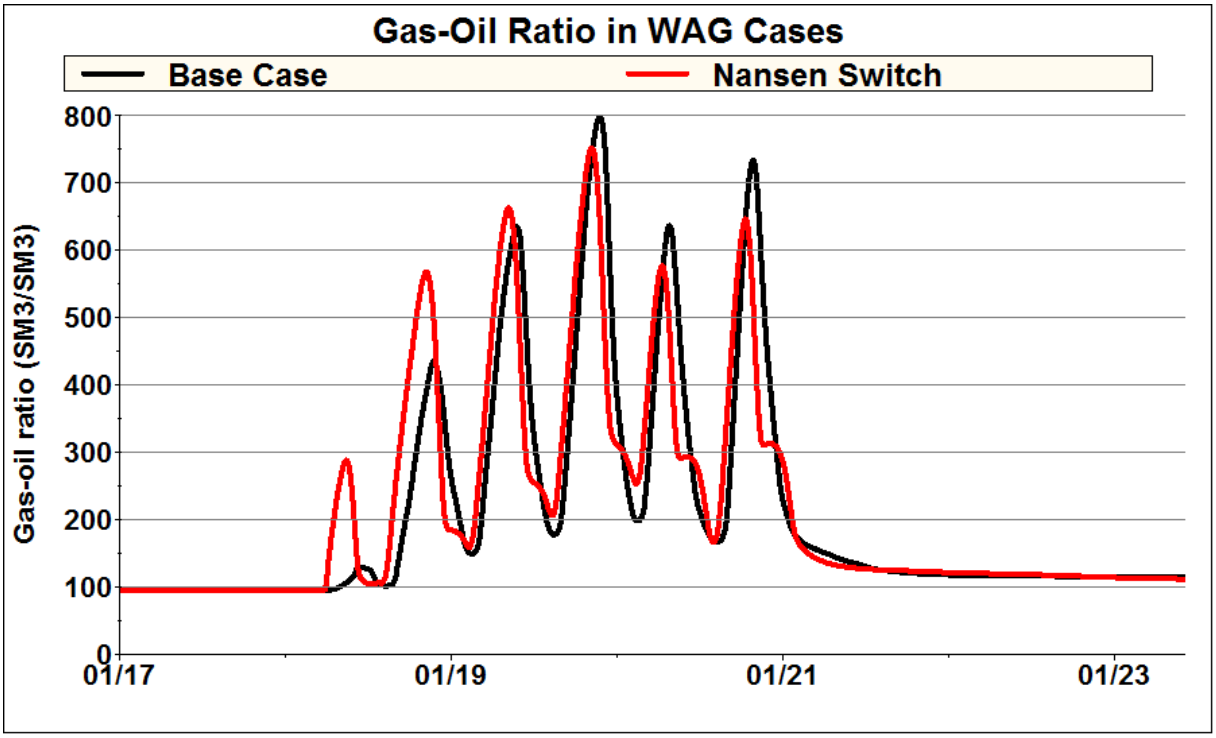

Figure 5-23 – Gas-oil ratio for the WAG base case and WAG Nansen switch case between 2017 and 2023.

5.4.2 Downwards Fining

In the downwards fining case the layers have been sorted by average horizontal permeability, with the most permeable on top. Oil rate and total oil production for the WAG and water cases in this setup is shown in Figure 5-24. WAG performance is not much different from the base case, shown in Figure 5-3. Again the incremental oil is produced by the final waterflood after WAG has ended. The incremental oil recovery at the end of simulation is 1.9 % of STOOIP, compared to 2.3 % for the base case. The oil rate and total oil recovery in the water base case and water downwards fining case, shown in Figure 5-25, are very similar. The in-place volumes of the downwards fining case are higher than the base case because the high quality layers are on top. Consequently the recovery factor in the downwards fining setup is 1.2 % lower than the base case, even if the total oil production is higher. WAG flood has a very consistent effect in the base case and downwards fining, but the oil rate is fluctuating more during WAG cycles in the downwards fining case. This is caused by faster and more significant breakthrough of gas. WAG flood performance is shown in Figure 5-26 and GOR is shown in Figure 5-27.

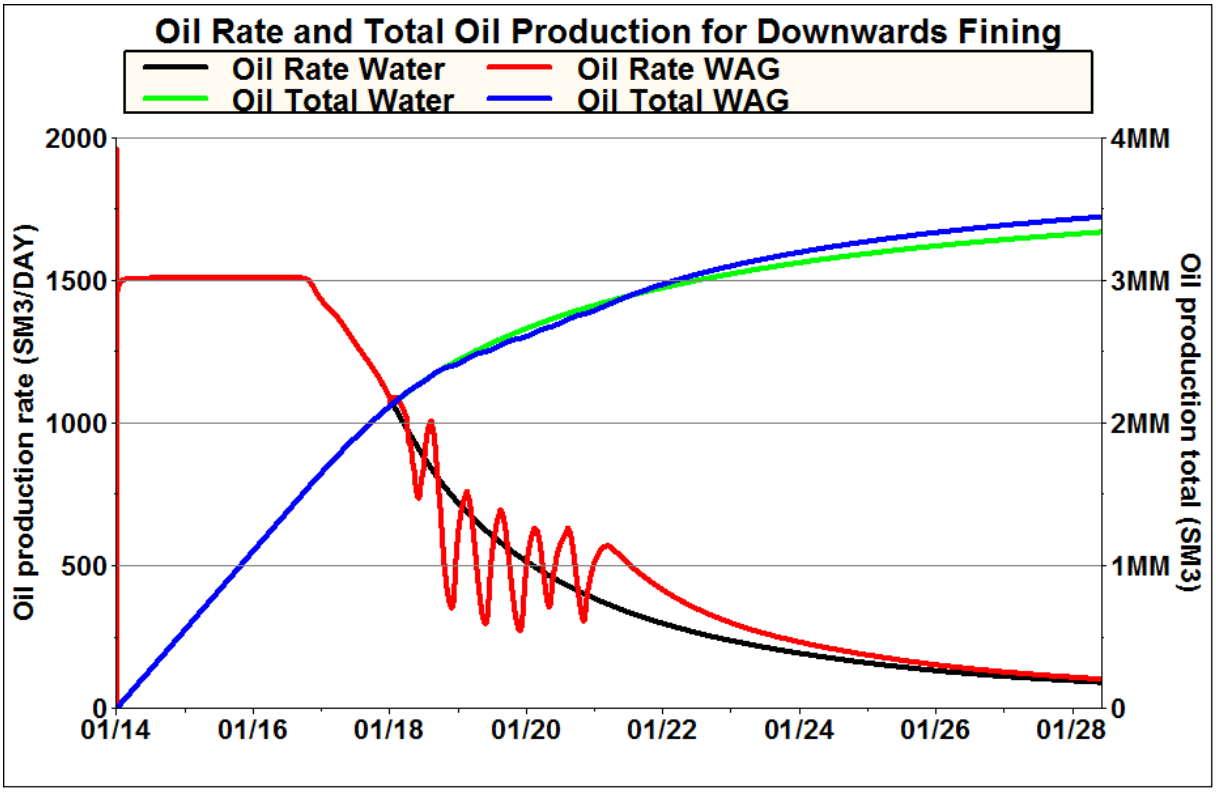

Figure 5-24 – Oil rate and total oil for the water and WAG downwards fining cases.

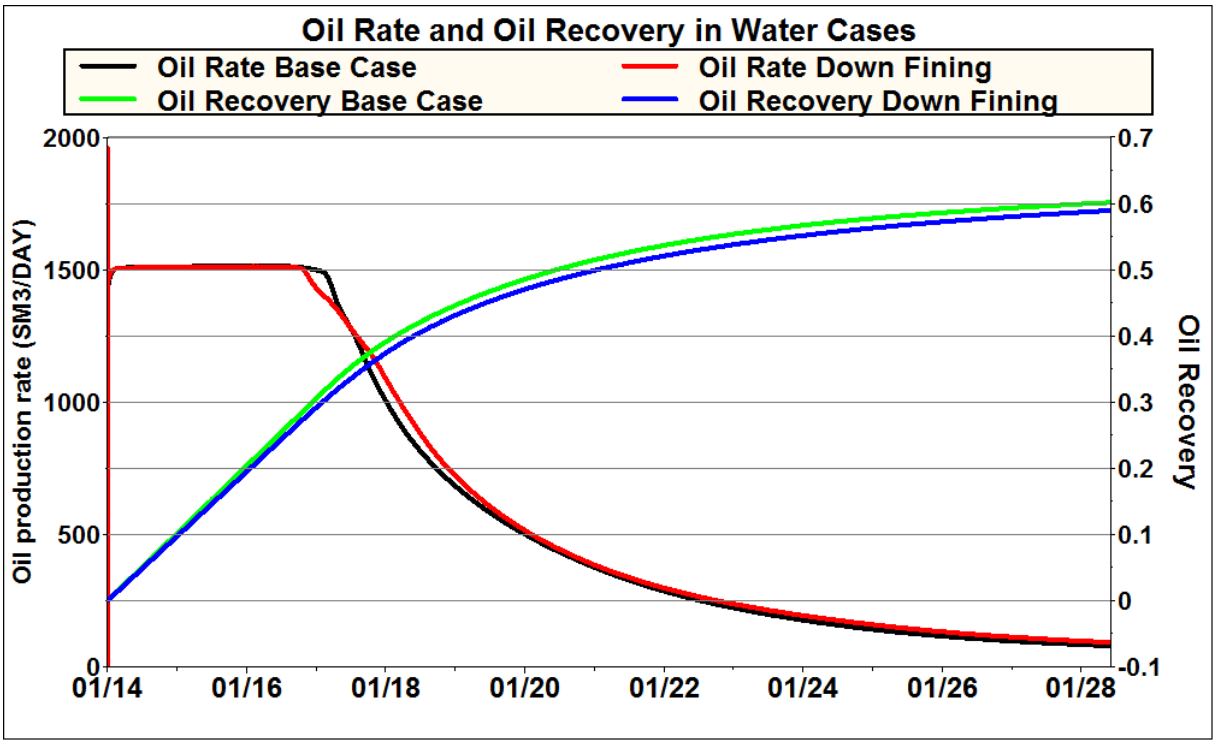

Figure 5-25 – Oil rate and oil recovery for the base case and downwards fining water case.

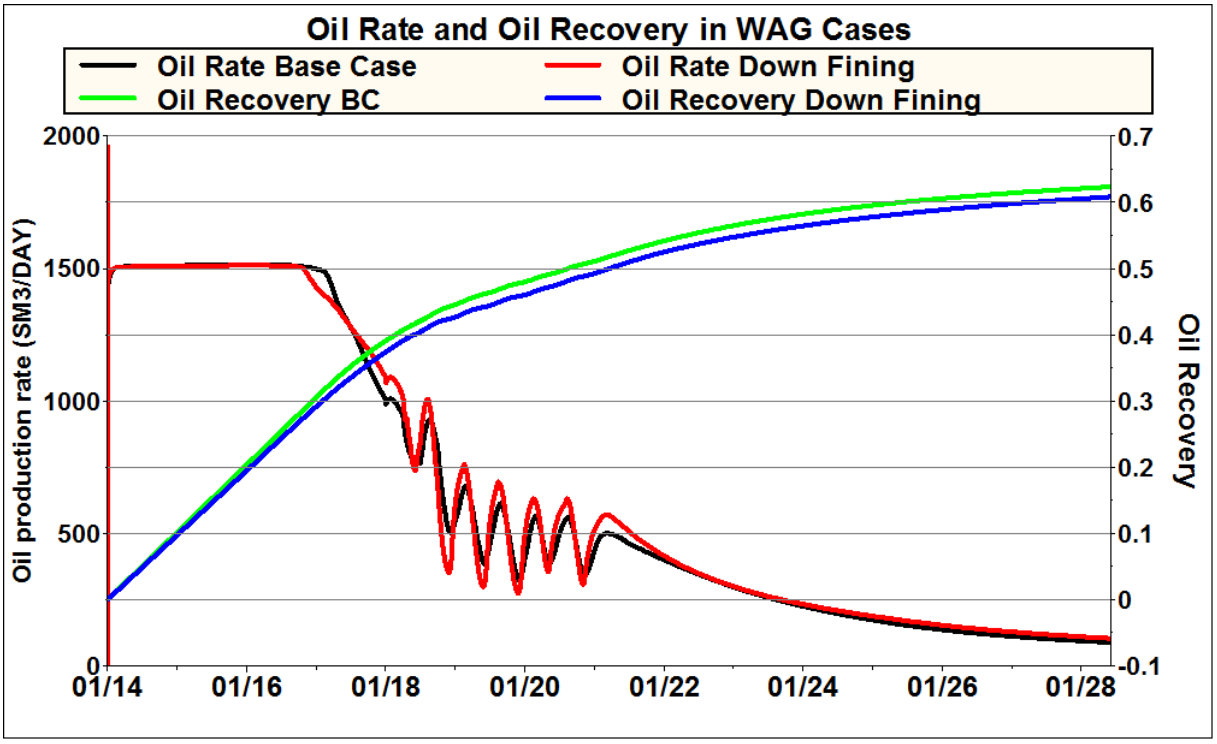

Figure 5-26 – Oil rate and oil recovery for the base case and downwards fining WAG case.

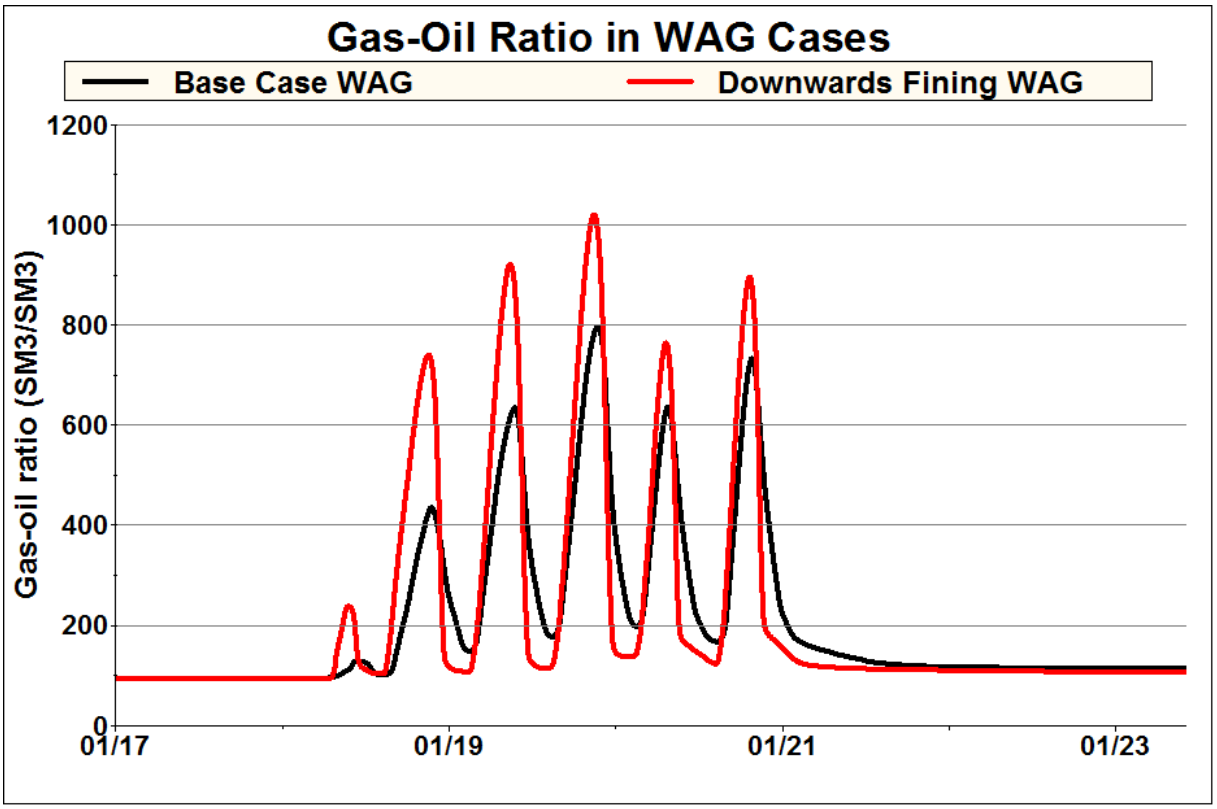

Figure 5-27 – Gas-oil ratio for the WAG base case and WAG downwards fining case between 2017 and 2023.

5.4.3 Upwards Fining

In the upwards fining case the layers have been sorted by average horizontal permeability, with the least permeable on top (see 4.4.3 for more information). Oil rate and total oil production for the WAG and water cases in this setup is shown in Figure 5-28. WAG performance is not much different from the base case, shown in Figure 5-3. Again the incremental oil is produced by the final waterflood after WAG has ended. The incremental oil recovery at the end of simulation is 2.4 % of STOOIP, compared to 2.3 % for the base case. Oil rate and total recovery for the water base case and water upwards fining case is shown in Figure 5-29. Water breaks through after one year in the upwards fining case compared to about three years for the base case (drop off plateau). The recovery is also 6.6 % lower. Note that STOOIP is 6 % lower for the upwards fining case than the base case because the high quality layers are deeper in the reservoir. Identical oil rate curves would then mean a higher recovery in the upwards fining case.

WAG flood performance is shown in Figure 5-30 and GOR is shown in Figure 5-31. WAG in the upwards fining sequence shows many of the same tendencies as the base case WAG.

However, the fluctuations in oil rate and GOR are lower, with lower peaks and not as deep valleys in GOR development.

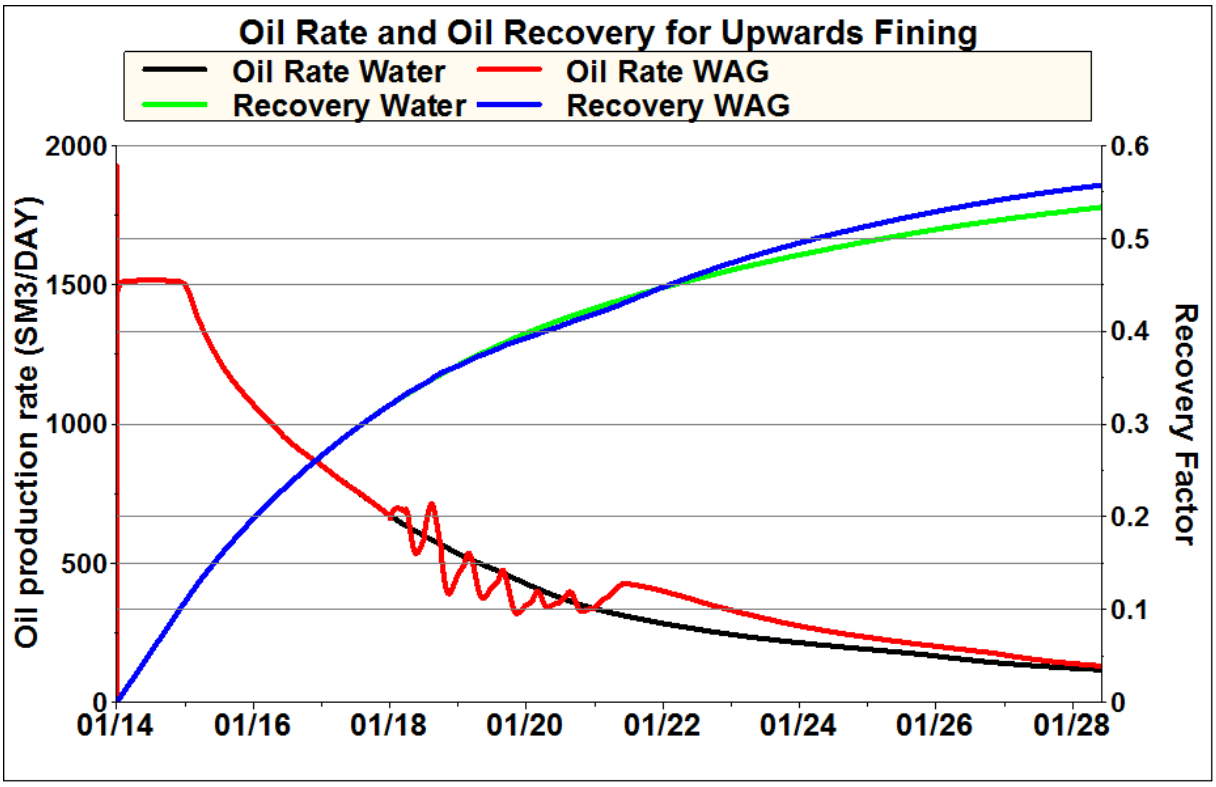

Figure 5-28 – Oil rate and oil recovery for the water and WAG upwards fining cases.

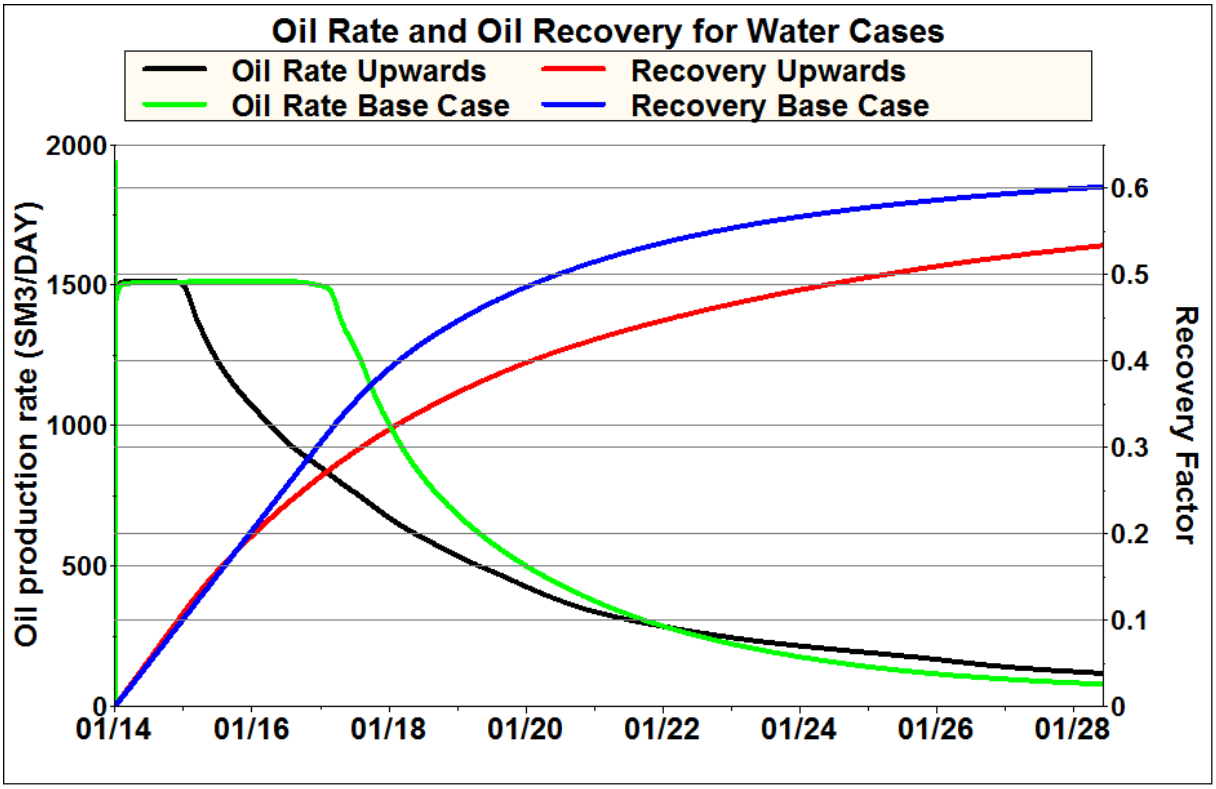

Figure 5-29 – Oil rate and oil recovery for the base case and upwards fining water case.

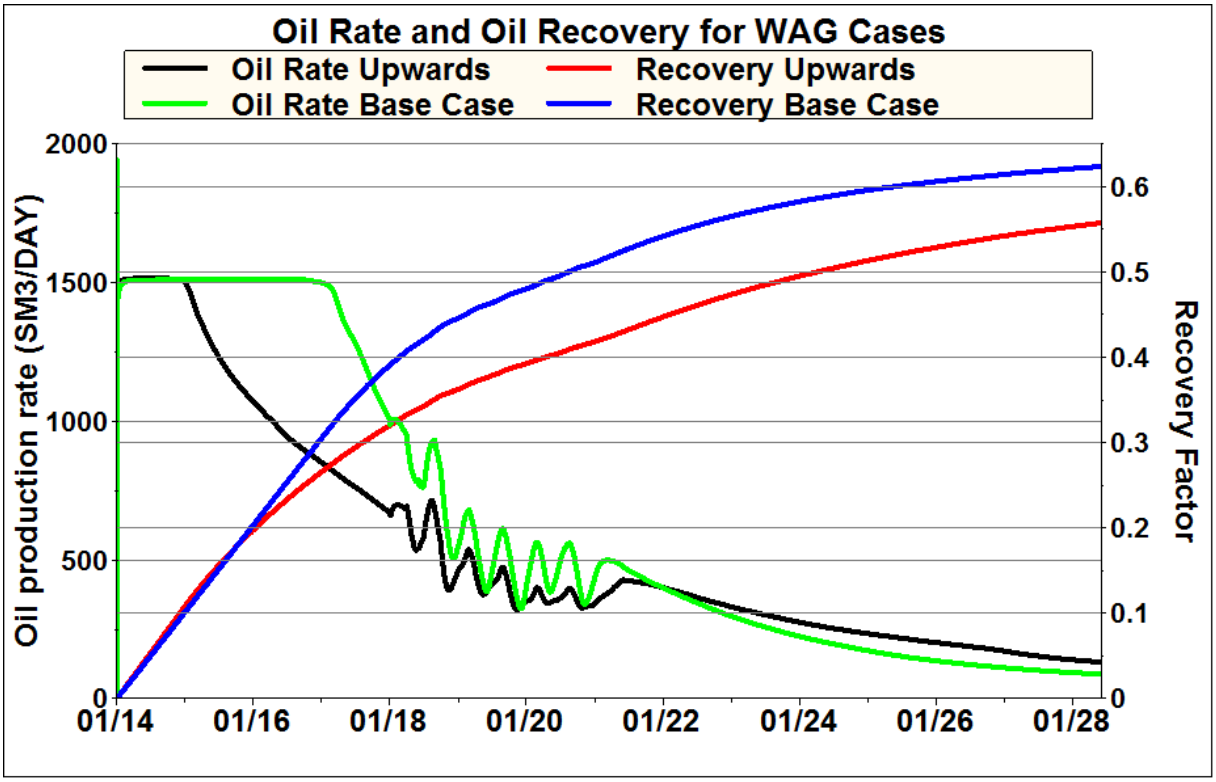

Figure 5-30 – Oil rate and oil recovery for the base case and upwards fining WAG case.

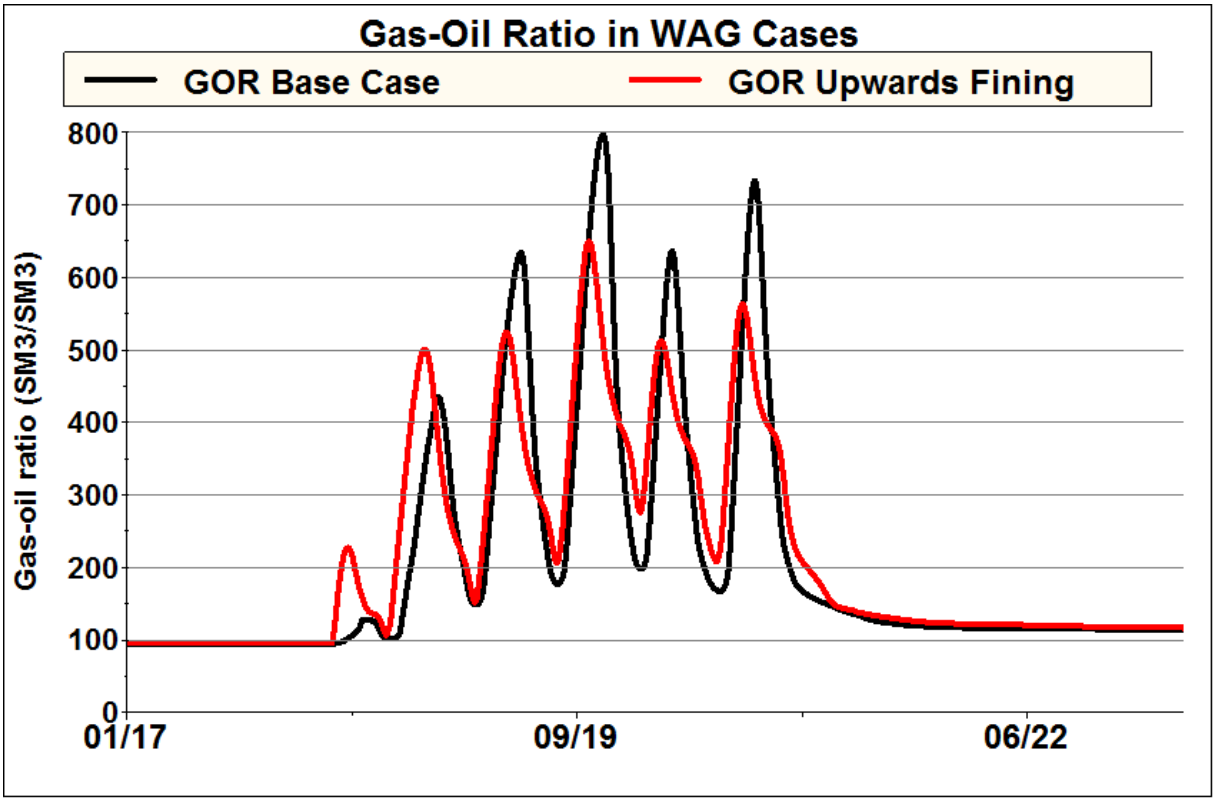

Figure 5-31 – Gas-oil ratio for the WAG base case and WAG upwards fining case between 2017 and 2023.

5.4.4 Upwards Fining Sequence with Interbedded Vertical Flow Barriers

This setup contains four units that are upwards fining. For more details see 4.4.4. Oil rate and total oil production for the WAG and water cases in this setup is shown in Figure 5-32. WAG performance is not much different from the base case, shown in Figure 5-3. Again the incremental oil is produced by the final waterflood after WAG has ended. The incremental oil recovery at the end of simulation is 2.6 % of STOOIP, compared to 2.3 % for the base case. Oil rate and total recovery for the water base case and water upwards fining with interbedded vertical flow barriers case is shown in Figure 5-33. Water breaks through almost immediately and the oil rate is lower than the base case for most of the simulation period. Note that the STOOIP in this setup is 12.5 % lower than the base case.

WAG flood performance is shown in Figure 5-34 and GOR is shown in Figure 5-35. WAG in the upwards fining sequence shows many of the same tendencies as the base case WAG. However, the fluctuations in oil rate and GOR are lower, with lower peaks and not as deep valleys in GOR development.

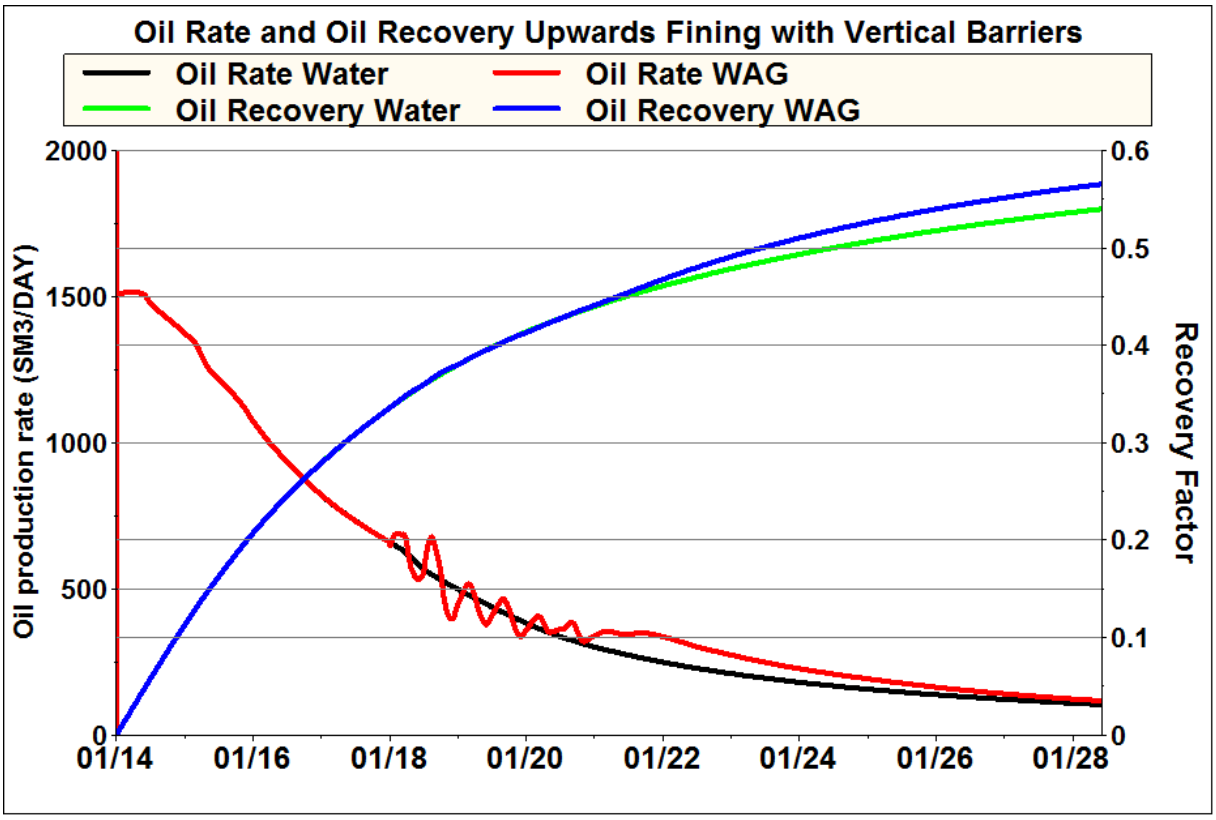

Figure 5-32 – Oil rate and oil recovery for the water and WAG upwards fining with vertical flow barrier cases.

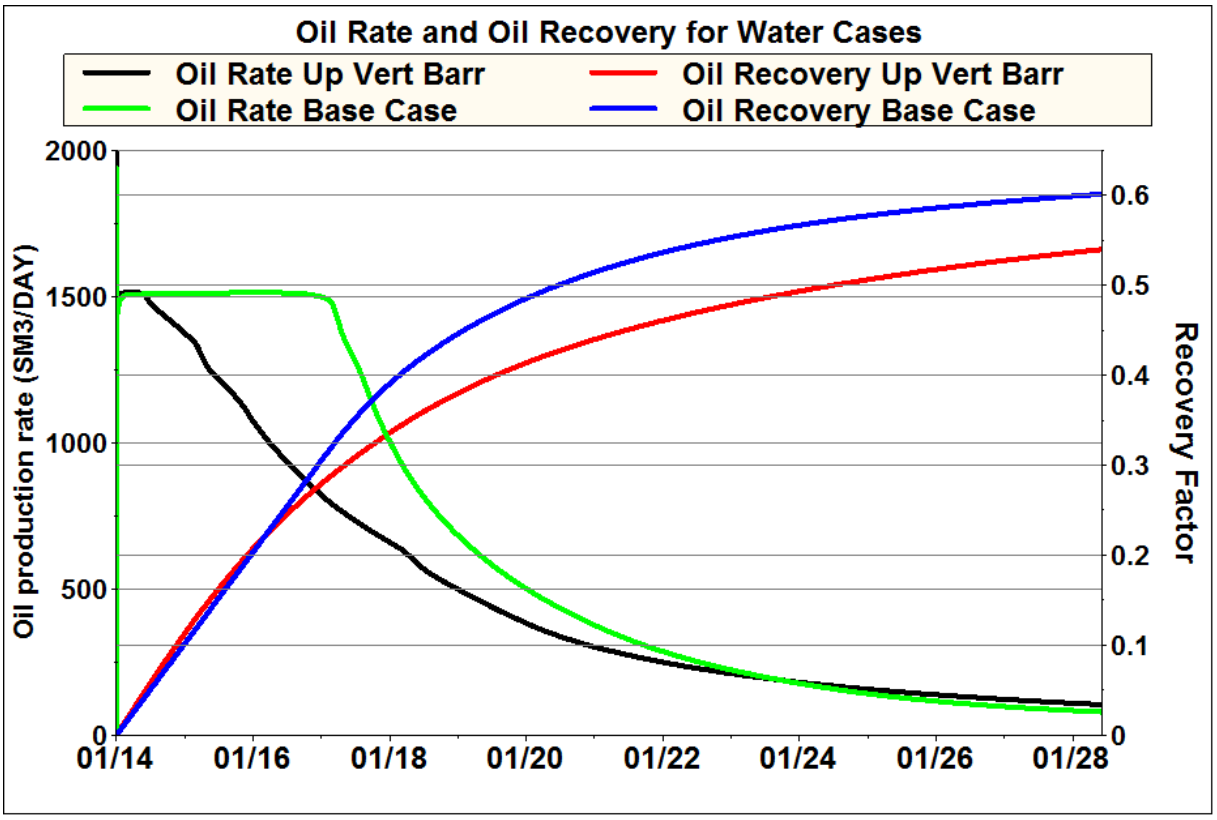

Figure 5-33 – Oil rate and oil recovery for the water base case and water upwards fining with vertical flow barrier case.

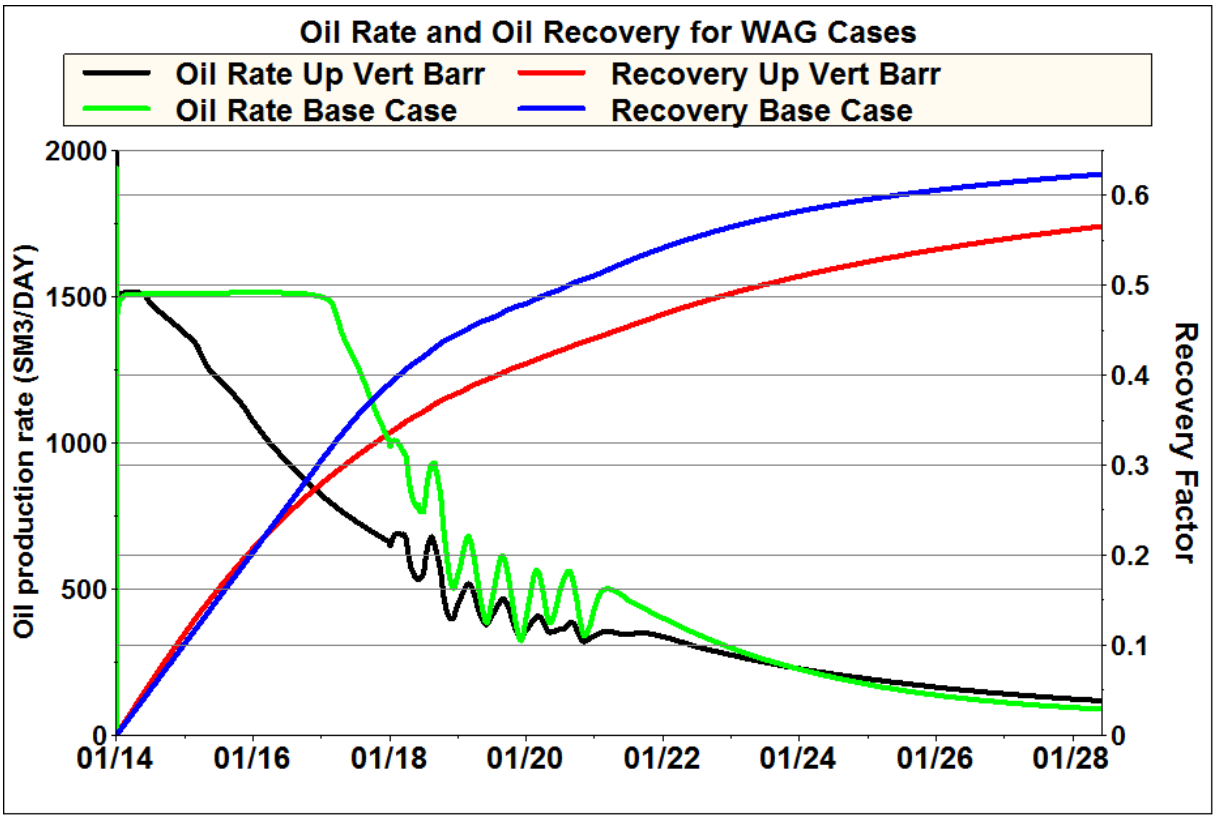

Figure 5-34 – Oil rate and oil recovery for the WAG base case and WAG upwards fining with vertical flow barrier case.

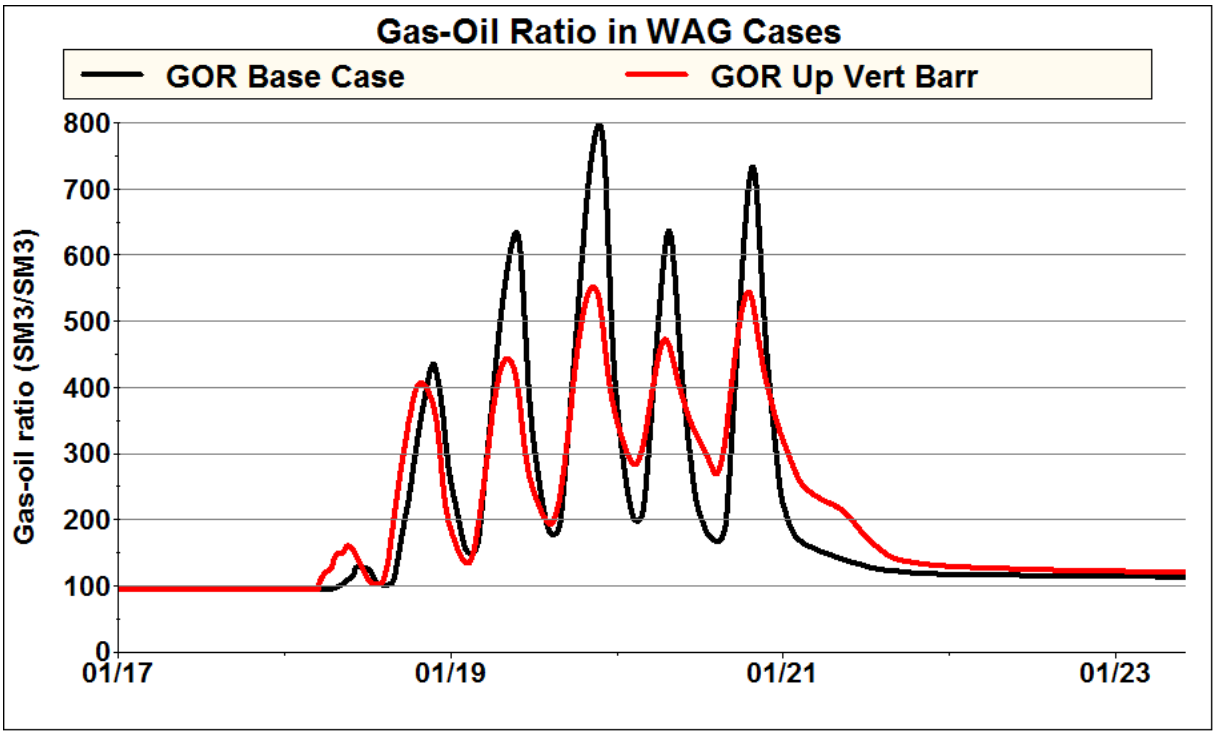

Figure 5-35 – Gas-oil ratio for the WAG base case and WAG upwards fining with vertical flow barrier case between 2017 and 2023.

5.4.5 Downwards Fining Sequence with Interbedded Vertical Flow Barriers

This setup contains four units that are downwards fining. For more details see 4.4.5. Oil rate and total oil production for the WAG and water cases in this setup is shown in Figure 5-32. WAG performance is not much different from the base case, shown in Figure 5-3. Again the incremental oil is produced by the final waterflood after WAG has ended. The incremental oil recovery at the end of simulation is 1.7 % of STOOIP, compared to 2.3 % for the base case. Oil rate and total recovery for the water base case and water downwards fining with interbedded vertical flow barriers case is shown in Figure 5-37. Water breaks through after one year and the oil rate is lower than the base case for most of the simulation period. Note that the STOOIP in this setup is 8.0 % lower than the base case. The oil recovery in is 2.6 % lower than the water base case.

WAG flood performance is shown in Figure 5-38 and GOR is shown in Figure 5-39. WAG in the downwards fining sequence with vertical barriers behaves similar to the base case from the 3rd cycle. Most of the difference in oil recovery is from the initial waterflooding, but the fluctuations in oil rate and GOR are higher, particularly in the first cycles.

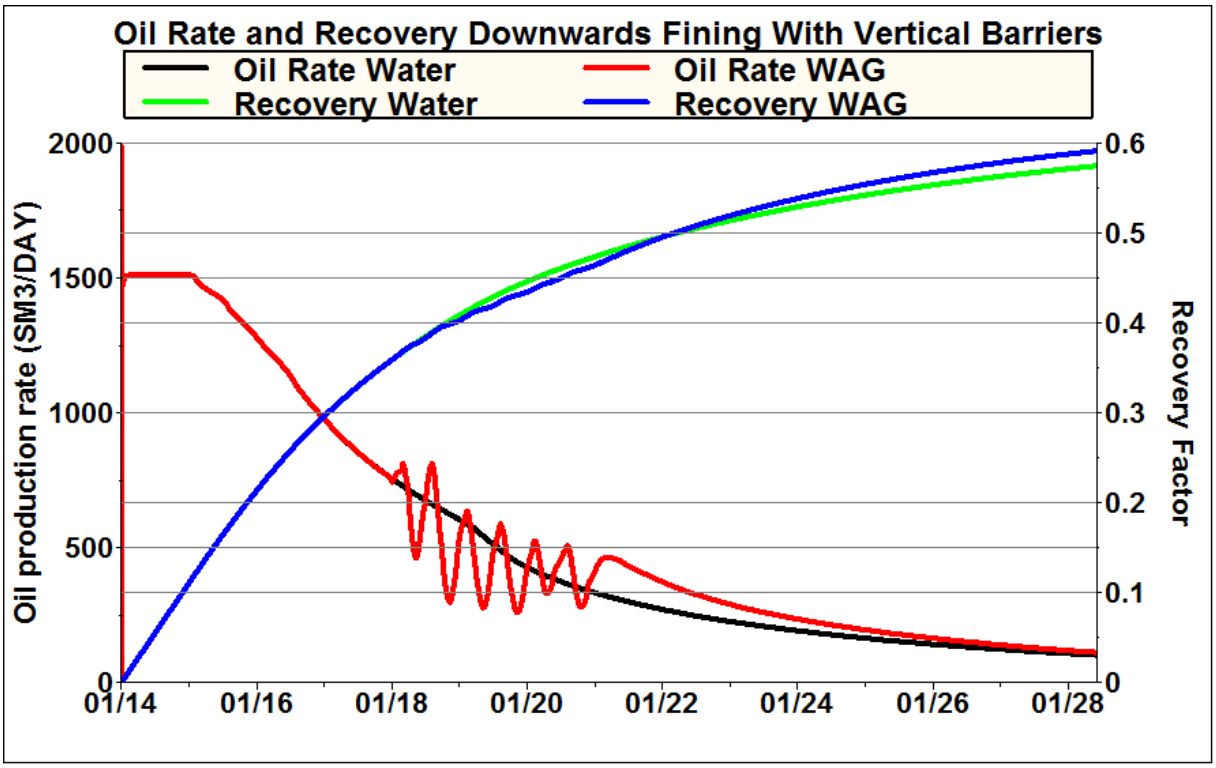

Figure 5-36 – Oil rate and oil recovery in downwards fining with vertical flow barrier cases.

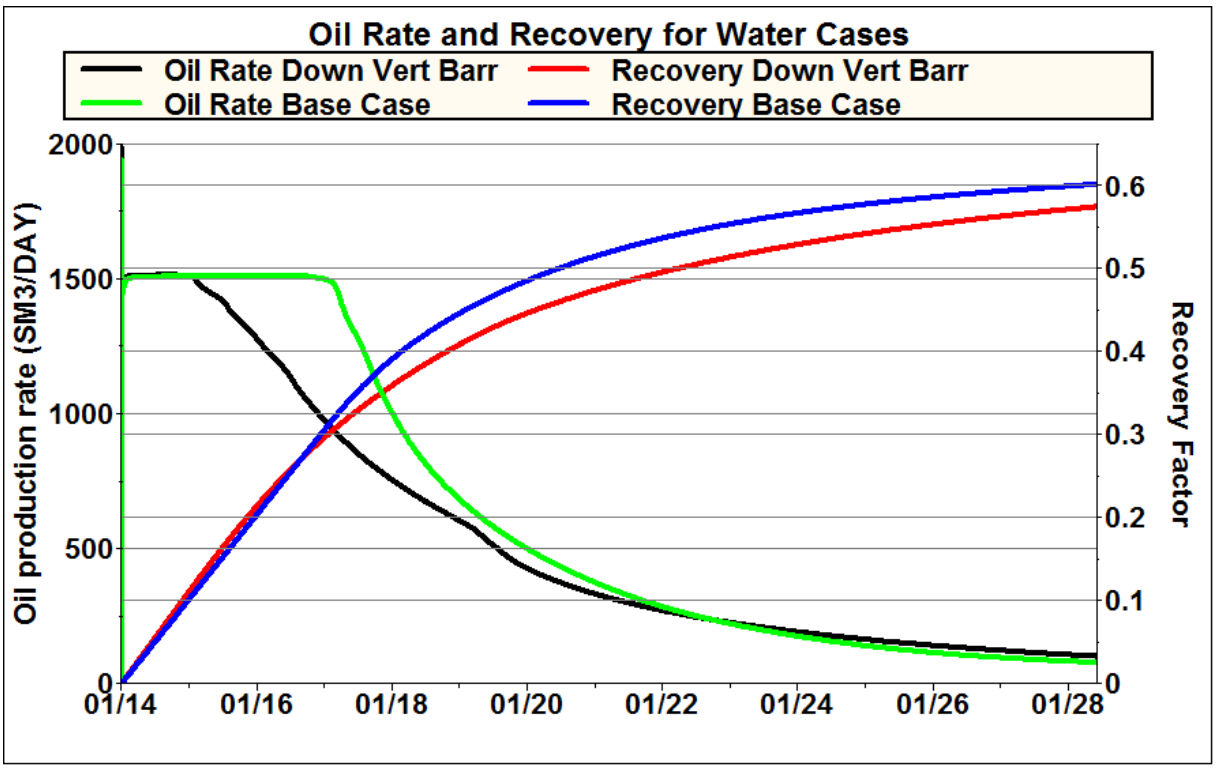

Figure 5-37 – Oil rate and oil recovery for the water cases in downwards fining with vertical flow barrier.

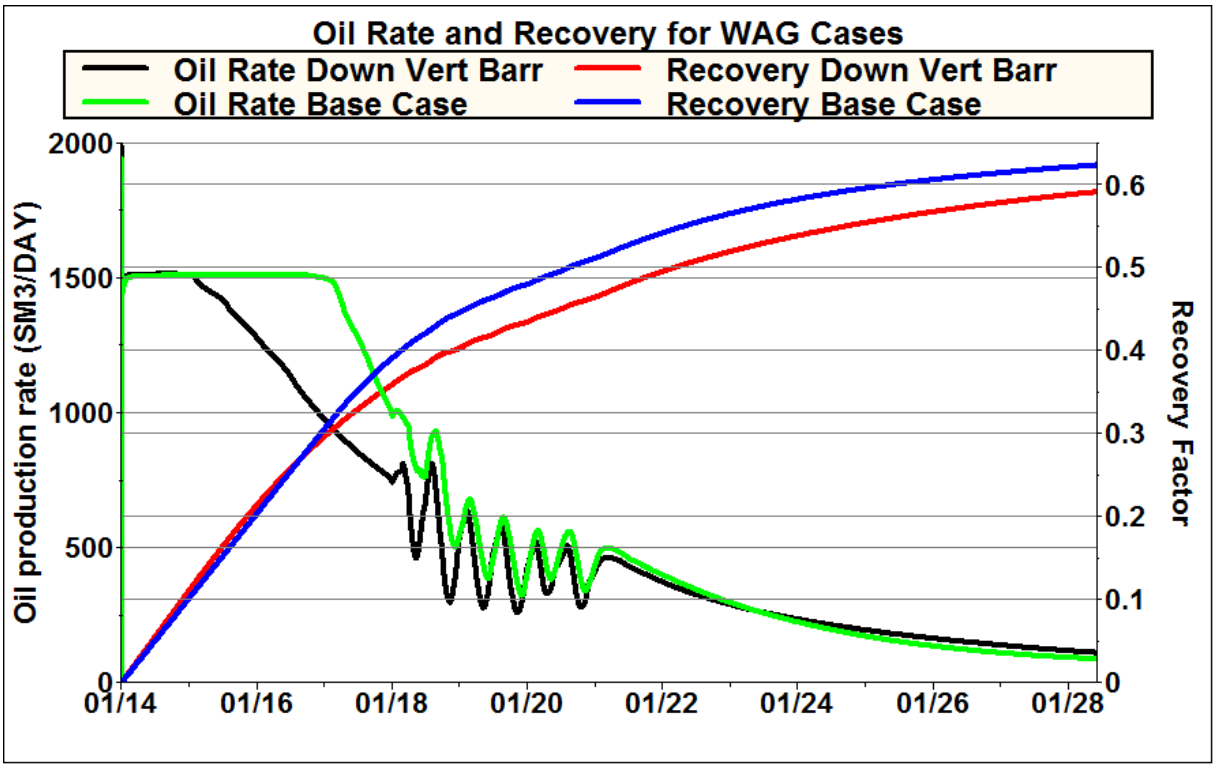

Figure 5-38 – Oil rate and oil recovery for the WAG base case and WAG downwards fining with vertical flow barrier case.

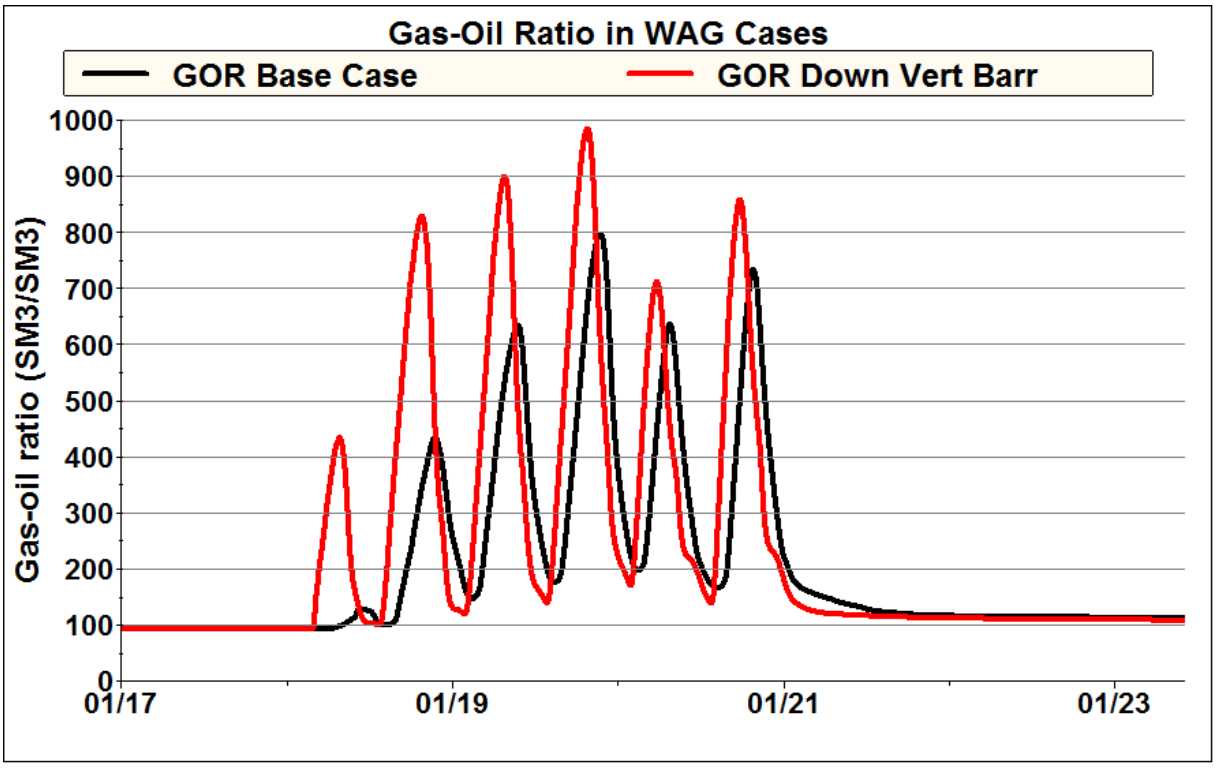

Figure 5-39 – Gas-oil ratio for the WAG base case and WAG downwards fining with vertical flow barrier case between 2017 and 2023.

5.4.5.1 Disabled Non-Neighbor Connections

Water and WAG cases of the downwards fining sequence with interbedded vertical flow barriers have been run with non-neighbor connections disabled. For further details see 4.4.5 and 6.2.5.

Disabling NNCs to keep the gas within the intended flow path did not have a large effect. Figure 5-40 shows the oil rate and oil recovery for the water and WAG downwards fining with vertical flow barrier cases with and without NNCs enabled and Figure 5-41 shows the GOR for the WAG cases. The recovery difference between the WAG cases was 0.06 % and 0.04 % for the water cases. The difference between waterflooding and WAG remained at 1.7 % for both instances. The GOR development did not change significantly, but the peaks are higher with NNCs disabled.

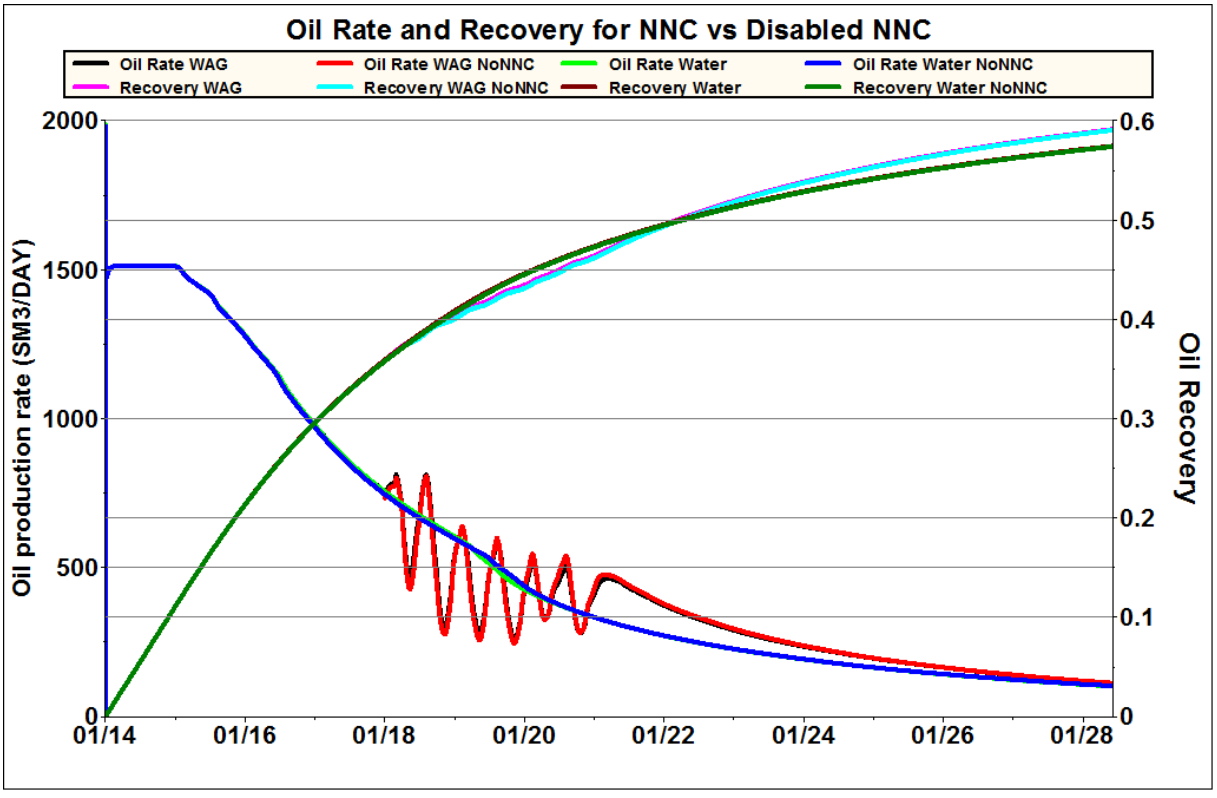

Figure 5-40 – Oil rate and oil recovery in downwards fining with vertical flow barrier cases with and without NNCs enabled.

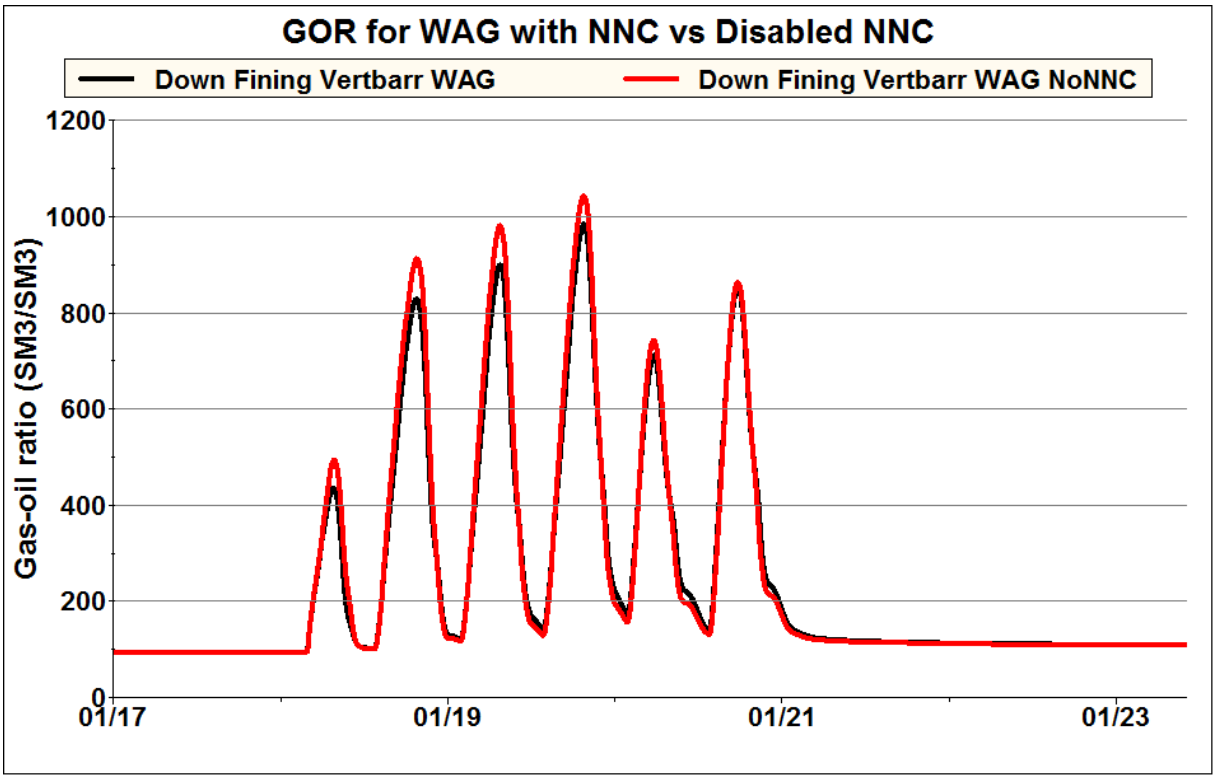

Figure 5-41 – Gas-oil ratio for the WAG downwards fining with vertical flow barrier case with and without NNCs enabled between 2017 and 2023.

6 Discussion

The discussion will first analyze the sensitivities and simulation setups individually to assess and explain the results. Then comparison of the cases and general trends are discussed.

6.1 Sensitivities

6.1.1 Relative Permeability Sensitivity

The base case has been run without hysteresis and with the WAGHYSTR keyword implemented. For a more detailed description see 4.3.1. Results are reported in 5.3.1. Hysteresis is only applied for the gas phase in the base case. Naturally the simulations are giving the same results until gas is introduced in the first WAG cycle. When there is no hysteresis on the gas phase the gas breakthrough in the first cycles are larger. This is according to expectations since only the critical gas saturation is trapped, while the remainder eventually will make its way to the producer. In the later cycles the gas breakthrough is delayed compared to the base case. The trapped gas will be mobilized in the base case and cause a rapid increase in relative gas permeability as gas saturation is increasing. Once water injection starts, the gas relative permeability will quickly drop to zero as the trapped gas saturation is reached. Consequently the GOR increases faster during the gas injection half cycle and drops off faster during the water injection half cycle in the base case, compared to without gas hysteresis.

When the WAGHYSTR keyword is included, the GOR behavior is similar to the base case, but a more extreme drop in GOR during the water injection half cycle is seen. Some of the explanation for this may be found in Figure 6-1, which shows the gas relative permeability in a selected block for the base case and the WAGHYSTR case. The gas relative permeability is generally slightly lower in the WAGHYSTR case and the imbibition is treated differently. This also causes the trapped gas saturation to be about 5 % higher in the WAGHYSTR case under the current maximum gas saturation, although the trapped gas saturation is equal if the cell reaches maximum possible gas saturation. The increased trapped gas saturation explains the reduced gas breakthrough in the first two WAG cycles. The linear behavior of the gas relative permeability curve in the WAGHYSTR case after the first two cycles could be the reason for the faster drop in later cycles. Once the gas relative permeability drops below 0.05 it drops

to zero over a shorter saturation interval than the base case. The water relative permeability in the same block for both cases is shown in Figure 6-2. The water relative permeability moves along the same curve (black) during primary imbibition, but when the gas is introduced the WAGHYSTR k_{rw} moves towards the three-phase curve. Although uncertain how this specifically affects the simulation, a possible interpretation is that the resulting reduced water mobility leads to quicker displacement of the free gas. If so it is another factor explaining the faster drop in GOR after each cycle in the WAGHYSTR case.

The WAGHYSTR case recovers 0.7 % additional oil while the “no hysteresis” case recovers 0.3 % less than the base case. The reduced water and gas relative permeabilities in the WAGHYSTR case will result in more favorable displacement of oil and can account for much of the incremental oil. Although residual oil saturation is not linked to trapped gas saturation in this case, trapped gas saturation will cause a slight increase in oil mobility because the residual oil to gas is lower than to water. The default Eclipse model for three-phase oil relative permeability is used, which assigns the gas-oil oil relative permeability to part of the oil in a cell with gas saturation. Since the gas-oil oil relative permeability is higher than the water-oil oil relative permeability, increased trapped gas saturation results in higher oil mobility.

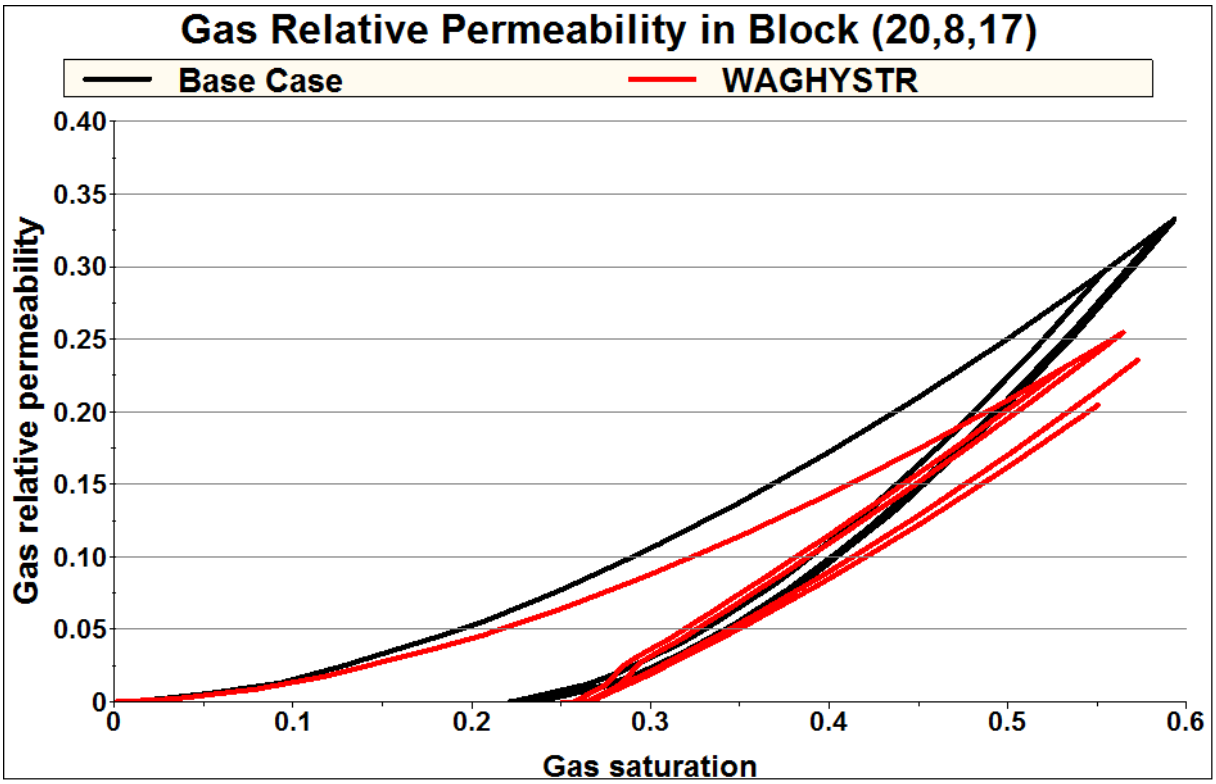

Figure 6-1 – Gas relative permeability in block (20, 8, 17) for the base case and WAGHYSTR case.

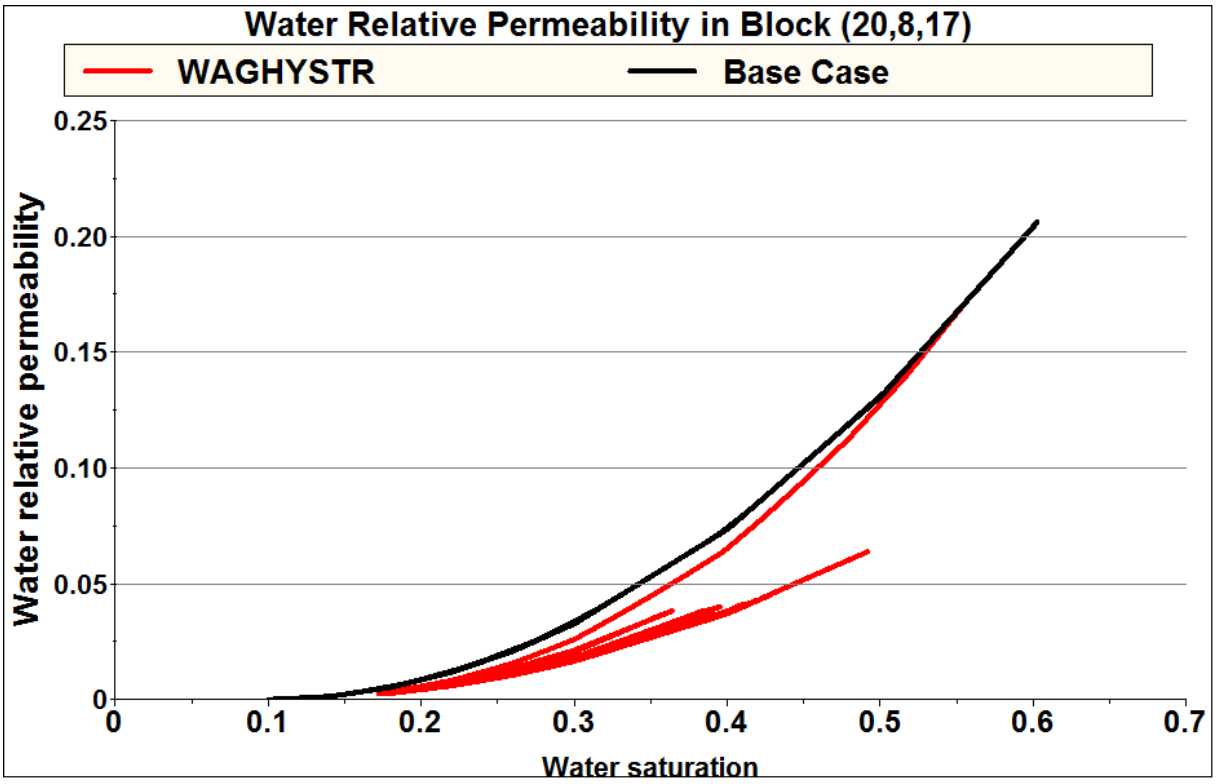

Figure 6-2 – Water relative permeability in block (20, 8, 17) for the base case and WAGHYSTR case.

6.1.2 Layer Thickness Sensitivity

The base case had a layer thickness of 1 m, but both WAG and water was run with 2 m and 4 m layer thickness. For more details on the setup see 4.3.2 and for results see 5.3.2. The small difference between the runs is remarkable and unexpected. The low vertical permeability could be one factor, by keeping the flow mostly in the layer where the injection occurs. Large differences in recovery were not expected, but thinner layers should create some differences in how the gas moves vertically and consequently in the GOR development. A closer look at the GOR development shows more differences than appears in Figure 5-7. At the end of the 4th gas injection on 1st October 2019, the GOR is 450 Sm^3/Sm^3 in the base case, 412 Sm^3/Sm^3 with layer thickness 2 m and 340 Sm^3/Sm^3 with layer thickness 4 m. The following GOR peak is at 23rd November for the base case, 2nd December for 2 m and 8th December for 4 m layer thickness. Gas flow to the production well is faster with thinner layers as one would expect, even if the overall shape is similar.

The secondary sensitivity with vertical injector gave similar results. The spread in WAG ultimate oil recovery is the same at 0.8 %, but the differences are more notable in the GOR development. Still the differences are not significant for the simulation results.

It would probably have been sufficient to use 2 m thick layers in the simulations to get satisfactory results, but it cannot be ruled out that layer thickness could have a larger influence in other simulation setups. Additionally the reduced layer thickness is not used to model the geology more accurately, the layers are simply repeated. More accurate modelling of the reservoir is required to make the effect of smaller cells more significant.

6.1.3 Oil Vaporization Sensitivity

The oil vaporization control parameter has been varied from 2 in the base case to 3 in the high case and 0.5 in the low case. For more details see 4.3.3 and for results see 5.3.3.

Increasing the oil vaporization control parameter from 2 to 3 did not make any noteworthy impact. This is as expected since oil vaporization into the gas is already quite inhibited by the base case constant of 2. Vaporization of oil is in other words not a large influence in the simulation and further reduction does not have significant effect. Increasing the impact of oil vaporization by reducing the parameter to 0.5 has more effect. The recovery factor is only increased by 0.34 %, but the best effect is seen when GOR is high. Since the gas can hold

more oil this is very natural. A too low control parameter is not recommended since the oil saturation can go to zero, or at least well below the defined residual oil saturation, in an area around the injector.

6.1.4 Production Rate Sensitivity

The base case production rate is 2000 Rm^3/day and the simulation has been run with production rates of 1500 Rm^3/day and 2500 Rm^3/day. For more details see 4.3.4 and for results see 5.3.4. WAG performance and behavior is similar in the high rate case and the base case. WAG performs 0.3 % better for the high rate case than the base case. The higher rate results in a larger amount of injected gas and could be the cause for this increase. The base case reservoir has most of the high quality layers high in the reservoir and the increased rate can reduce the amount of gas that is allowed to migrate to the top layers. The low rate case allows more time for the gas to migrate to the top and has lower benefit from WAG. In hindsight it would have been an idea to adjust the cycle time to have a consistent PV of injected gas.

6.1.5 Vertical Permeability Sensitivity

The base case vertical permeability is 0.01 of horizontal permeability. The simulation has been run with Kv/Kh of 0.05 and 0.1 additionally. For more details see 4.3.5 and for results see 5.3.5.

The injection well is horizontal and injects in the top layer in the heel and bottom level at the toe. Naturally an increased vertical permeability allows the water to migrate to additional layers and improves the reservoir sweep. Since the WAG schedule also injects water for most of the time the recovery is increased for these cases as well. However, the advantage of WAG dwindles as the vertical permeability increases. A high vertical permeability allows the gas to migrate very fast to the top of the reservoir. As a result, gas is able to contact less of the reservoir and the GOR development is more extreme. This is the main cause of the reduced WAG efficiency as vertical permeability increases. In other cases, where permeable units are on the bottom, gas can be unable to migrate to the top layers under a regime of very low vertical permeability and higher vertical permeability can be advantageous to WAG performance.

6.2 Stratification Sequences

6.2.1 Nansen and Eiriksson 2 Switch

In this setup the Nansen and Eiriksson 2 units are switched. See 4.4.1 for more details and 5.4.1 for results. The highly permeable Nansen unit is now placed lower in the reservoir, which allows the gas injected in this unit to migrate up in the reservoir, instead of directly breaking through at the producer. Comparison of the waterflood base case and Nansen switch case shows the water breaks through faster in the Nansen switch case. The current well setup has a well distance between injector and producer of 1000 m at the heel of the injector and 550 m at the toe. The result is that well distance at the perforations in the highly permeable Nansen layer is less for the Nansen switch case than the base case. Figure 6-3 shows the water saturation in the Nansen switch water case in 2016 and clearly the water breaks through in the Nansen unit first.

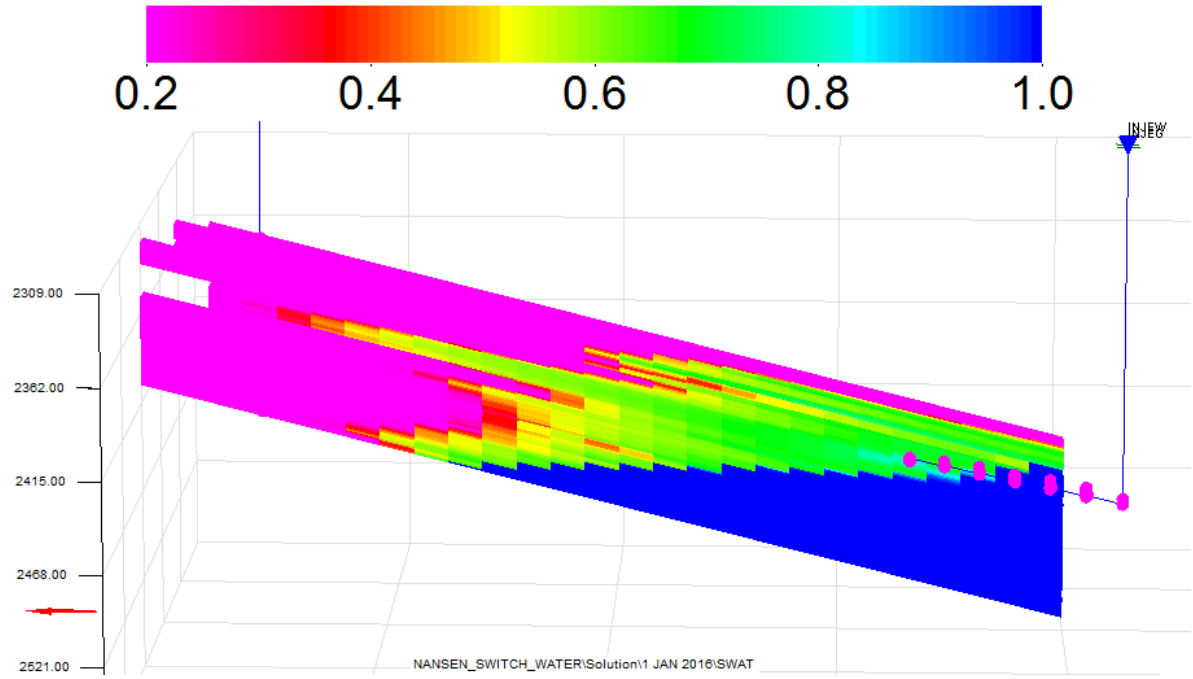

Figure 6-3 – Water saturation in XZ slice with Y=12 at 1 Jan 2016 in Nansen switch.

Placing the Nansen unit further down was expected to increase the efficiency of WAG since the gas would not be trapped in the top layer in the Nansen unit and cause massive gas breakthrough. That turned out to be an incorrect expectation. Gas breakthrough is even faster and larger than the base case and the gas is still mainly flowing in the top layer of the Nansen unit. The low vertical permeability does not allow gas to move away from this very permeable layer and combined with the reduced well distance this causes faster gas

breakthrough. After the 3rd gas cycle at 1st October 2019 the GOR is 558 Sm^3/Sm^3 of which about 100 Sm^3/Sm^3 is solution gas. 65 % of the produced gas is from the top layer in the Nansen unit at a GOR of 3000 Sm^3/Sm^3. The bottom layer in the Eiriksson 2 unit, directly above the gas producing Nansen layer, shows some indications of free gas production at a GOR of 250. However, the volumes are limited and the next layer is producing at solution gas GOR, clearly demonstrating that the gas has not been able to contact as much of the reservoir as hoped. The combination of gas accumulating in the Nansen top layer and the reduced well distance for this layer is causing the faster breakthrough.

6.2.2 Downwards Fining

In this setup the layers are sorted by average permeability with the most permeable layer on top. See 4.4.2 for more details and 5.4.2 for results.

A downwards fining sequence is expected to be the least favoring for WAG injection. The majority of the gas will be injected in the upper, high quality layers and the gas can quickly move to the top layer. The result is a small contact volume and fast breakthrough of gas. WAG in this setup is indeed less effective than the base case, but the difference is not as large as expected. WAG has ultimate recovery 1.9 % over the water case in this setup, compared to 2.3 % in the base case. Figure 6-4 confirms that gas does not contact much of the reservoir in the area where gas is injected high in the reservoir. Except for the top layer, gas saturation is barely above the critical gas saturation. Where gas is injected in the lower quality layers deeper in the formation, the gas is able to contact much more of the reservoir. Figure 6-5, a slice where gas is injected deeper in the reservoir, shows that the gas is able to contact more of the reservoir in this area. Gas does not reach the top layer as a consequence of three combined factors: The vertical permeability is very low, one layer has a very heterogeneous permeability distribution and the amount of gas injected in this area is limited. The layer in question has high permeability around the injector, but is nearly impermeable around the producer. As a result the average permeability is high and the layer is placed fairly high in the formation. The absence of this layer would in this case probably lead to better vertical sweep, but in combination with higher vertical permeability it could result in reduced vertical sweep.

The GOR development, shown in Figure 5-27, clearly shows that gas breaks through faster and in large volume in the downwards fining case. Especially in the first three cycles gas production is significantly larger than the base case. This is expected, since most of the gas is injected in high quality layers close to the top of the formation where gas contacts a small fraction of the reservoir volume.

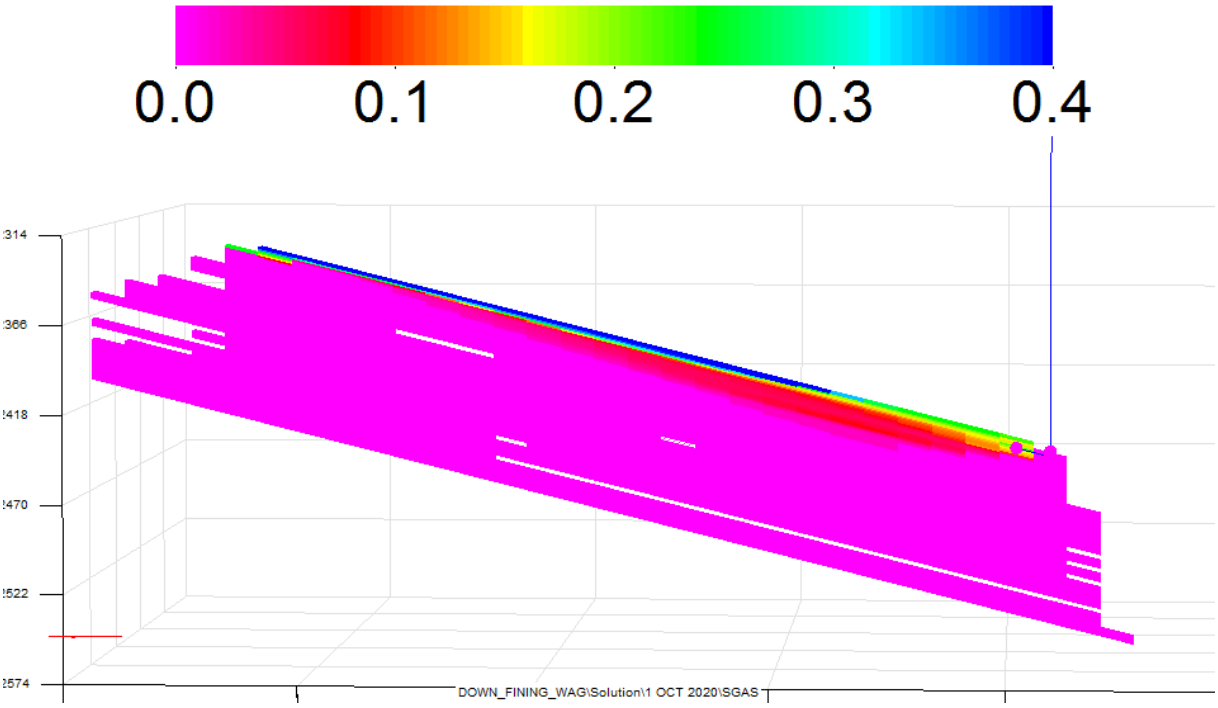

Figure 6-4 – Gas saturation at 1 October 2020 in downwards fining WAG in XZ slice Y=7.

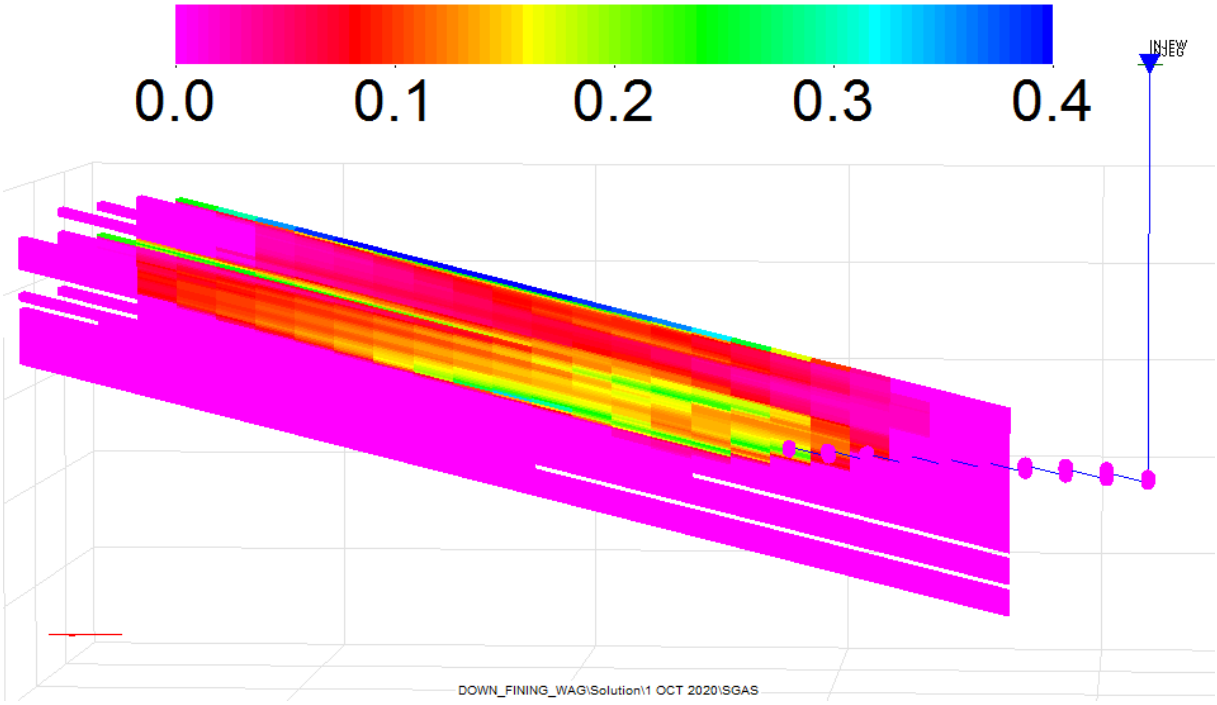

Figure 6-5 – Gas saturation at 1 October 2020 in downwards fining WAG in XZ slice Y=15.

6.2.3 Upwards Fining

In this setup the layers are sorted by average permeability with the least permeable layer on top. See 4.4.3 for more details and 5.4.3 for results.

An upwards fining sequence is expected to be very favorable to WAG, because the gas will be able to move away from the highly permeable layers, delaying and reducing gas breakthrough and increasing the vertical sweep. WAG did perform marginally better in this scenario, but only 0.1 % better than the base case at 2.4 % incremental recovery. Figure 6-6 shows that the gas is not able to reach the top of the reservoir. This is mainly because of the low vertical permeability and the layer discussed in 6.2.2. In the middle of the reservoir there is a large accumulation of gas blocked by this layer. Most of the gas is injected in the toe of the well. In this section of the well the distance to the producer is only 500 m, meaning there is a reduced volume available for gas sweep compared to the base case. In the base case most of the gas is injected in the heel of the injection well where the distance to the producer is around 1000 m. The well placement of the producer is sub-ideal in this and several of the other cases.

The gas breakthrough is faster than the base case in the first two cycles, mainly due to the reduced distance between the main injection point and the producer. In the later cycles the peaks are lower and the drop-off slower. This is natural as the base case gas does not contact significant new volumes in the later cycles, while the upwards fining case have some movement into shallower layers.

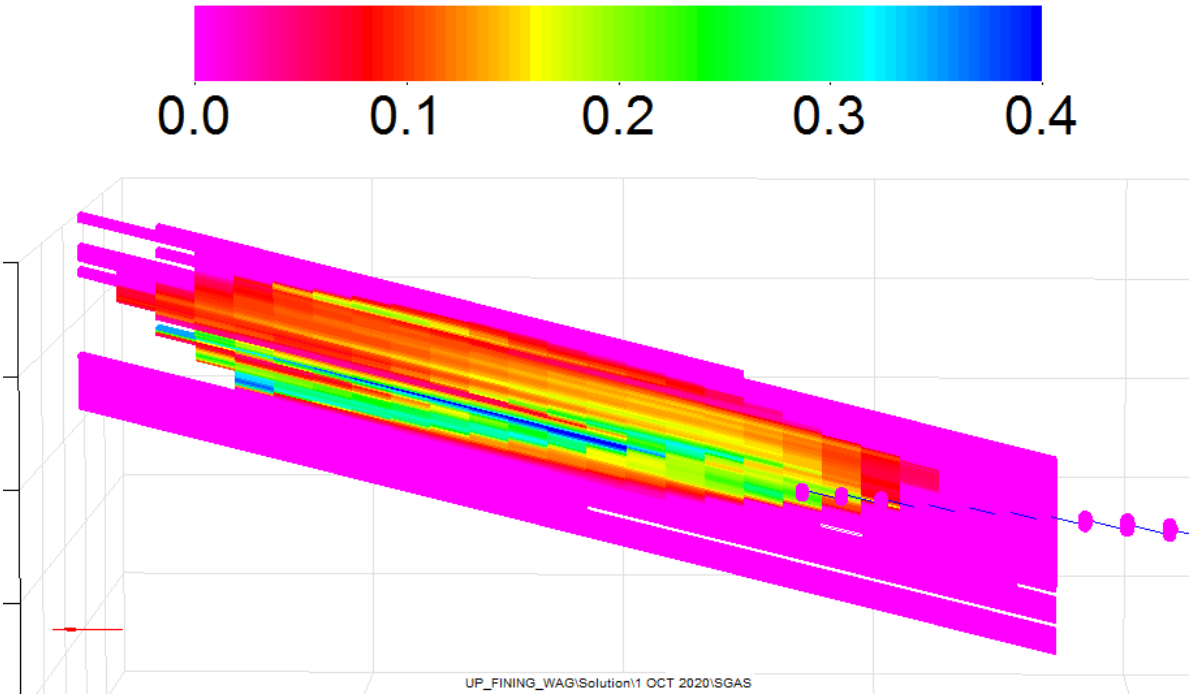

Figure 6-6 – Gas saturation at 1 October 2020 in upwards fining WAG in XZ slice Y=16.

6.2.4 Upwards Fining with Interbedded Vertical Flow Barriers

The "upwards fining with interbedded vertical flow barriers" setup contains four units that are upwards fining. See 4.4.4 for more details and 5.4.4 for results. The cases with upwards and downwards fining sequences with interbedded vertical flow barriers should be more comparable with each other, as highly permeable layers are placed within each unit. With the horizontal injector the gas and water will be injected more evenly over the perforation length and will not be as affected by the varying distance between producer and injector. On the other hand the low quality layers bounding each unit do not allow much flow across, so the gas is mostly contained within the unit it is injected. Figure 6-7 shows a slice where gas injection is in the bottom unit. Some gas has made its way to the unit above, but judging by the very low gas saturation in the layers between the units, it is more likely that most of this gas has moved laterally from the injection point in the upper unit.

The GOR fluctuates less in this setup than in the base case. This is expected behavior as gravity moves gas to the upper layers of each unit, where reservoir quality is worse. The gas in these layers will move slowly to the producer lower peaks and shallower valleys in the GOR development. Due to the low vertical permeability and high permeability contrast most of the free gas is still produced through the high quality layer at the bottom of the unit,

while the top layers in each unit produces close to or no free gas. This situation could change with a higher vertical permeability.

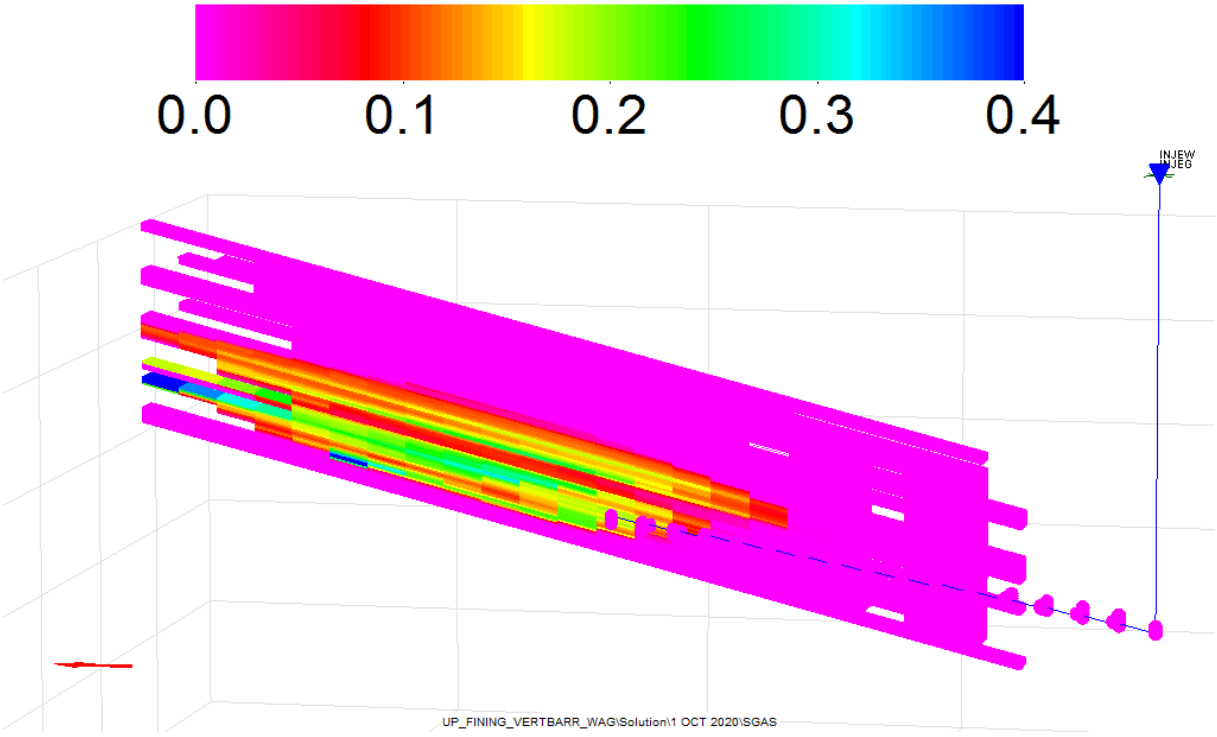

Figure 6-7 – Gas saturation in upwards fining WAG with interbedded vertical flow barriers in XZ slice Y=22 at 1 October 2020.

6.2.5 Downwards Fining with Interbedded Vertical Flow Barriers

This setup contains four units that are downwards fining. See 4.4.5 for more details and 5.4.5 for results.

Oil recovery by waterflooding is expected to increase for this setup compared to the opposite setup, because most of the water will be injected at the top of each unit and can move down to displace oil in the lower quality layers. This is also the case as the recovery in the downwards setup is 3.4 % higher than the upwards setup. WAG efficiency is expected to decrease, since most of the gas is injected at the top of the unit with limited possibility to move up. This expectation is also met as WAG efficiency in this setup is 1.7 % against 2.6 % in the opposite setup. Figure 6-8 shows the gas saturation at the end of the last gas cycle. The gas mostly stays within the top layer of each unit, but small volumes are migrating to the units above. Overall the vertical sweep is poor. Figure 6-9 shows the gas saturation in slice Y=11. This area has better vertical sweep in the top section of the reservoir, caused by unintended non-neighbor connections (NNCs) created over cells made inactive by the

MINPV keyword. The simulations could easily have been re-run to correct this error, but this would require re-graphing and re-writing of all the results. The error is not believed to have much influence in the other setups as the layer with the majority of deactivated cells is surrounded by low quality layers, generating low transmissibility over the connection. The exception is this setup, where the inactive layer is positioned between a high and low quality layer, and the upwards fining sequence with interbedded vertical flow barriers, where this layer is on top and no NNC is created over the inactive layer.

The simulations with NNCs disabled showed that the reduced gas sweep did not affect the simulation results significantly. GOR peaked slightly higher as can be expected when the gas is unable to move up in the layers. Since this setup is most likely the setup affected most by this error, it is assumed that it would not influence the other setups in any notable manner.

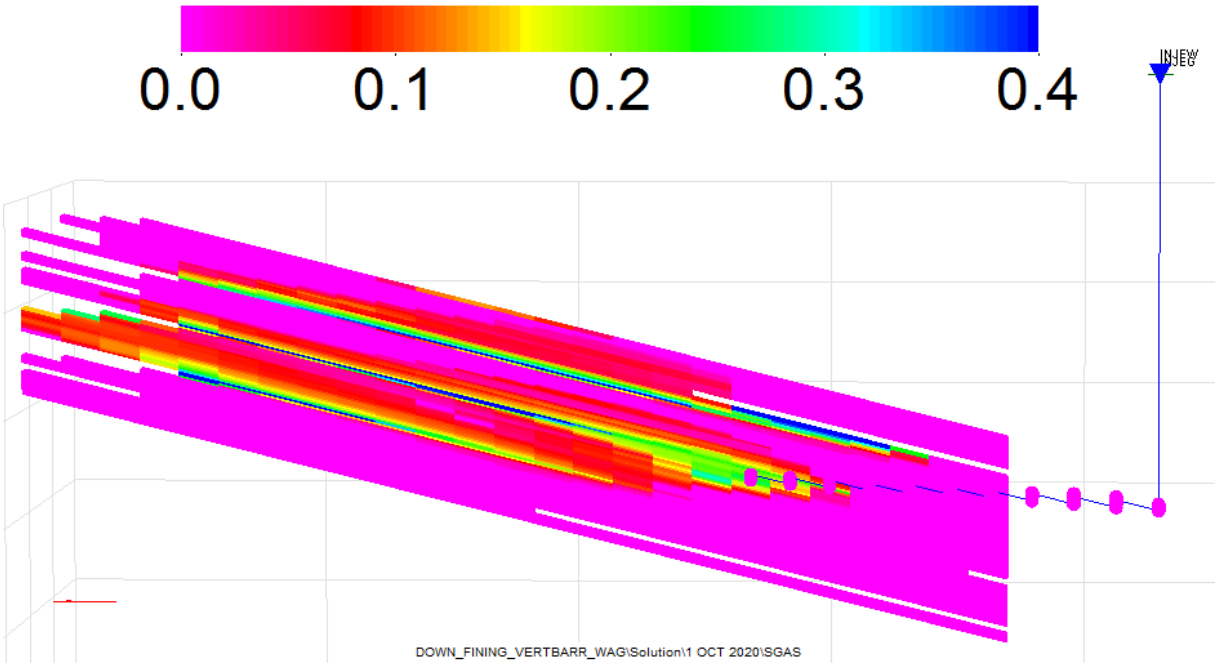

Figure 6-8 – Gas saturation in downwards fining WAG with interbedded vertical flow barriers in XZ slice Y=16 at 1 October 2020.

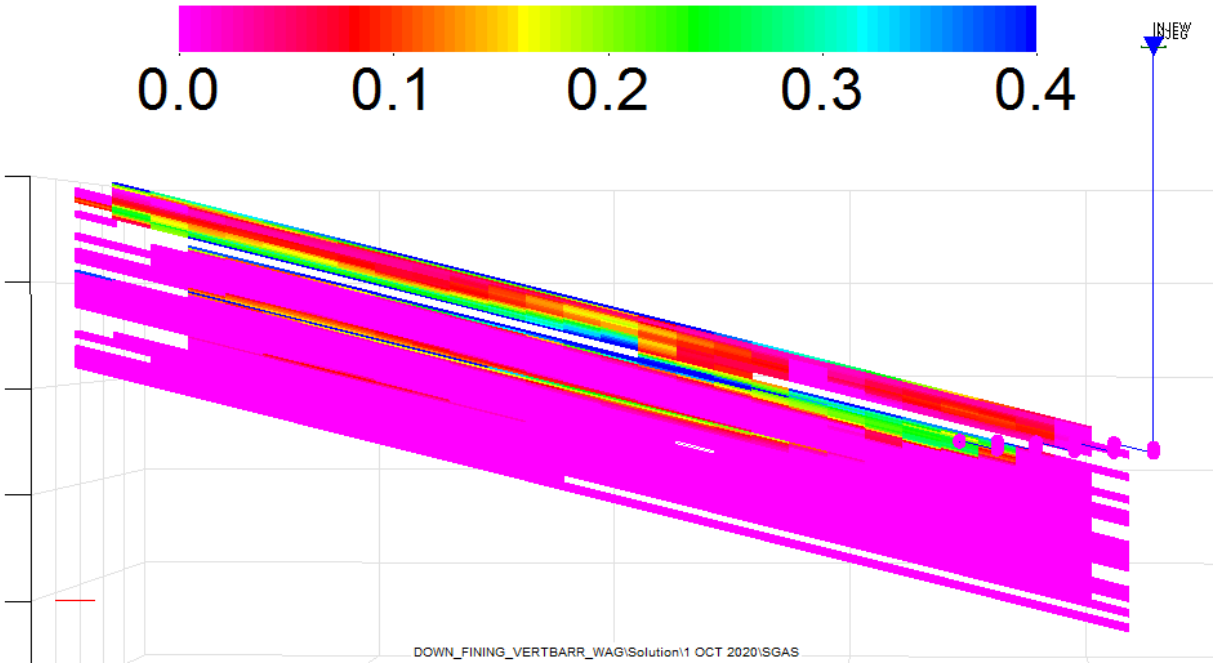

Figure 6-9 – Gas saturation in downwards fining WAG with interbedded vertical flow barriers in XZ slice Y=11 at 1 October 2020.

6.3 General Remarks on Results

6.3.1 Sensitivities

Of the five sensitivities run, only relative permeability hysteresis and vertical permeability has a large impact on recovery. Relative permeability hysteresis does not impact water floods, but it does affect the efficiency of a WAG process. In particular the GOR development is very different for each case and obtaining a history match without an accurate hysteresis model can be difficult. The vertical permeability has a large effect on waterflood, as the increased vertical permeability allows water to sweep more of the reservoir. In the WAG cases, increased vertical permeability had a negative effect, although the ultimate recovery increased from the waterflood part of the simulation. It would be interesting to see the effect of higher vertical permeability in other setups than the base case. In the upwards fining sequence almost no gas was able to reach the top of the reservoir and an increase in vertical permeability could have increased both recovery by waterflood and additional recovery of WAG. Obviously vertical permeability plays a large role when heterogeneities and fluids of different densities are involved.

6.3.2 Stratification Sequences

The general trend of the results is that WAG is more efficient in an upwards fining environment than a downwards fining environment. However the differences are not as big as expected. All setups showed additional WAG recovery between 1.5 and 3.0 %. The upwards and downwards fining setups are more complex to analyze because the lateral extension of the main gas influenced area varies between the cases. The main injection section is seen in Figure 6-10 for the upwards fining and downwards fining case. Despite the reduced impact area of gas in the upwards fining case the incremental recovery is higher than the downward fining case.

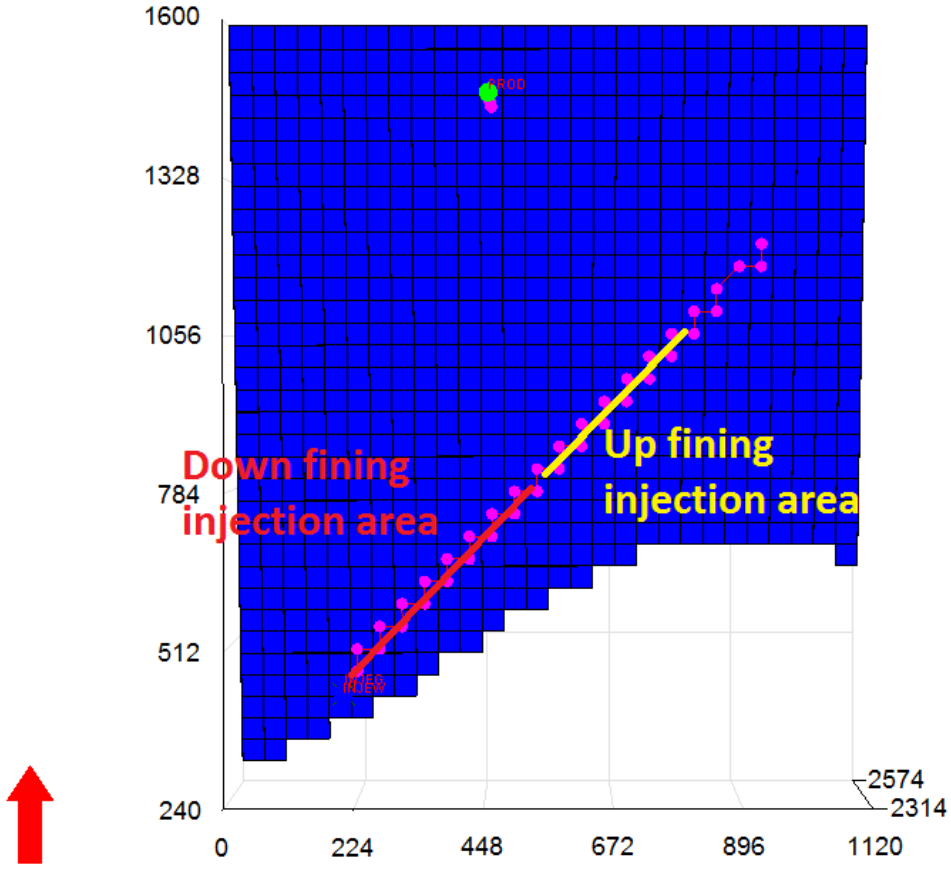

Figure 6-10 – Main injection intervals for downwards and upwards fining setups.

In the setups with four units upwards or downwards fining the high quality layers are distributed evenly over the entire formation. Consequently injection occurs over the entire perforation interval and the difference in sweep area between upwards and downwards fining is minor. The upwards fining setup with interbedded vertical flow barriers recovers 1 % more oil from WAG over waterflooding than the downwards fining case. This may not sound like much, but considering the downwards fining WAG case recovers 1.7 % more than

the water case, WAG is 50 % more effective in an upwards fining environment. In the single unit upwards and downwards fining cases WAG is also 25 % more effective in the upwards fining environment despite the areal differences.

A downwards fining setup is better for a pure waterflood because water is denser than the oil and will seek down in the lower quality layers. Since the waterflood recovery is higher there is less residual oil available for WAG extraction.

WAG still recovers more oil than waterflooding in a downwards fining environment. In a waterflood most of the water flows in the high permeable layers. In the single unit downwards fining setup nearly 60 % of the produced reservoir volume is produced through the top three layers in the water case in 2024. The trapped gas in the WAG case is mostly in the top layers and will somewhat limit the flow in these layers by reducing the water saturation and the water relative permeability. This diverts more of the water to the lower and not as well swept layers. The flow through the top three layers are only reduced by 1.4 % from 57.4 to 56 % of the total flow in the WAG case, but a higher oil rate in these layers means the water rate is reduced by 4 %. Although this effect is likely only a minor contributor to the increased recovery it should not be ignored. The effect could also be larger in reservoirs with very dominating high streaks. This effect could be under predicted because decrease in water relative permeability in three-phase zones is not included in these simulations. This effect is discussed in 2.2.3.

The downwards fining sequences are plagued by very fast breakthrough of gas and the gas is produced over a short time frame. It is possible that equivalent benefit could be achieved with a smaller amount of gas if, for instance, the gas injection period was reduced to one month. If this is the case, WAG in downwards fining sequences is not necessarily 25-50 % less profitable than upwards fining sequences as long as the gas has sales value (i.e. an export option exists).

7 Conclusion

- WAG provides additional recovery over waterflood for all setups investigated in this study.
- WAG is 25-50 % more efficient in an upwards fining sequence than a downwards fining sequence under the circumstances investigated in this study. The cause is a combination of gas sweep efficiency, amount of residual oil available for WAG extraction and reduced gas breakthrough.
- Vertical permeability plays an important role in the segregation of fluids and thus also in a WAG process. Different vertical permeability had a large impact on the results in the base case and effects of similar magnitude are expected in the other setups. Further investigation is recommended.
- Fast and significant breakthrough of gas is seen in all cases. Heterogeneities and channeling is an issue for WAG processes even in otherwise favoring geological structures, i.e. upwards fining sequences.

8 Recommendations for Further Work

8.1 Possible Improvements

In hindsight it is always easy to see that some things should or could have been done differently. That is also the case for this study. Three elements have been identified that could have been solved in a different way.

8.1.1 Well setup

The horizontal injector was necessary to enable gas injection in all units. However the placement of the producer was too focused on the optimal solution in the base case. The injector toe being closer to the producer than the injector heel was only beneficial in the base case because most of the fluids were injected in the heel. That way water and gas from the heel and toe broke through at approximately the same time. In other cases, most notably the upwards fining case, most of the injection was in the toe, making gas and water break through much faster and reducing the possible lateral extension of gas sweep. The producer should have been placed further into the corner of the grid to achieve a more even distance from the producer to every part of the injector.

8.1.2 WAG schedule

In several of the setups the gas breaks through within a month. Continuous gas injection for three months leads to a significant gas breakthrough and a subsequent decline in production rate during the breakthrough period. An option is to shorten the gas injection periods and instead continue the WAG period over a longer time. The large breakthroughs of gas repeated every six months delay the incremental oil production until after the WAG period. This would be unacceptable in a real field application if WAG both required up-front capital investment and delayed the oil production. Ideally the WAG schedule and well placement would be optimized for each setup, but this requires significant time and resources. A schedule with shorter gas injection periods and/or longer water injection periods would not be ideal in some of the setups, but would at least reduce the issue of massive gas breakthrough in the downwards fining cases.

8.1.3 Vertical Permeability

The vertical permeability is low, being 0.01 of the horizontal permeability. A higher vertical permeability had major impact on the recovery in the base case and it would be interesting to see the effect in the other setups. Clearly vertical permeability is an important factor in WAG application and the results could change with higher vertical permeability. In the Nansen switch case and the upwards fining cases, increased vertical permeability could increase WAG recovery, while in the base case and downwards fining cases it could reduce the WAG recovery. WAG recovery is certainly reduced with increased vertical permeability in the base case (see 5.3.5).

8.2 Future Work

WAG as an EOR method is considered a mature technology, both onshore and offshore. However, uncertainties persist and WAG continues to be researched all over the world. A natural continuation of this study would be a further investigation into the effect of vertical permeability on upwards and downwards fining sequences.

The model in this study is mainly built on theoretical assumptions and is not backed by experimental data. To ensure more accurate flow description, laboratory experiments can be used in combination with simulations. Three-phase core floods are particularly important to get accurate flow description in WAG floods. Compositional fluid description is preferred in WAG simulations due to the ability to model mass exchange between the gas and oil. A compositional model is recommended for future work.

9 Nomenclature

API	American Petroleum Institute
bara	bar Absolute
BHP	Bottom Hole Pressure
C	Land's Constant
°C	Degrees Celcius
EOR	Enhanced Oil Recovery
FAWAG	Foam Assisted Water Alternating Gas
FVF	Formation Volume Factor
GOC	Gas Oil Contact
GOR	Gas-Oil Ratio
HC	Hydrocarbon
IFT	Interfacial Tension
IWAG	Immiscible Water Alternating Gas
k_h	Horizontal Permeability
k_{rg}	Gas Relative Permeability
$k_{rg,max}$	Gas Relative Permeability at Maximum Gas Saturation
k_{ro}	Oil Relative Permeability
$k_{ro,max}$	Oil Relative Permeability at Maximum Oil Saturation
k_v	Vertical Permeability
k_{rw}	Water Relative Permeability
$k_{rw,max}$	Water Relative Permeability at Residual Oil Saturation
MCM	Multicontact Miscibility
mD	MilliDarcy
MMP	Minimum Miscible Pressure
MMSTB	Million Stock Tank Barrels
MWAG	Miscible Water Alternating Gas
N/G	Net/Gross
n^g	Corey Exponent for Gas

n^o	Corey Exponent for Oil
n^w	Corey Exponent for Water
NNC	Non-Neighbor Connection
NTNU	Norwegian University of Science and Technology
OWC	Oil Water Contact
psia	Pounds per Square Inch Absolute
PV	Pore Volume
PVT	Pressure-Volume-Temperature
Rm^3	Reservoir Cubic Meter
Rs	Solution Gas in Oil
Rv	Vaporized Oil in Gas
Sm^3	Standard Cubic Meter
S_g	Gas Saturation
S_{gc}	Critical Gas Saturation
S_{gi}	Initial Gas Saturation
S_{go}	Maximum Trapped Gas Saturation
S_{om}	Three-phase Residual Oil Saturation
S_{org}	Residual Oil Saturation to Gas
S_{orw}	Residual Oil Saturation to Water
STOOIP	Stock Tank Original Oil in Place
S_w	Water Saturation
SWAG	Simultaneous Water Alternating Gas
S_{wc}	Connate Water Saturation
THP	Tubing Head Pressure
WAG	Water Alternating Gas

10 Bibliography

Abdallah, W., Buckley, J., Carnegie, A., Edwards, J., Herold, B., Fordham, E., . . . Ziauddin, M. (2007). Fundamentals of Wettability. *Oilfield Review*(Summer), 44-61.

Ahmadloo, F., Ashgari, K., & Jamaloei, B. (2009). Experimental and Theoretical Studies of Three-Phase Relative Permeability. *SPE Annual Technical Conference and Exhibition.* New Orleans, Loisiana, USA: Society of Petroleum Engineers. doi:http://dx.doi.org/10.2118/124538-MS

Awan, A., Teigland, R., & Kleppe, J. (2008). A Survey of North Sea Enhanced-Oil-Recovery Projects Initiated During the Years 1975 to 2005. *SPE Reservoir Evaluation & Engineering, 11*(03), 497-512. doi:http://dx.doi.org/10.2118/99546-PA

Baker, L. (1988). Three-Phase Relative Permeability Correlations. *SPE Enhanced Oil Recovery Symposium.* Tulsa, Oklahoma, USA: Society of Petroleum Engineers. doi:http://dx.doi.org/10.2118/17369-MS

Beggs, H. D., & Robinson, J. R. (1975). Estimating the Viscosity of Crude Oil Systems. *Journal of Petroleum Technology, 27*(09), 1140-1141. doi:http://dx.doi.org/10.2118/5434-PA

Braun, E., & Holland, R. (1995). Relative Permeability Hysteresis: Laboratory Measurements and a Conceptual Model. *SPE Reservoir Engineering, 10*(03), 222-228. doi:http://dx.doi.org/10.2118/28615-PA

Brodie, J. A., Zhang, P., Hetland, S. M., Moulds, T. P., & Jhaveri, B. (2012). BP North Sea Gas Injection Projects: Sustaining Offshore Production. *Abu Dhabi International Petroleum Conference and Exhibition.* Abu Dhabi: Society of Petroleum Engineers. doi: http://dx.doi.org/10.2118/161189-MS

Carlson, F. (1981). Simulation of Relative Permeability Hysteresis to the Nonwetting Phase. *SPE Annual Technical Conference and Exhibition.* San Antonio, Texas, USA: Society of Petroleum Engineers. doi:http://dx.doi.org/10.2118/10157-MS

Chew, J.-N., & Connally, C. A. (1959). A Viscosity Correlation for Gas-Saturated Crude Oils. *Petroleum Transactions, 216*, 23-25. Retrieved March 9, 2015, from www.onepetro.org

Christensen, J., Stenby, E., & Skauge, A. (1998). Review of WAG Field Experience. *International Petroleum Conference and Exhibition of Mexico.* Villahermosa, Mexico: Society of Petroleum Engineers. doi: http://dx.doi.org/10.2118/39883-MS

Corey, A., Rathjens, C., Henderson, J., & Wyllie, M. (1956). Three-Phase Relative Permeability. *Journal of Petroleum Technology, 8*(11), 63-65. doi:http://dx.doi.org/10.2118/737-G

Cosentino, L. (2001). *Integrated Reservoir Studies.* Paris, France: Editions Technip.

Crogh, N. A., Eide, K., & Morterud, S. (2002). WAG Injection at the Statfjord Field, A Success Story. *European Petroleum Conference.* Aberdeen, United Kingdom: Society of Petroleum Engineers. doi: http://dx.doi.org/10.2118/78348-MS

Donaldson, E. C., Chilingarian, G. V., & Yen, T. F. (1989). *Enhanced Oil Recovery II: Processes and Operations.* Amsterdam, NLD: Elsevier Science & Technology. Retrieved from www.ebrary.com

Donnez, P. (2007). *Essentials of Reservoir Engineering.* Paris, France: Editions Technip.

Element, D., Masters, J., Sargent, N., Jayasekera, A., & Goodyear, S. (2003). Assessment of Three-Phase Relative Permeability Models Using Laboratory Hysteresis Data. *SPE International Improved Oil Recovery Conference in Asia Pacific.* Kuala Lumpur, Malaysia: Society of Petroleum Engineers. doi:http://dx.doi.org/10.2118/84903-MS

Glasø, Ø. (1980). Generalized Pressure-Volume-Temperature Correlations. *Journal of Petroleum Technology, 32*(05), 785-795. doi:http://dx.doi.org/10.2118/8016-PA

Goda, H., & Behrenbruch, P. (2004). Using a Modified Brooks-Corey Model to Study Oil-Water Relative Permeability for Diverse Pore Structures. *SPE Asia Pacific Oil and Gas Conference and Exhibition.* Perth, Australia: Society of Petroleum Engineers. doi: http://dx.doi.org/10.2118/88538-MS

Green, D. W., & Willhite, P. G. (1998). *SPE Textbook Series, Volume 6: Enhanced Oil Recovery.* Richardson, TX, USA: Society of Petroleum Engineers. Retrieved from http://www.ebrary.com

Haadjizadeh, M., Narayanan, R., & Waldren, D. (2001). Modeling Miscible WAG Injection EOR in the Magnus Field. *SPE Reservoir Simulation Symposium.* Houston, Texas, USA: Society of Petroleum Engineers. doi: http://dx.doi.org/10.2118/66378-MS

Hall, K. L., & Yarborough, L. (1977). A New Equation of State for Z-factor Calculations. *SPE Reprint Series No. 13, 1*, 227-235.

Hamon, G., Suzanne, K., Billiotte, J., & Trocme, V. (2001). Field-Wide Variations of Trapped Gas saturation in Heterogeneous Sandstone Reservoirs. *SPE Annual Technical Conference and Exhibition.* New Orleans, Louisiana, USA: Society of Petroleum Engineers. doi:http://dx.doi.org/10.2118/71524-MS

Holm, L. (1986). Miscibility and Miscible Displacement. *Journal of Petroleum Technology, 38*(08), 817-818. doi:http://dx.doi.org/10.2118/15794-PA

Holmgren, C., & Morse, R. (1951). Effect of Free Gas Saturation on Oil Recovery by Water Flooding. *Journal of Petroleum Technology, 3*(05), 135-140. doi:http://dx.doi.org/10.2118/951135-G

Instefjord, R., & Todnem, A. C. (2002). 10 Years of WAG Injection in Lower Brent at the Gullfaks Field. *European Petroleum Conference.* Aberdeen, United Kingdom: Society of Petroleum Engineers. doi: http://dx.doi.org/10.2118/78344-MS

Keelan, D. K., & Pugh, V. J. (1975). Trapped-Gas Saturations in Carbonate Formations. *Society of Petroleum Engineers Journal, 15*(02), 149-160. doi:http://dx.doi.org/10.2118/4535-PA

Killough, J. (1976). Reservoir Simulation With History-Dependent Saturation Functions. *Society of Petroleum Engineers Journal, 16*(01), 37-48. doi:http://dx.doi.org/10.2118/5106-PA

Knudsen, T. W. (1999). The Gullfaks satellites: New subsea technology, start up and operational experience. *Offshore Europe Oil and Gas Exhibition and Conference.*

Aberdeen, UK: Society of Petroleum Engineers. doi:http://dx.doi.org/10.2118/56909-MS

Kralik, J., Manak, L., Jerauld, G., & Spence, A. (2000). Effect of Trapped Gas on Relative Permeability and Residual Oil Saturation in an Oil-Wet Sandstone. *SPE Annual Technical Conference and Exhibition.* Dallas, Texas, USA: Society of Petroleum Engineers. doi:http://dx.doi.org/10.2118/62997-MS

Lake, L. W. (1989). *Enhanced Oil Recovery.* Upper Saddle River, New Jersey: Prentice Hall.

Land, C. (1968). Calculation of Imbibition Relative Permeability for Two- and Three-Phase Flow From Rock Properties. *Society of Petroleum Engineers Journal, 8*(02), 149-156. doi:http://dx.doi.org/10.2118/1942-PA

Larsen, J., & Skauge, A. (1998). Methodology for Numerical Simulation With Cycle-Dependent Relative Permeabilities. *SPE Journal, 3*(02), 163-173. doi:http://dx.doi.org/10.2118/38456-PA

Larsen, J., & Skauge, A. (1999). Simulation of the Immiscible WAG Process Using Cycle-Dependent Three-Phase Relative Permeabilities. *SPE Annual Technical Conference and Exhibition.* Houston, Texas, USA: Society of Petroleum Engineers. doi:http://dx.doi.org/10.2118/56475-MS

Lee, A. L., Gonzalez, M. H., & Eakin, B. E. (1966). The Viscosity of Natural Gases. *Journal of Petroleum Technology, 18*(08), 997-1000. doi: http://dx.doi.org/10.2118/1340-PA

Leverett, M., & Lewis, W. (1941). Steady Flow of Gas-oil-water Mixtures through Unconsolidated Sands. *Transactions of the AIME, 142*(01), 107-116. doi:http://dx.doi.org/10.2118/941107-G

Lien, S., Lie, S., Fjellbirkeland, H., & Larsen, S. (1998). Brage Field, Lessons Learned After 5 Years of Production. *European Petroleum Conference.* The Hague, Netherlands: Society of Petroleum Engineers. doi: http://dx.doi.org/10.2118/50641-MS

Ma, T., & Youngren, G. (1994). Performance of Immiscible Water-Alternating-Gas (IWAG) Injection at Kuparuk River Unit, North Slope, Alaska. *SPE Annual Technical Conference*

and Exhibition. New Orleans, Loisiana, USA: Society of Petroleum Engineers. doi:http://dx.doi.org/10.2118/28602-MS

Naar, J., & Henderson, J. (1961). An Imbibition Model - Its Application to Flow Behavior and the Prediction of Oil Recovery. *Society of Petroleum Engineers Journal, 1*(02), 61-70. doi:http://dx.doi.org/10.2118/1550-G

Pejic, D., & Maini, B. (2003). Three-Phase Relative Permeability of Petroleum Reservoirs. *SPE Latin American and Caribbean Petroleum Engineering Conference.* Port-of-Spain, Trinidad and Tobago: Society of Petroleum Engineers. doi:http://dx.doi.org/10.2118/81021-MS

Saraf, D., Batycky, J., Jackson, C., & Fisher, D. (1982). An Experimental Investigation of Three-Phase Flow of Water-Oil- Gas Mixtures Through Water-Wet Sandstones. *SPE California Regional Meeting.* San Francisco, California, USA: Society of Petroleum Engineers. doi:http://dx.doi.org/10.2118/10761-MS

Schlumberger. (2011). *Eclipse Technical Description Version 2011.1.*

Schneider, F., & Owens, W. (1976). Relative Permeability Studies of Gas-Water Flow Following Solvent Injection in Carbonate Rocks. *Society of Petroleum Engineers Journal, 16*(01), 23-30. doi:http://dx.doi.org/10.2118/5554-PA

Sebastian, H., & Lawrence, D. (1992). Nitrogen Minimum Miscibility Pressures. *SPE/DOE Enhanced Oil Recovery Symposium.* Tulsa, Oklahoma, USA: Society of Petroleum Engineers. doi: http://dx.doi.org/10.2118/24134-MS

Sheng, J. J. (2013). *Enhanced Oil Recovery: Field Case Studies.* Lubbock, TX: Gulf Professional Publishing.

Skauge, A., & Larsen, J. (1994). Three-Phase Relative Permeabilitites and Trapped Gas Measurements Related to WAG Processes. *International Symposium of the Society of Core Analysists*, (p. 227.234). Stavanger, Norway.

Skauge, A., & Sorbie, K. (2014). Status of Fluid Flow Mechanisms for Miscible and Immiscible WAG. *SPE EOR Conference at Oil and Gas West Asia.* Muscat, Oman: Society of Petroleum Engineers. doi:http://dx.doi.org/10.2118/169747-MS

Slotte, P., & Stenmark, H. (1996). Snorre WAG pilot. In S. M. Skjæveland, & L. Hinderaker (Eds.), *RUTH: 1992-1995 Program Summary* (pp. 85-92). Stavanger: Norwegian Petroleum Directorate.

Stalkup, F. I. (1983). Status of Miscible Displacement. *Journal of Petroleum Technology, 35*(04), 815-826. doi:http://dx.doi.org/10.2118/9992-PA

Standing, M. B., & Katz, D. L. (1942). Density of Natural Gases. *Transactions of the AIME, 146*(01), 140-149. doi:http://dx.doi.org/10.2118/942140-G

Statoil. (2005). Gullfaks Satelitter med Fokus på Rimfaks Statfjord og Lunde. Bergen, Norway.

Stone, H. (1970). Probability Model for Estimating Three-Phase Relative Permeability. *Journal of Petroleum Technology, 22*(02), 214-218. doi:http://dx.doi.org/10.2118/2116-PA

Stone, H. (1973). Estimation of Three-Phase Relative Permeability and Redual Oil Data. *Journal of Canadian Petroleum Technology, 12*(04), 53-61. doi:http://dx.doi.org/10.2118/73-04-06

Sutton, R. P. (1985). Compressibility Factors for High-Molecular-Weight Reservoir Gases. *SPE Annual Technical Conference and Exhibition.* Las Vegas, Nevada, USA: Society of Petroleum Engineers. doi:http://dx.doi.org/10.2118/14265-MS

Sørbel, J. (2014). *Water Alternating Gas in Stratified Reservoirs.* Trondheim, Norway: NTNU.

Treiber, L., & Owens, W. (1972). A Laboratory Evaluation of the Wettability of Fifty Oil-Producing Reservoirs. *Society of Petroleum Engineers Journal*, 531-540. doi:http://dx.doi.org/10.2118/3526-PA

Vazquez, M., & Beggs, H. D. (1980). Correlations for Fluid Physical Properties. *Journal of Petroleum Technology, 32*(06), 968-970. doi:http://dx.doi.org/10.2118/6719-PA

Wu, R., & Batycky, J. (1990). Evaluation of Miscibility from Slim Tube Tests. *Journal of Canadian Petroleum Technology, 29*(06). doi:http://dx.doi.org/10.2118/90-06-06

Zhang, P., Brodie, J., Daae, V., Erbas, D., & Duncan, E. (2013). BP North Sea Miscible Gas Injection Projects Review. *SPE Offshore Europe Oil and Gas Conference and*

Exhibition. Aberdeen, United Kingdom: Society of Petroleum Engineers. doi:http://dx.doi.org/10.2118/166597-MS

Appendix A. Relative Permeability Tables and Graphs

Appendix A.1 Nansen Unit

Table 1 – Nansen oil-water relative permeability

Sw	Krw	Kro
0.1	0	1
0.14	0.001	0.838
0.18	0.005	0.695
0.22	0.012	0.569
0.26	0.021	0.459
0.3	0.033	0.364
0.4	0.073	0.187
0.5	0.131	0.079
0.6	0.204	0.023
0.7	0.294	0.003
0.8	0.400	0
1	1	0

Table 2 – Nansen drainage gas-oil relative permeability

S liq	Krg	Kro
0.24	0.5	0
0.3	0.4367	0.0005
0.35	0.3865	0.0030
0.4	0.3386	0.0093
0.45	0.2931	0.0211
0.5	0.2501	0.0400
0.55	0.2098	0.0679
0.6	0.1721	0.1063
0.65	0.1373	0.1570
0.7	0.1056	0.2217
0.75	0.0771	0.3022
0.8	0.0521	0.4001
0.9	0.0142	0.6549
0.98	0	0.9231
1	0	1

Table 3 – Nansen imbibition gas-oil relative permeability

S liq	Krg	Kro
0.24	0.5000	0
0.3	0.3998	0.0005
0.35	0.3229	0.0030
0.4	0.2523	0.0093
0.45	0.1885	0.0211
0.5	0.1319	0.0400
0.55	0.0832	0.0679
0.6	0.0435	0.1063
0.65	0.0144	0.1570
0.7	0	0.2217
0.75	0	0.3022
0.8	0	0.4001
0.85	0	0.5171
0.9	0	0.6549
1	0	1.0000

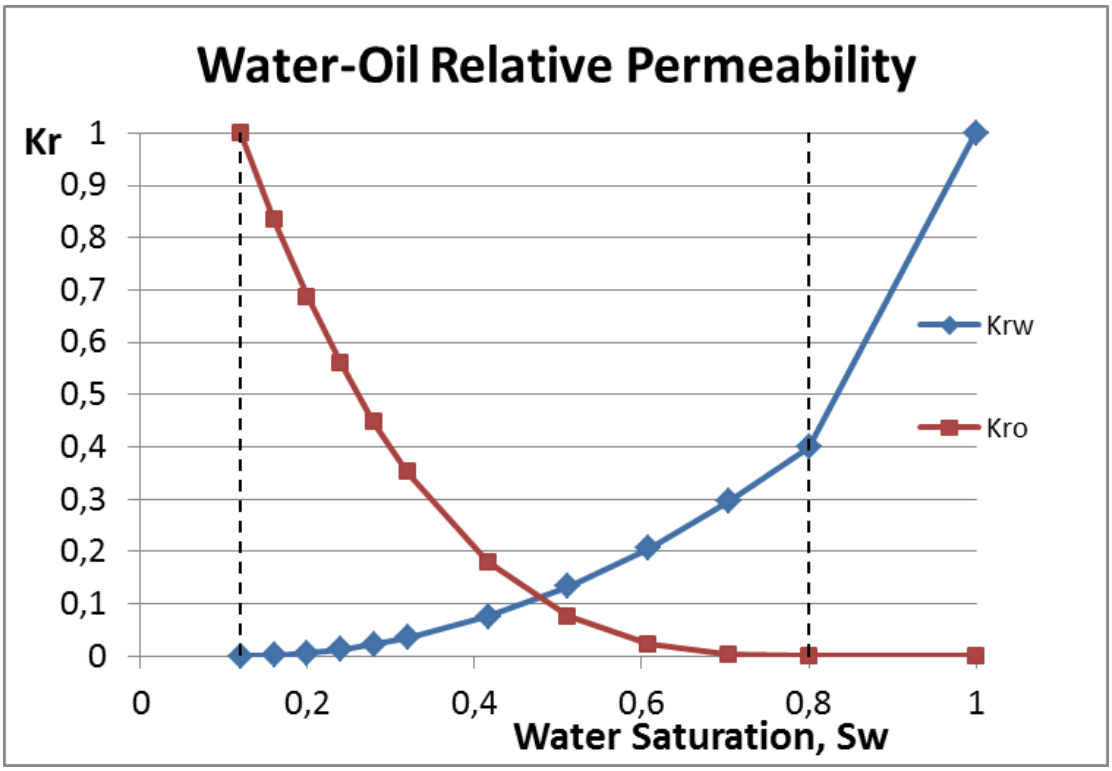

Figure 1 – Nansen oil-water relative permeability

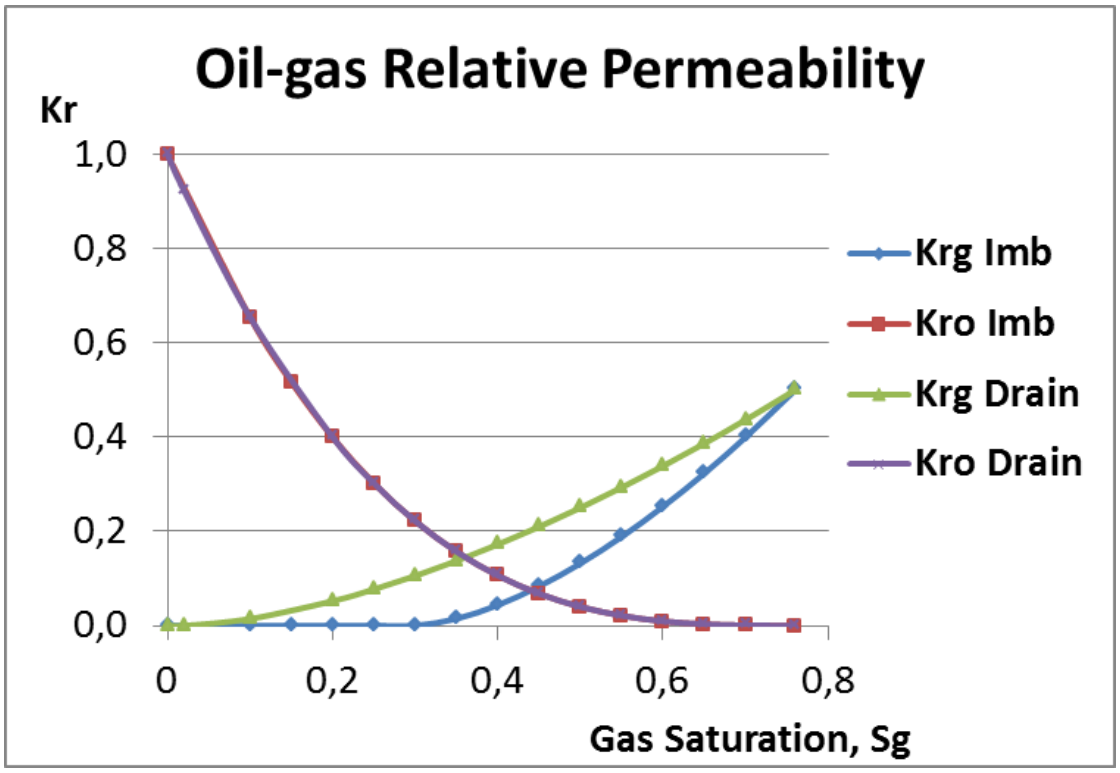

Figure 2 – Nansen oil-gas relative permeability

Appendix A.2 Eiriksson 2

Table 4 – Eiriksson 2 oil-water relative permeability

Sw	Krw	Kro
0.12	0	1
0.16	0.001	0.834
0.2	0.006	0.687
0.24	0.012	0.559
0.28	0.022	0.447
0.32	0.035	0.352
0.416	0.076	0.180
0.512	0.133	0.076
0.608	0.206	0.023
0.704	0.295	0.003
0.8	0.4	0
1	1	0

Table 5 – Eiriksson 2 drainage gas-oil relative permeability

S liq	Krg	Kro
0.26	0.5	0
0.3	0.456	0.000
0.35	0.404	0.002
0.4	0.354	0.007
0.45	0.306	0.017
0.5	0.261	0.034
0.55	0.219	0.060
0.6	0.180	0.097
0.65	0.144	0.146
0.7	0.110	0.210
0.75	0.081	0.290
0.8	0.054	0.389
0.9	0.015	0.647
0.98	0	0.921
1	0	1

Table 6 – Eiriksson 2 imbibition gas-oil relative permeability

S liq	Krg	Kro
0.26	0.50	0
0.3	0.4293	0.0002
0.35	0.3467	0.0018
0.4	0.2709	0.0068
0.45	0.2024	0.0169
0.5	0.1416	0.0341
0.55	0.0894	0.0602
0.6	0.0467	0.0970
0.65	0.0154	0.1464
0.7	0	0.2102
0.75	0	0.2903
0.8	0	0.3886
0.85	0	0.5068
0.9	0	0.6469
1	0	1

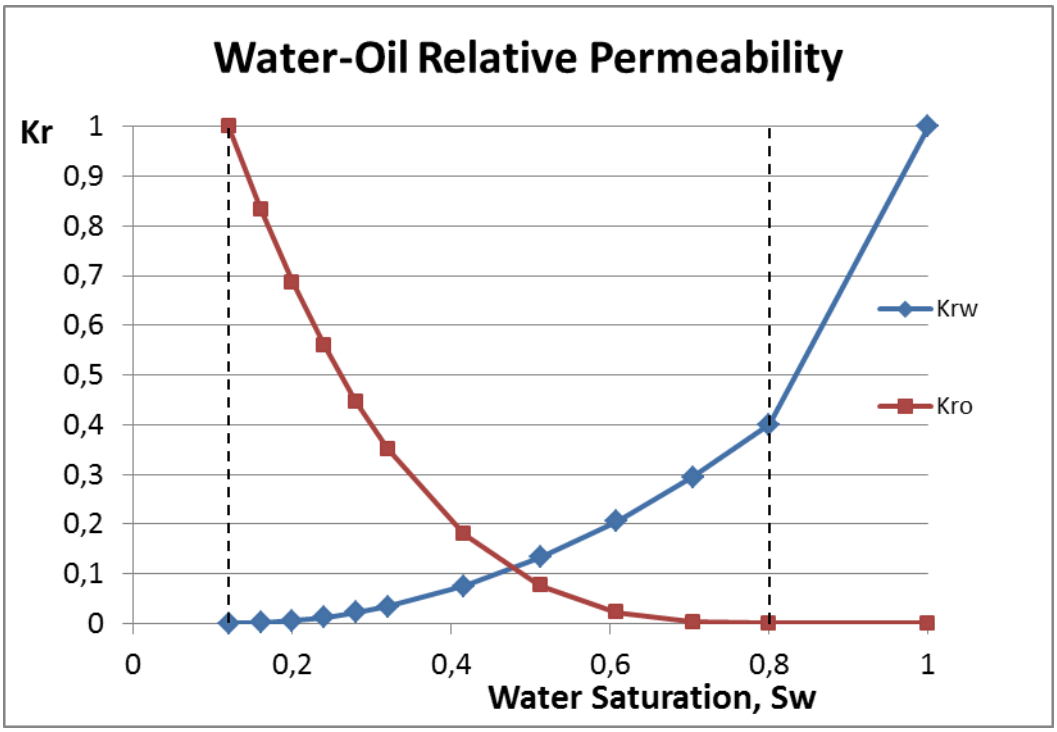

Figure 3 – Eiriksson 2 oil-water relative permeability

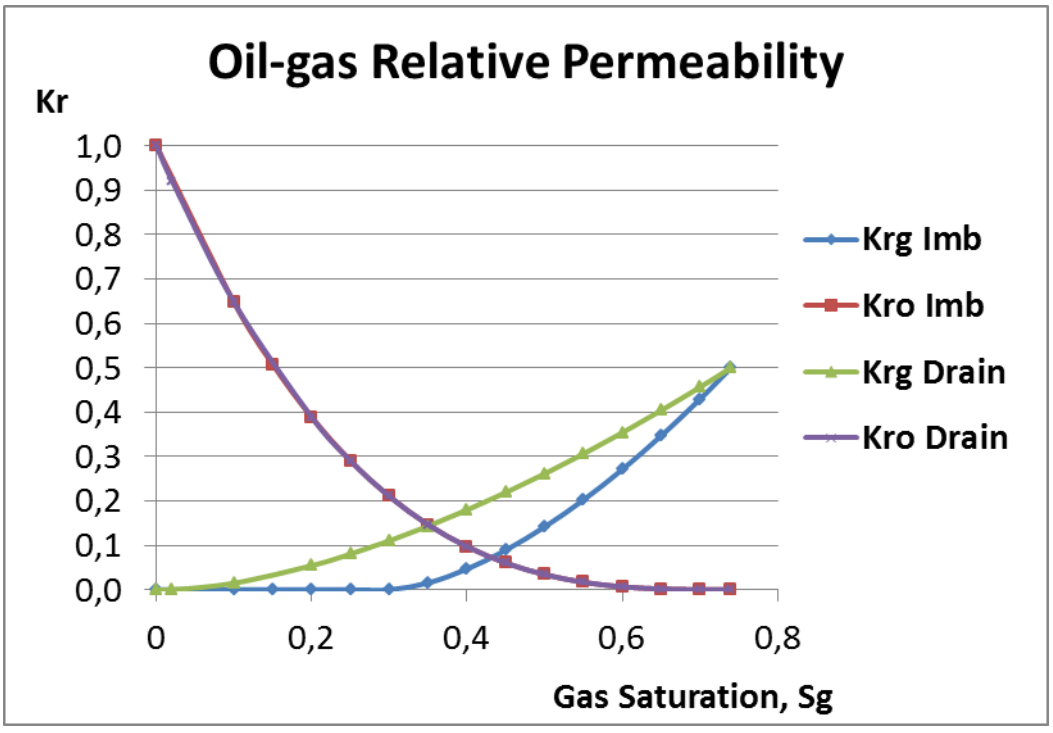

Figure 4 – Eiriksson 2 oil-gas relative permeability

Appendix A.3 Eiriksson 1 and Raude

Table 7 – Eiriksson 1 and Raude oil-water relative permeability

Sw	Krw	Kro
0,20	0	1
0,24	0,002	0,797
0,28	0,008	0,624
0,32	0,019	0,478
0,36	0,034	0,357
0,40	0,053	0,258
0,47	0,096	0,132
0,54	0,153	0,056
0,61	0,222	0,016
0,68	0,305	0,002
0,75	0,4	0
1	1	0

Table 8 – Eiriksson 1 and Raude drainage gas-oil relative permeability

S liq	Krg	Kro
0,40	0,5	0
0,45	0,4293	0,0006
0,50	0,3627	0,0046
0,55	0,3004	0,0156
0,60	0,2426	0,0370
0,65	0,1896	0,0723
0,70	0,1416	0,1250
0,75	0,0991	0,1985
0,80	0,0625	0,2963
0,85	0,0327	0,4219
0,90	0,0108	0,5787
0,95	0	0,7703
1	0	1

Table 9 – Eiriksson 1 and Raude imbibition gas-oil relative permeability

S liq	Krg	Kro
0,40	0,50	0
0,45	0,3735	0,0006
0,50	0,2614	0,0046
0,55	0,1649	0,0156
0,60	0,0862	0,0370
0,65	0,0284	0,0723
0,70	0	0,1250
0,75	0	0,1985
0,80	0	0,2963
0,85	0	0,4219
0,90	0	0,5787
0,95	0	0,7703
1	0	1

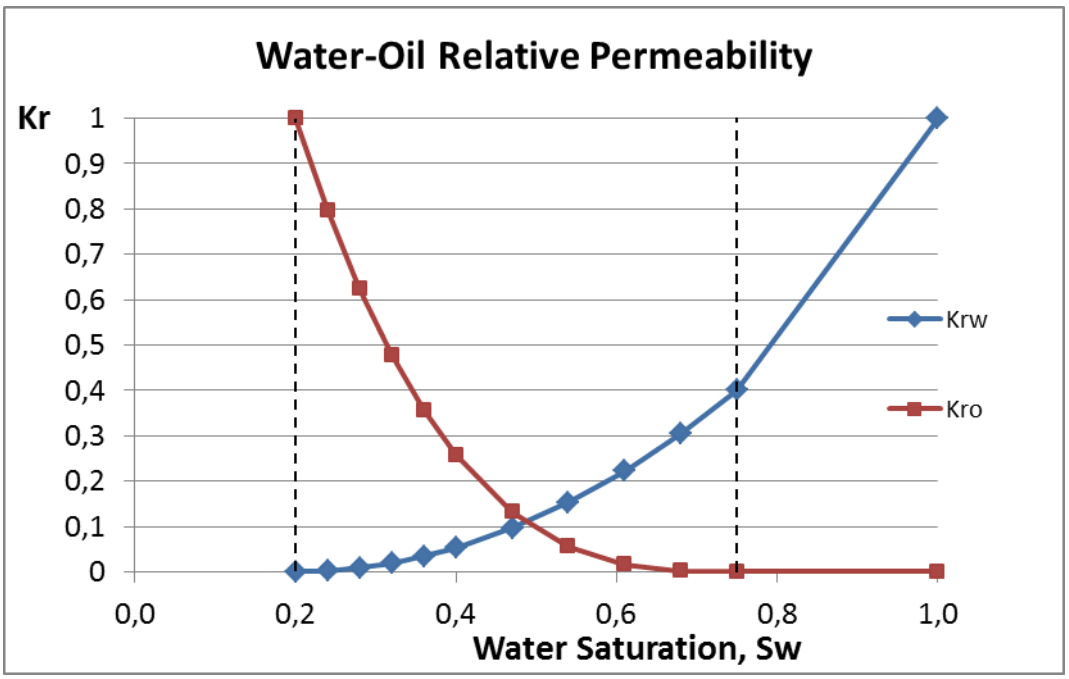

Figure 5 – Eiriksson 1 and Raude oil-water relative permeability

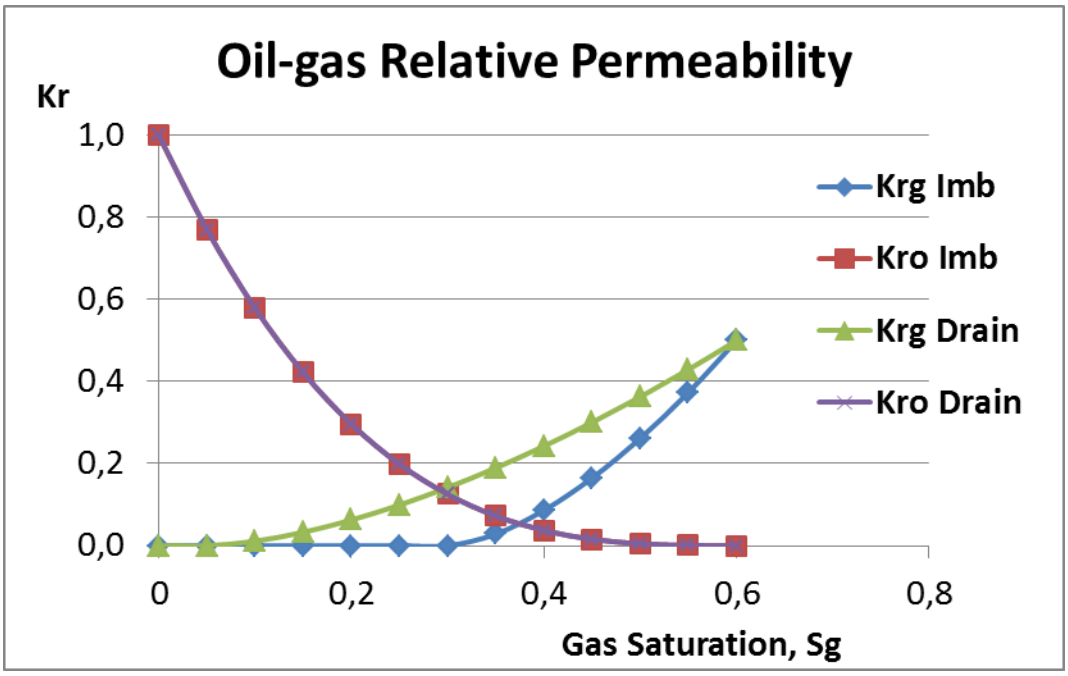

Figure 6 – Eiriksson 1 and Raude oil-water relative permeability

Appendix B. Eclipse 100 Code

Example data file of the WAG base case. The summary section has been cut for space considerations.

```
--
--  RIMFAKS STATFJORD - RFS 2003 JUNI 2003
--
--Zone         Layer          FIPNUM
--
--Nansen       1-5       1
--Eiriksson-2b 6-9       2
--Eiriksson-2a 10-13     3
--Eiriksson-1b 14-17     4
--Eiriksson-1a 18-20     5
--Raude-2b     21-22     6
--Raude-2a     23-24     7
--Raude-1b     25-25     8
--Raude-1a     26-26     9
------------------------------------------------------------
RUNSPEC
------------------------------------------------------------

TITLE
 BASE_CASE_WAG

DIMENS
-- NX  NY  NZ
   45  37  104 /

OIL
WATER
GAS
DISGAS
VAPOIL

METRIC

GRIDOPTS
  'YES'  /

SATOPTS
 'HYSTER' /

FAULTDIM
200 /

TABDIMS
6 1 25 /

REGDIMS
```

```
 10 /

VFPPDIMS
-------------------------------------------------------------------
--Rates    THP  WFR   GFR       ALQ     Tables (max values)
-------------------------------------------------------------------
   20    10   10    10     1     5 /

WELLDIMS
20 150 4 10 /

UNIFIN
UNIFOUT

START
1 'JAN' 2014 /

NSTACK
  60 /

MESSAGES
  2* 200 150 2* 10000 10000 10000 15000  /

NUPCOL
4 /

--NOSIM

-------------------------------------------------------------------
GRID
-------------------------------------------------------------------

INIT
NEWTRAN
GRIDFILE
2 /

NOECHO

INCLUDE
..\..\..\INCLUDE_MODIFIED\GRID_1M_DZ.INC /
--..\..\..\INCLUDE_MODIFIED\GRID_2M_DZ.INC /
--..\..\..\INCLUDE_MODIFIED\GRID_4M_DZ.INC /

MAPUNITS
 'METRES' /

MAPAXES
 0 100 0 0 100 0 /

GRIDUNITS
```

X

```
 'METRES' /

INCLUDE
..\..\..\INCLUDE_MODIFIED\MODIFIED_ACTNUM_1M.ACTNUM /
--..\..\..\INCLUDE_MODIFIED\MODIFIED_ACTNUM_2M.ACTNUM /
--..\..\..\INCLUDE_MODIFIED\MODIFIED_ACTNUM_4M.ACTNUM /

INCLUDE
..\..\..\INCLUDE_MODIFIED\MODIFIED_PERMX_1M.PERMX /
--..\..\..\INCLUDE_MODIFIED\MODIFIED_PERMX_2M.PERMX /
--..\..\..\INCLUDE_MODIFIED\MODIFIED_PERMX_4M.PERMX /

INCLUDE
..\..\..\INCLUDE_MODIFIED\MODIFIED_PORO_1M.PORO /
--..\..\..\INCLUDE_MODIFIED\MODIFIED_PORO_2M.PORO /
--..\..\..\INCLUDE_MODIFIED\MODIFIED_PORO_4M.PORO /

INCLUDE
..\..\..\INCLUDE_MODIFIED\MODIFIED_NTG_1M.NTG /
--..\..\..\INCLUDE_MODIFIED\MODIFIED_NTG_2M.NTG /
--..\..\..\INCLUDE_MODIFIED\MODIFIED_NTG_4M.NTG /

COPY
 PERMX PERMY /
 PERMX PERMZ /
/

-- vertikal permeabilitet er 1% av horisontal permeabilitet
MULTIPLY
 'PERMZ' 0.01  /
/

EQUALS
ACTNUM 0 1 45 29 37 1 104 /
ACTNUM 0 41 45 1 37 1 104 /
/

-- Nuller ut inaktive celler for å redusere regnetiden
MINPV
  5 /

PINCH
 0.01 /

------------------------------------------------------------
EDIT
------------------------------------------------------------

------------------------------------------------------------
PROPS
------------------------------------------------------------
```

```
INCLUDE
--..\..\..\INCLUDE_MODIFIED\HYSTERESIS_REL_PERM.INC /
..\..\..\INCLUDE_MODIFIED\MODIFIED_REL_PERM_HYST.INC /

EHYSTR
 0.1 1 1.0 /

INCLUDE
..\..\..\INCLUDE_MODIFIED\PVTH2H /

-----------------------------------------------------------------
REGIONS
-----------------------------------------------------------------

EQUALS
 'EQLNUM' 1   1 45  1 37  1 104 /    -- En likevektsregion --
/

INCLUDE
..\..\..\INCLUDE_MODIFIED\SATNUM_BASE_CASE.INC /


FIPNUM
33300*1 53280*2 46620*3 39960*4 /



-----------------------------------------------------------------
SOLUTION
-----------------------------------------------------------------
-- inkluderes for å unngå at Sor rundt gassinjektor blir lik
null.
VAPPARS
  2.0  0   /   Oil vaporization control

EQUIL
--   DATUM DATUM  OVK   OVK   GOK   GOK    RSVD   RVVD   SOLN
--     DYBDE  TRYKK   DEPTH  PCOW   DYBDE  PCOG    TABELL  TABELL
METODE
     2450. 250    2450  0.0   2075   0.0   1      1 /

RSVD
2317 100
2450 90 /

RVVD
2000 0.0001
2075 0.00012 /

NOECHO
```

```
------------------------------------------------------------
SUMMARY
------------------------------------------------------------

------------------------------------------------------------
SCHEDULE
------------------------------------------------------------

RPTRST
  'BASIC=5' FREQ=12 'CONV=10' /

RPTSCHED
WELLS=4 FIP=2 CPU /

TSTEP
 0.1  /

TSTEP
 0.1  /

TUNING
 0.1 2.0 2* 1.5 4* 0.1   /
             /
 2* 40       /

GRUPTREE
  G1 FIELD /
/

INCLUDE
..\..\..\INCLUDE_MODIFIED\SCH_WAG_BASE_CASE.SCH /
--..\..\..\INCLUDE_MODIFIED\MODIFIED_SCH_2M_DZ.SCH /
--..\..\..\INCLUDE_MODIFIED\MODIFIED_SCH_4M_DZ.SCH /

END
```

Include File with PVT Data
PVTH2H:

```
--         ***   G A S   D A T A   ***

--                 PVT PROPERTIES OF WET GAS
--
-- To generate a dry gas table change keyword to PVDG,
-- remove the vaporized oil column (Rv) and all / except
-- the last, and apply relevant gas FVF and viscosity data
--
------------------------------------------------------------
--PRESSURE  VAPORIZED  GAS FVF      GAS
--   Pg       OGR  Rv     Bg      VISCOSITY
--   Bar      Sm3/Sm3   rm3/Sm3      cP
```

```
--------------------------------------------------------------
PVTG
  110.0   0.00009108  0.011005    0.01695
          0.000046    0.01117     0.0168
          0.000000    0.01127     0.0166  /

  140.0   0.00011619  0.008564    0.01851
          0.000058    0.00874     0.0182
          0.000000    0.00885     0.0179  /

  170.0   0.00015321  0.007050    0.02048
          0.000077    0.00724     0.0198
          0.000000    0.00736     0.0193  /

  200.0   0.00020228  0.006048    0.02297
          0.000101    0.00625     0.0218
          0.000000    0.00637     0.0207  /

  230.0   0.00026379  0.005363    0.02605
          0.000132    0.00556     0.0241
          0.000000    0.00569     0.0223  /

  260.0   0.00033751  0.004886    0.02980
          0.000169    0.00507     0.0266
          0.000000    0.00519     0.0239  /

  290.0   0.00042144  0.004555    0.03429
          0.000211    0.00471     0.0295
          0.000000    0.00482     0.0254  /

  320.0   0.00050957  0.004325    0.03950
          0.000255    0.00445     0.0327
          0.000000    0.00454     0.0270  /

  350.0   0.00059104  0.004163    0.04512
          0.000296    0.00424     0.0360
          0.000000    0.00431     0.0285  /

  382.0   0.00066066  0.004034    0.05114
          0.000330    0.00407     0.0396
          0.000000    0.00410     0.0300  /

  438.2   0.00080085  0.003904    0.06422
          0.000400    0.00385     0.0468
          0.000000    0.00382     0.0326  /

  469.7   0.00093084  0.003904    0.07581
          0.000465    0.00378     0.0527
          0.000000    0.00372     0.0340  /

  488.6   0.00105175  0.003949    0.08645
```

```
          0.000526    0.00377     0.0579
          0.000000    0.00368     0.0348  /
/


-------------------------------------


--          ***   O I L   D A T A   ***
PVTO

--    RSO     PRESSURE      B-OIL      VISCOSITY
--              (BAR)                    (CP)

   36.72      75.00       1.185      0.72467
             125.00       1.171      0.80416
             175.00       1.159      0.88460
             225.00       1.149      0.96552
             275.00       1.140      1.04646
             325.00       1.132      1.12702 /


   48.82     100.00       1.218      0.67515
             150.00       1.203      0.74491
             200.00       1.191      0.81531
             250.00       1.180      0.88598
             300.00       1.170      0.95658
             350.00       1.161      1.02680 /


   61.47     125.00       1.253      0.61426
             175.00       1.237      0.68339
             225.00       1.223      0.75220
             275.00       1.211      0.81778
             325.00       1.201      0.88143
             375.00       1.192      0.94397 /


   74.83     150.00       1.288      0.54501
             200.00       1.271      0.58559
             250.00       1.257      0.62550
             300.00       1.244      0.66490
             350.00       1.233      0.70423
             400.00       1.223      0.74458 /


   89.01     175.00       1.326      0.49587
             225.00       1.308      0.53098
             275.00       1.292      0.56541
```

```
            325.00      1.279     0.59916
            375.00      1.267     0.63220
            425.00      1.257     0.66450 /

  104.11    200.00      1.366     0.45227
            250.00      1.346     0.48282
            300.00      1.330     0.51275
            350.00      1.316     0.54208
            400.00      1.303     0.57080
            450.00      1.292     0.59890 /

  120.24    225.00      1.408     0.41329
            275.00      1.387     0.44000
            325.00      1.370     0.46613
            375.00      1.355     0.49173
            425.00      1.342     0.51681
            475.00      1.330     0.54135 /

  137.54    250.00      1.452     0.37822
            300.00      1.431     0.40165
            350.00      1.413     0.42457
            400.00      1.397     0.44700
            450.00      1.382     0.46897
            500.00      1.370     0.49048 /

  156.20    275.00      1.501     0.34646
            325.00      1.478     0.36709
            375.00      1.458     0.38724
            425.00      1.441     0.40696
            475.00      1.426     0.42628
            525.00      1.413     0.44519 /

  176.42    300.00      1.552     0.31748
            350.00      1.528     0.33570
            400.00      1.508     0.35347
            450.00      1.490     0.37086
            500.00      1.474     0.38787
            550.00      1.460     0.40454 /

  198.50    325.00      1.609     0.29083
            375.00      1.584     0.30694
            425.00      1.562     0.32266
            475.00      1.543     0.33801
            525.00      1.526     0.35303
            575.00      1.511     0.36774 /
```

222.84	350.00	1.671	0.26605
	400.00	1.644	0.28033
	450.00	1.621	0.29422
	500.00	1.601	0.30779
	550.00	1.583	0.32106
	600.00	1.567	0.33405 /
250.54	375.40	1.743	0.24233
	425.40	1.714	0.25494
	475.40	1.689	0.26720
	525.40	1.667	0.27915
	575.40	1.648	0.29084
	625.40	1.631	0.30227 /
286.43	413.73	1.826	0.22254
	463.73	1.796	0.23359
	513.73	1.770	0.24432
	563.73	1.747	0.25479
	613.73	1.727	0.26501
	663.73	1.708	0.27501 /
322.37	450.08	1.909	0.20672
	500.08	1.877	0.21655
	550.08	1.850	0.22609
	600.08	1.826	0.23540
	650.08	1.804	0.24448
	700.08	1.785	0.25337 /
358.36	484.43	1.989	0.19375
	534.43	1.957	0.20261
	584.43	1.929	0.21121
	634.43	1.904	0.21959
	684.43	1.881	0.22777
	734.43	1.861	0.23577 /
394.40	516.44	2.070	0.18287
	566.44	2.036	0.19093
	616.44	2.007	0.19876
	666.44	1.981	0.20639
	716.44	1.958	0.21384
	766.44	1.937	0.22112 /
430.49	545.82	2.150	0.17351

```
            595.82      2.116     0.18093
            645.82      2.085     0.18812
            695.82      2.058     0.19513
            745.82      2.034     0.20197
            795.82      2.013     0.20866 /
 /


DENSITY
  833. 1027.  0.88 /

PVTW
    478.0      1.057     5.2E-5    0.246    0.0 /

ROCK
      470.8     8.00E-5 /
```